UNIVERSITÉ DU QUÉBEC À MONTRÉAL

A LOW-DIMENSIONAL HILLSLOPE-BASED CATCHMENT MODEL FOR LAYERED GROUNDWATER FLOW: CONCEPTUAL DEVELOPMENT, TESTING, AND APPLICATION

SUBMITTED IN THE PARTIAL FULFILMENT OF THE
REQUIREMENTS FOR THE DEGREE OF
DOCTOR OF PHILOSOPHY
IN EARTH AND ATMOSPHERIC SCIENCES

DÉPARTEMENT DES SCIENCES DE LA TERRE ET DE L'ATMOSPHÈRE

STEFAN BRODA

JANUARY 2011

UNIVERSITÉ DU QUÉBEC À MONTRÉAL

DÉVELOPPEMENT, TEST ET APPLICATION D'UN MODÈLE D'ÉCOULEMENT SOUTERRAIN DE VERSANT

PRÉSENTÉ COMME EXIGENCE PARTIELLE
DU DOCTORAT EN SCIENCES DE LA TERRE ET DE
L'ATMOSPHERE

DÉPARTEMENT DES SCIENCES DE LA TERRE ET DE
L'ATMOSPHÈRE

STEFAN BRODA

JANVIER 2011

ABSTRACT

Low flow prediction is a sensitive element in watershed management. During these periods, baseflow can become a major component of the hydrological response of a catchment. The groundwater flow component in catchment-based hydrological models is often oversimplified, if existent at all. This is generally due to a lack of detailed aquifer characterization, combined with significant additional computational cost for groundwater flow modules. In this thesis the focus is on developing a sparse-parameter, low- dimensional, and computationally efficient yet accurate model for layered groundwater flow. The proposed model has stand-alone uses, but it also designed with a view to incorporation into land surface-based hydrological models.

For subsurface flow on a local scale, the transient-state hillslope-storage Boussinesq (hsB) model (Troch *et al.*, 2003; Paniconi *et al.*, 2003) is selected and coupled with a steady state analytic element (AE) model (Strack, 1989; Haitjema, 1995) representing deep, two-dimensional (horizontal) regional groundwater flow. The coupling approach involves relaxing the no-flow boundary at the hillslope bottom for the hsB model and introducing a Darcy-type leakage term, representing vertical fluxes through a hypothetical aquitard. In order to gain a comprehensive understanding of leakage beyond its classical application in horizontal and infinite aquifers, leakage driving factors such as hillslope planform geometry, base inclination, aquifer properties, and boundary conditions are evaluated by means of a three-dimensional Richards equation based model (Paniconi and Putti, 1994; Camporese *et al.*, 2010). The principal observations from this analysis are i) leakage can generally percolate in both directions, partitioning the hillslope into three distinct zones of downward leakage (upgradient), upward leakage (downgradient), and a transition zone in between; ii) hillslope inclination and planform geometry are the driving forces of the leakage partitioning, with an especially large proportion of upward leakage occurring in convergent hillslopes. These findings are used in the iterative coupling implementation for the hsB/AE model, where each hillslope unit and its underlying deep aquifer is subdivided into three zones of constant leakage. The hsB/AE model is tested on a set of hypothetical hillslopes and a two-hillslope open-book catchment. Comparisons with the results of the Richards equation model demonstrate, in addition to computational efficiency, i) generally good matches in terms of hydraulic heads, leakage rates, and outflow patterns; ii) best results for low and mildly inclined hillslopes of uniform and divergent geometry; iii) reasonable matches in terms of cumulative outflow volumes for the open-book catchment. Deviations from the Richards model are attributed to i) the missing unsaturated zone representation in the hillslope aquifer; ii) the Dupuit-Forchheimer assumption the AE model is based on neglecting resistance to vertical flow in the deep aquifer. An application of the hsB/AE model on a 30 km^2 headwater catchment located in southern Quebec concludes this thesis. The model reproduces reasonably well the baseflow at the catchment outlet during low-flow periods. However, significant deviations are observed during peak flow events, for the reasons mentioned above.

The research described in this thesis represents a first implementation of a catchment scale low-dimensional model constructed on the basis of commonly accepted conceptualizations of shallow subsurface flow in hillslopes on the one hand and deeper groundwater flow in aquifers on the other, taking account of the interactions between these two units via a carefully analyzed leakage process. Some of the limitations in this first implementation can be readily surmounted, for instance by incorporating unsaturated zone extensions of the hsB model (e.g., Hilberts *et al.*, 2005) and transient flow versions of the AE model (e.g., Kuhlman and Neuman, 2009). These efforts are left for future research.

Keywords: hillslope hydrology, leakage, Boussinesq equation, Richards equation, analytic elements, layered aquifer systems, model coupling

RÉSUMÉ

La prévision des débits d'étiage est une question importante dans la gestion des bassins versants. Pendant les périodes de basses eaux, l'écoulement de base peut devenir une composante majeure des débits en rivière. Dans les modèles hydrologiques, la composante de l'écoulement souterrain est souvent très simplifiée. Ceci découle le plus souvent d'une caractérisation insuffisante des aquifères et les temps de calculs prohibitifs des modèles intégrant de manière complète l'écoulement souterrain. Cette thèse développe un modèle représentant les écoulements souterrains peu profonds et profonds qui nécessitent peu de paramètres et dont les calculs sont efficaces et fiables. Le modèle proposé peut être utilisé à la place d'un modèle d'écoulement souterrain en différences finies ou en éléments finis, mais il a été conçu dans le but d'être incorporé à un modèle hydrologique de bassin versant.

Le modèle d'écoulement transitoire de versant "hillslope-storage Boussinesq" (hsB) (Troch et al, 2003, Paniconi et al., 2003) est sélectionné pour représenter l'écoulement souterrain peu profond à l'échelle locale. Le modèle hsB est couplé avec le modèle GLOW d'écoulement permanent basé sur la méthode des éléments analytiques (EA) (Strack, 1989; Haitjema, 1995) qui représente l'écoulement régional profond 2D horizontal. L'approche de couplage utilisée nécessite d'intégrer un terme de percolation à la base du modèle hsB. Ce terme de percolation est représenté par un flux vertical de Darcy à travers un aquitard hypothétique séparant le versant local de l'aquifère 2D régional. Afin de mieux comprendre les facteurs contrôlant la percolation, les facteurs tels que la géométrie du versant, l'inclinaison de la base, les propriétés des aquifères et les conditions limites sont évalués à l'aide d'un modèle 3D basé sur l'équation de Richards (Paniconi et Putti, 1994 ; Camporese *et al.*, 2010).

Les observations principales de cette analyse sont: i) l'eau peut circuler vers le bas ou vers le haut entre les aquifères de peu profonds et profonds et séparer les versants en trois zones distinctes: une zone de flux descendant à l'amont, une zone de flux descendant à l'aval et une zone de transition entre les deux; ii) l'inclinaison des versants et leur géométrie déterminent la partition des flux échangés. Ces résultats sont utilisés dans la mise en œuvre du couplage entre les modèles hsB et EA, où chaque versant et l'aquifère sous-jacent sont subdivisés en trois zones de percolation constante. Le modèle hsB/EA est testé sur différents types de versants et sur un bassin hypothétique formé de deux versants convergeant vers un cours d'eau. La comparaison avec les résultats d'un modèle numérique 3D basé sur l'équation de Richards et utilisé comme référence démontrent i) que les charges hydrauliques, les taux de percolation et les débits aux exutoires sont généralement bien simulés; ii) de meilleurs résultats ont été obtenus pour les versants peu ou très peu inclinés aux géométries uniformes et divergentes ; iii) les débits cumulés sont simulés de manière convenable pour le bassin hypothétique.

Les écarts entre le modèle de référence sont attribués au fait que la zone non-saturée n'est pas représentée dans le modèle hsB et à l'hypothèse de Dupuit-Forchheimer du modèle EA qui néglige l'écoulement vertical dans la nappe profonde. Le fait que le modèle EA ne permette pas de simuler l'écoulement en régime transitoire est une autre limitation du modèle hsB/EA (e.g. Kuhlman et Neuman, 2009). Une application du modèle hsB/EA sur un bassin versant de 30 km^2 situé dans la région de Covey Hill au sud du Québec a été réalisée. Dans cette application du modèle hsB/EA, les débits de base sont assez bien reproduits à l'exutoire du bassin versant pendant les périodes d'étiage.

Toutefois, des écarts importants sont observés au cours des débits de pointe. Les erreurs sur les charges sont également non négligeables dans les zones où un gradient vertical a été observé. Ces erreurs peuvent être attribuées en parties aux limitations du modèle développé.

Mots clés: hydrologie des versants, percolation, équation de Boussinesq, équation de Richards, éléments analytiques, eaux souterraines stratifié, modèle couplé

In Memoriam

Für meine Mutter und meinen Vater, in tiefsten Respekt und Liebe.

(To my mother and father with deepest respect and love.)

ACKNOWLEDGEMENTS

First and foremost, I would like to thank my advisor Marie Larocque for the success of this dissertation. From the day I arrived at UQAM, your enthusiasm about all facets of hydrogeology have inspired me. During our countless discussions you were always a guide for solving occurring problems, but also during discussions aside dissertation related subjects I could acquire important experiences for my personal and professional endeavours. Marie, you made me realize how much potential I have and always challenged me to the limit in order to make me improve.

Sincere thanks go to Claudio Paniconi, you have been an excellent co-advisor from the very beginning. Aside from your many insightful contributions to my work, you taught me above all else to be precise in the communication of my ideas. This was especially evident in your critique of my writing. I also appreciate your patience and willingness to work with me over the last years. You were always available to answer my silly questions which I hadn't carefully considered. It means a big deal for me to count as one of your graduates.

I also want to thank Henk Haitjema from Bloomington University, Indiana, for his ongoing effort of extending and improving his great modeling software, and for patiently explaining elementary concepts to an analytic element novice like me.

I appreciate the assistance of Sylvain Gagné, Lysandre Tremblay, Nadège Baptiste, and Viorel Horoi for providing me with invaluable information about the study site, tirelessly running countless simulations with the three-dimensional numerical model, and assisting me with GIS pre-processing. Extended thanks go to Frédérik Toupin, who was always available concerning anything related to coding and other software issues. Furthermore, I also extend a most grateful thank to Guillaume Houle at McGill university who provided me with insight in efficient MATLAB coding and to fellow graduate Mauro Sulis at INRS-ETE for his help and sharing his experiences of his very own graduate life with me.

My most gratitude must go to my wife Mélanie, for her love and devotion throughout my graduate school years. From the beginning you have encouraged me to pursue my academic goals. You have been unwaveringly supportive, despite the long hours and financial sacrifices of graduate school. This thesis would certainly not exist without you.

To my family and friends in Canada, thank you for welcoming me into your life. You helped me keep afloat amidst the inevitable storms of graduate student's years, my life has been enriched by your presence. To my friends in Germany, especially Constanze, Hajo, and Danny, I thank you all for not forgetting me and being tirelessly supportive, even though I ran off thousands of miles away from you – Danke!

Thanks also go to the other members of my thesis jury, Laxmi Sushama (UQAM), Alain Rouleau (UQAC) and Alain Tremblay (UQAM), granting me the possibility to defend my thesis within a brief delay.

Last but not least, I would like to acknowledge that my research was funded by Ouranos and the Natural Sciences and Engineering Research Council of Canada (CRDPJ-319968-04) and partially funded through a doctoral stipend of the FQRNT and a student stipend by GEC3 at McGill University.

TABLE OF CONTENTS

LIST OF FIGURES

LIST OF TABLES

CHAPTER I

INTRODUCTION

1.1 Background

The availability and quality of water resources can be compromised, sometimes irreversibly, by natural and anthropogenic factors such as climate change or excessive exploitation of groundwater and surface water reservoirs. Such factors can have severe impacts on, for instance, the recharge dynamics of an aquifer or the low flow regime of a river basins. A proper understanding of the continuous interactions between atmospheric, surface, and subsurface components of the hydrological cycle is thus crucial to ensure the sustainable use of water resources. Despite the strong interactions between surface and subsurface waters, the management of these resources has traditionally focused on surface water, soil water and groundwater as separate entities (Sophocleous, 2002; Winter *et al.*, 1998). As a result, simplified models are commonly used to represent groundwater flow in hydrological models used for flood prediction and water resources management. However, the imprecision associated with these models becomes a limiting factor during low flow periods when aquifers represent the major contributor to river flow.

Various approaches for coupling groundwater models with surface flow models exist, and can be separated into four categories: 1) fully-integrated distributed models, of which examples include HydroGeoSphere (VanderKwaak and Sudicky, 1999; Therrien *et al.*, 2005) and CATHY (Paniconi and Putti, 1994; Camporese *et al.*, 2010); 2) loosely coupled groundwater and surface water models, e.g., SWAT and MODFLOW (Sophocleous and Perkins, 2000); 3) extensions of existing surface water or land use models to include some representation of groundwater flow, e.g., ANSWERS (Bouraoui *et al.*, 1997); and 4)

extensions of existing groundwater models to include some representation of surface water flow, e.g., MODFLOW-WhaT (Thoms and Johnson, 2005). While the models in category one are the most complex and physically-based, computational costs and calibration efforts can be quite onerous. The models in the other categories simplify and/or neglect compartments of the hydrological cycle and therefore the interactions between surface water and groundwater bodies are less accurately represented. A summary of some selected coupled models is presented in Table 1.1, wherein the physical descriptions of the surface and subsurface flow components and the interfaces between these components is briefly described.

The application of fully-coupled, integrated surface water/groundwater models (category 1) is generally not appropriate for large scale aquifer systems or river basins, since these models require a large number of parameters to simulate surface and groundwater flow components, and, as already stated, calibration and verification can be quite difficult. Moreover, numerical accuracy, together with convergence and stability properties, are a function of the spatio-temporal discretization and can thus lead to high computational costs. This can be a limiting criteria for water management purposes. In category 2 models, Morita and Yen (2002) applied an infiltrability term at the ground surface as a common internal boundary condition. This term describes the potential infiltration rate or infiltration capacity under the condition of given surface water depth and soil water content just below the surface, and must be compared with the available water supply. The authors report difficulties in the calibration process which they attribute to the increased number of calibration parameters. Gunduz and Aral (2005) solved surface and groundwater flow equations within one global matrix at once, rather than solving separate matrices for each flow domain, while improving the solution iteratively. However, the unsaturated zone was neglected. They also rely on a lateral flow per channel length conceptualization that provides a link between the two systems. Sophocleous and Perkins (2000) applied the hydrologic fluxes calculated by a semi-distributed agricultural watershed model as boundary conditions in MODFLOW. Although models in categories 3 and 4 are easier to develop, calibrate and run than fully-integrated models, the simplifications inherent in these approachesmay render them inappropriate to simulation of the entire water cycle. These simplifications are often related to the representation of groundwater flow or of surface/subsurface water interactions. Liang and Xie (2003) for example use a model which

is not based on groundwater flow equations and is thus primarily used to study surface water dynamics. Thoms and Johnson (2005) used a source/sink exchange flux to couple groundwater and surface water flow equations. The exchange term is evaluated using the conductance concept, representing an interface between the two entities.

In surface-groundwater flow coupling, the challenge lies in closing the gap between computational efficiency, parameter demand and model accuracy. Hence the development of parsimonious yet accurate models describing the entire water cycle with a high degree of parameter identifiability remains a major subject of current research. The basic concept of models in category 2, i.e. taking advantage of strengths of existing models, appears to be particularly promising. This is the direction followed in this thesis. This research is triggered by the recently gaining recognition of hillslopes as fundamental building blocks in hydrological models on the watershed scale (e.g., Matonse and Kroll, 2009). A low-dimensional hillslope model has recently been developed (Troch *et al.*, 2003; Paniconi *et al.*, 2003) and subsequently extended to account for varying bedrock slopes and a partial representation of the unsaturated zone (Hilberts *et al.*, 2004; 2005). These models, derived from the Boussinesq equation, are able to treat complex geometries in a simplified fashion by introducing an averaging procedure over the width function in the lateral flow direction, a conceptualization also used by Fan and Bras (1998) for the kinematic flow equation. The resulting "hillslope-storage Boussinesq" (hsB), model collapses a three-dimensional hillslope soil mantle to a one-dimensional computational space, thereby making the model very efficient in terms of numerical parameterization and numerical resolution as well as a good alternative to higher dimensional, more detailed numerical models.

Table 1.1 Summary of selected coupled groundwater and surface water models

	Surface Flow		Subsurface Flow		Interface
Reference	**Dimension**	**Equation**	**Dimension**	**Equation**	
Fully-integrated surface water and groundwater models (category 1)					
Paniconi and Putti (1994) Camporese et al. (2010)	1D (path-based) overland and channel flow	Convection-diffusion equation complemented with Manning-type relationship	3D unsaturated/ saturated	Richards	Boundary condition-based coupling
Reggiani et al. (1998; 1999)	Representative elementary watershed approach (REW): global balance laws for mass momentum and energy formulated on REW-scale (each REW is subdivided in five zones: unsaturated, saturated, saturated overland flow zone, concentrated overland flow, channel reach); averaged directly at REW scale, each REW is considered as a spatial unit represented by watershed scale parameters and variables, and enables interaction between saturated zone and channel reaches				
Therrien et al. (2005) Therrien and Sudicky (1996)	2D overland	Diffusion-wave approximation of Saint-Venant equation	3D unsaturated/ saturated	Richards	Dual nodes (Darcy flux through thin interface layer)
VanderKwaak and Sudicky (1999) VanderKwaak and Loague (2001)	2D	Diffusion-wave equation	3D variably saturated	Richards	1D Darcy and advection-dispersion equation describe fluxes between continua
Kollet and Maxwell (2006)	2D overland flow	Manning	3D variable saturated	Richards	Surface node represent surface-subsurface domain simultaneously, overland simulator is upper boundary

Table 1.1 continued

	Surface Flow		Subsurface Flow		Interface
Reference	**Dimension**	**Equation**	**Dimension**	**Equation**	
Coupled existing groundwater and surface water models (category 2)					
Gunduz and Aral (2005)	1D channel flow	Saint Venant	2D	Vertically averaged mass conservation in unconfined aquifer	Solving single global matrix at once, linkage via lateral flow term
Morita and Yen (2002)	2D overland flow	Noninertia approximation of Saint Venant, written as 2D heat diffusion equation	3D	Modified Richards equation, written as 3D heat diffusion equation	Using common boundary condition of infiltration through ground surface (infiltrability)
Sophocleous and Perkins (2000)	2D overland flow	Variable storage coefficient method, Muskingum routing method	3D	Mass balance law and Darcy	Recharge, tributary inflows to stream network, irrigation and evaporation from shallow groundwater is specified as MODFLOW boundary condition
Extension of existing surface water models (category 3)					
Arnold et al. (1993)	2D overland flow	Modification of SCS curve number method (varies non-linearly from dry to wet at field capacity)	1D	Use of non-steady-state response of gw-flow to periodic recharge	Via water balance for shallow aquifer storage

Table 1.1 continued

	Surface Flow		Subsurface Flow		Interface
Reference	**Dimension**	**Equation**	**Dimension**	**Equation**	
Extension of existing surface water models (category 3) - continued					
Bouraoui et al. (1997)	2D overland flow	Modified discharge-water depth equation of Manning type	2D	Darcy approach	Modification of distributed parameters surface nonpoint source model
Liang and Xie (2003)	2D overland flow	Linear routing scheme	2D	Variable infiltration capacity, baseflow = f(soil moisture in lowest layer)	Prescribed flux across groundwater table
Extension of existing groundwater models (category 4)					
Anderson (2005)	1D channel flow	Dupuit approximation	2D	Steady state, confined	Leaky stream bed, heterogeneity of hydraulic conductivity below stream
Thoms and Johnson (2005)	2D overland	Kinematic wave approximation	3D variable saturated	Richards	Effective conductivity for overland flow cells
Hantush (2005)	1D channel flow	Linear Muskingum channel storage model, simple mass balance equation	1D	Boussinesq linearized form, unconfined flow	Linear response functions relating channel discharge and stream-aquifer discharge in rates and volumes

Shallow subsurface flow processes in hillslopes are considered to occur from local to catchment scales. However, in many environments groundwater often flows more rapidly near the surface and slower deeper in the aquifer. Cloke *et al.* (2003) indicated significant interactions between hillslope aquifers and deep aquifers which are important for understanding long-term subsurface flow responses (see also Tromp-van Meerveld and Weiler, 2008 as well as Hopp and McDonnell, 2009). Therefore, a complete representation of the subsurface, i.e. a layered groundwater flow system acting on the local and regional scales, needs to be developed all in keeping with the guiding principles of parameter sparsity and computational efficiency.

1.2 Research objectives

The general objective of this dissertation is to propose a computationally efficient watershed scale subsurface flow model for layered groundwater flow. The specific objectives are as follows: 1) to investigate leakage processes in view of an extension of a Boussinesq equation-based model to layered aquifers; 2) to couple the Boussinesq approach to a groundwater flow model; 3) to test and compare the combined model with a benchmark by means of numerical experiments and 4) to assess the model's ability to simulate observed hydrographs and hydraulic heads on a real world catchment. In future research work, the proposed model will be coupled to a land surface model for representation of processes such as evapotranspiration, surface runoff and interflow flow.

1.3 Outline of the dissertation

In Chapter 2 the hsB model is extended to allow for leakage from the hillslope bottom and some preliminary numerical experiments on a uniform hillslope are conducted.

In Chapter 3 an extensive leakage evaluation is carried out with the three-dimensional Richards equation model. Numerical experiments are conducted on hillslopes of different

planform shapes and inclinations as well as different aquifer properties and boundary conditions.

Chapter 4 presents the combination of the hsB model with an analytic element (AE)-based model, representing, respectively, shallow groundwater flow and deep regional groundwater flow. The coupled hsB/AE model is tested on single hillslopes of different planform shapes, inclinations, and aquifer properties, as well as on a synthetic multi-hillslope catchment of 1 km^2 surface area. Leakage patterns, outflow hydrographs and groundwater levels are compared to the three-dimensional Richards equation model.

Chapter 5 describes an application of the new combined model to a real catchment. The study area is a headwater catchment located within the transboundary (Québec/New York) regional scale Châteauguay watershed. The 30 km^2 catchment is delineated into multiple hillslopes. The model is calibrated and validated on measured groundwater heads and baseflow rates.

In Chapter 6 the most significant results of this thesis are summarized and conclusions for future research are drawn.

Preface to Chapter II

In the following chapter, the original hillslope-storage Boussinesq model is extended to account for leakage through the hillslope base. The general behavior of the hsB model with constant leakage is examined and compared to results of a three-dimensional Richards equation model. The aim of this inspection is to assess whether the hsB model is an adequate candidate for coupling with a groundwater flow model. This chapter is based on the paper "Broda, S., Paniconi, C., Larocque, M. (2008). Evaluation of the hillslope-storage Boussinesq model with leakage. In Calibration and Reliability in Groundwater Modelling (Proceedings of ModelCARE 2007) edited by J.C. Refsgaard, K. Kovar, E. Haarder & E. Nygaard, *IAHS Red Book* 320, 182-187, IAHS Press, Copenhagen, Denmark."

CHAPTER II

EVALUATION OF THE HILLSLOPE-STORAGE BOUSSINESQ MODEL WITH LEAKAGE

Abstract The hillslope-storage Boussinesq (hsB) model (Troch *et al.*, 2003) has been extended to allow for leakage through a hypothetical aquitard at the hillslope bottom. A leakage term has been incorporated by extending the mass balance and combining it with the Boussinesq equation. To evaluate the extended hsB model, simulated water table levels are compared with results of a three-dimensional surface–subsurface flow model solving the Richards equation. Numerical experiments are performed on an inclined straight hillslope. Results from the extended hsB model are in reasonable agreement with those from the benchmark model, indicating that the hsB model can be used to simulate recharge to a deep semi-confined aquifer. The leakage rates calculated by the 3D model show significant spatial variability, indicating the requirement for further extension of the hsB model to account for spatially distributed leakage.

2.1 Introduction

Coupled surface water–groundwater models are increasingly used in studies of water cycle dynamics at the watershed scale. These models often incorporate a parsimonious representation of aquifer flow, including subsurface and deep groundwater contributions to river flow. A possible candidate to the simulation of subsurface flow is the one-dimensional (1D) hillslope-storage Boussinesq (hsB) model, which has recently been the object of significant extensions and improvements. The latest versions of the hsB model now consider non-constant bedrock slopes (Hilberts *et al.*, 2004), as well as drainable porosity variations in the unsaturated zone (Hilberts *et al.*, 2005). The low-dimensional nature, physical basis, and sparse parameter needs of the hsB model make it appealing for application to a large variety of real-world hydrogeological problems. The increasing interest in modelling regional scale catchments for integrated water management purposes motivates further development of the hsB model for an eventual coupling with a surface hydrological model and with a deep aquifer model.

This paper deals with the extension of the hsB model (1D) to account for leakage through the hillslope bottom, expanding the model's applicability to simulate recharge to deep aquifers through the incorporation of an additional source/sink term in the subsurface flow mass balance equation. This question has been addressed by Koussis *et al.* (1998), but solely for the linearized Boussinesq model. Simulated water tables are compared to those calculated with CATHY (CATchment Hydrology; Bixio *et al.*, 2000; Camporese *et al.*, 2010), a coupled surface-subsurface model based on the 3D Richards equation and taken to be the benchmark for comparison purposes (Paniconi *et al.*, 2003).

2.2 Material and methods

2.2.1 Incorporation of the leakage term

The leakage concept has been extensively explored and applied in different contexts: in urban water management to assess sewage water exfiltration from pipes to the soil and vice versa (Karpf and Krebs, 2005); in geotechnical engineering to predict possible aquifer

contamination below landfill liners (Foose *et al.*, 2001); and in hydrogeology for pumping test analysis in leaky aquifers (Hantush and Jacob, 1954).

The leakage concept is based on Darcy's law, and allows a vertical groundwater transfer between two aquifers bounding an aquitard:

$$L = -K_v \frac{h_2 - h_1}{D} = C(h_2 - h_1) \tag{2.1}$$

where L [$L\,T^{-1}$] is the leakage flux, K_v [$L\,T^{-1}$] and D [L] are the vertical hydraulic conductivity and thickness of the aquitard, and h_1 and h_2 [L] are the heads in the aquifers bounding the aquitard. Parameter C is the conductance, commonly called the leakage coefficient [T^{-1}].

In the hillslope-storage Boussinesq model, a width function was incorporated into the classical Boussinesq equation in order to extend its applicability to hillslopes of arbitrary geometry (Troch *et al.*, 2003). In this paper a leakage term has been added, so that the mass balance equation describing subsurface flow along a hillslope of variable geometry can be written as:

$$\frac{\partial S}{\partial t} = -\frac{\partial Q}{\partial x} + Nw - Lw \tag{2.2}$$

where S [L^2] is the subsurface water storage, Q [L^3T^{-1}] is the subsurface flux, N [LT^{-1}] is the recharge, L [LT^{-1}] is the leakage through the hillslope bottom, w [L] is the hillslope width, t [T] is the time, and x [L] is the distance to the outlet along the hillslope.

The subsurface flux for the hillslope-storage Boussinesq model is (Troch *et al.*, 2003):

$$Q = -\frac{KS}{f}\left[\cos\alpha \frac{\partial}{\partial x}\left(\frac{S}{fw}\right) + \sin\alpha\right] \tag{2.3}$$

where K [LT^{-1}] is the hydraulic conductivity, f [-] is the drainable porosity, and α [rad] is the angle that the aquifer bottom makes with the horizontal.

The extended hsB equation accounting for leakage through the hillslope bottom is obtained by combination of equation 2 and 3:

$$f\frac{\partial S}{\partial t} = \frac{K\cos\alpha}{f}\frac{\partial}{\partial x}\left[\frac{S}{w}\left(\frac{\partial S}{\partial x} - \frac{S}{w}\frac{\partial w}{\partial x}\right)\right] + K\sin\alpha\frac{\partial S}{\partial x} + fNw - fLw \qquad (2.4)$$

In this study the drainable porosity is kept constant and therefore is independent of the leakage. Equation (2.4) is discretized in the spatial coordinate (Δx = 1 m) and then solved using a variable-order ordinary differential equation solver. It should be noted that leakage is a source/sink term, thereby providing the possibility to represent return flow from a possible deep aquifer.

2.2.2 Behavior of the hsB model with leakage

Figure 2.1 depicts water tables and outflow rates calculated by the hsB model with constant leakage rates applied over the entire simulation time of 100 days, with a dry hillslope as initial condition and recharge of 10 mm/d applied for the first 50 days followed by zero recharge until the end of the simulation, conditions selected to best demonstrate the hsB model performance. As one can expect, leakage can have a significant impact on calculated water tables and outflow rates.

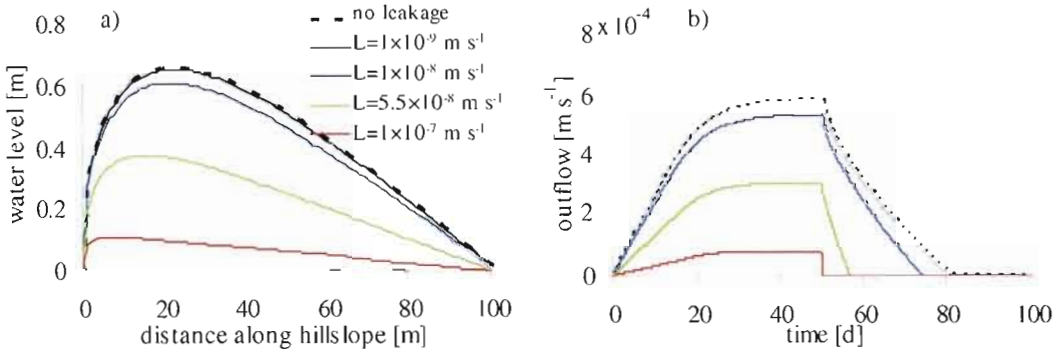

Figure 2.1 Comparison of water table profiles at t = 50 days (a) and outflow rates (b) calculated with the hsB model for different constant leakage rates.

2.2.3 Model set-up for comparison of hsB and CATHY models

Preliminary evaluation of the 1D hsB model with leakage was performed on a straight hillslope with planar geometry and a constant bedrock slope of 5% (Fig. 2.2a). The hillslope has a length of 100 m and a 2 m soil depth, corresponding to a shallow phreatic aquifer. The spatial discretization is Δx = 1 m. The hsB simulations are run for 10 days, with a 1 h time step. In this paper, a drainage scenario is performed.

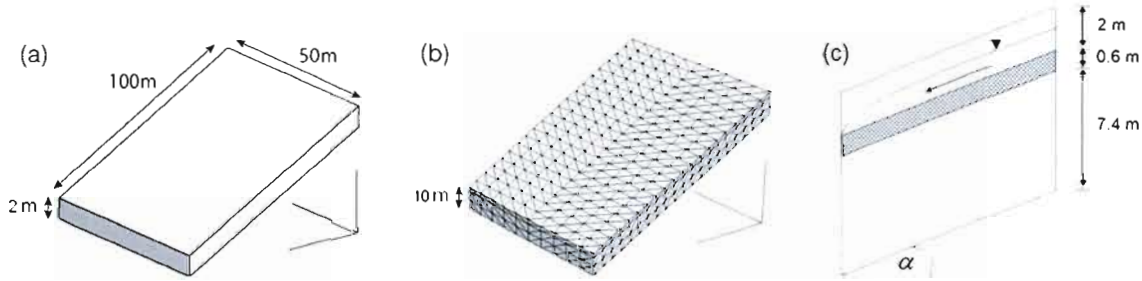

Figure 2.2 Schematic of (a) the test hillslope, (b) discretization used for the CATHY model, and (c) vertical cross-section of the hillslope representation in the CATHY model.

The set-up for the 3D CATHY model consists of a hillslope with the same horizontal extent (Fig. 2.2b). Vertically, a total depth of 10 m is applied, discretized in 20 layers with varying thicknesses and including the aquitard. The first 2 m of the hillslope represent the equivalent of the hsB hillslope, where unconfined groundwater flow occurs in a shallow phreatic aquifer. The next 0.6 m represents the aquitard, followed by 7.4 m representing the deep aquifer (Fig. 2.2c). Horizontally, a mesh increment of Δx = 0.5 m was used. The entire domain consists of 144 000 tetrahedral elements and 29 547 nodes.

In the hsB model, the storage is set to zero at the downslope limit. In the CATHY model, a fixed head boundary condition (Dirichlet type) ranging from 2 m to 2.80 m depth is assigned at the downslope end, corresponding to a river with a depth of 0.80 m cutting the aquifer. No-flow conditions were applied for both models at the hillslope upper and lateral boundaries. The initial water table is set to 0.4 m in the hsB model, and to 8.4 m in the CATHY model

(i.e., 0.4 m height within the unconfined aquifer). A sandy soil type was used for the shallow phreatic aquifer and for the deep aquifer in CATHY. Its hydraulic conductivity is 2.8×10^{-4} m s^{-1} and its drainable porosity is 0.30. The aquitard is represented, for different test cases, with three different hydraulic conductivities, ranging from 1×10^{-6} to 1×10^{-8} m s^{-1}.

Free drainage was first simulated with CATHY for a 10-day period. The simulated leakage rates through the aquitard were spatially averaged for each time step, adapted to the hsB reference frame to account for the hillslope inclination, and used as the leakage term (L) in a ten-day free-drainage simulation with the hsB model. Further hsB developments will provide for a stand-alone version in which the calculation of leakage is accomplished directly in hsB.

2.3 Results

Figure 2.3 illustrates simulated water tables from the hsB and CATHY models for the free-drainage simulation. The hydraulic conductivity of the aquitard has a large influence on the simulated water table. Reasonable matches between the two models are obtained for low-conductivity aquitards for all time steps. When hydraulic conductivity increases, the shape and timing of the response curves are less similar.

It should be noted that the configuration of the two models is not exactly the same, thus there are several issues that require further investigation in comparing the results. For example, the outlet is represented by zero storage at the lower boundary in the hsB model, whereas in the CATHY model the Dirichlet nodes represent a river of 0.80 m depth. Tests have shown that simulated leakage rates and heads from the CATHY model are influenced by the position of the Dirichlet nodes. These differences in parameterization might explain the consistently lower CATHY water tables compared to those of the hsB model. The set-up of the Dirichlet nodes, combined with the applied hydraulic conductivity of the aquitard, causes a water table drop throughout the hillslope in comparison to those calculated by the hsB model. Additionally, the hsB model used in this study does not consider storage-dependent drainable porosity, so that systematic overestimation of water table heights with the hsB model is to be expected (Hilberts *et al.*, 2005). The wave shaped water tables calculated by CATHY are due

to numerical artifacts (Paniconi *et al.*, 2003) and are expected to disappear with a higher spatial resolution of the modeling grid.

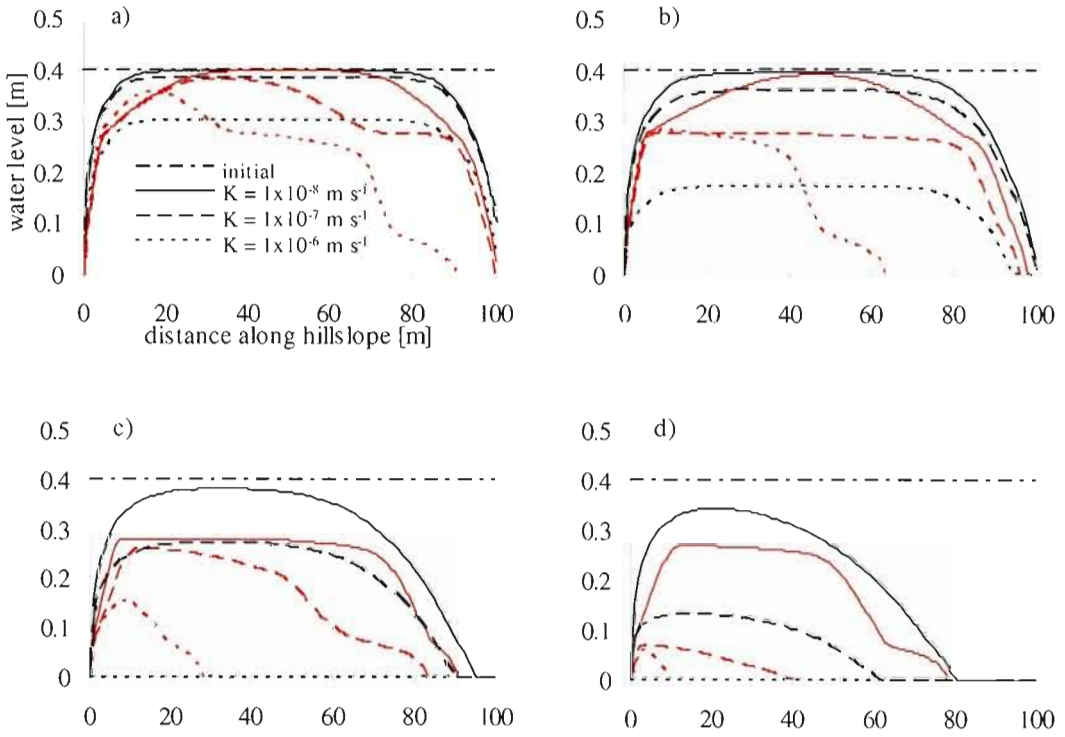

Figure 2.3 Comparison of water table profiles calculated with hsB (black lines) and CATHY (red lines) for different hydraulic conductivities of the aquitard after (a) 1 day, (b) 2 days, (c) 5 days, and (d) 10 days.

Figure 2.4 depicts calculated outflow hydrographs from the two models (aquitard conductivity = 1×10^{-7} m s^{-1}). At a lower slope angle the hsB outflow rates match slightly better the results from CATHY, demonstrating that with increasing slope a larger part of the deep saturated aquifer contributes to outflow. Furthermore, the CATHY model provides additional water through the unsaturated zone and capillary fringe, contributing to higher outflow rates.

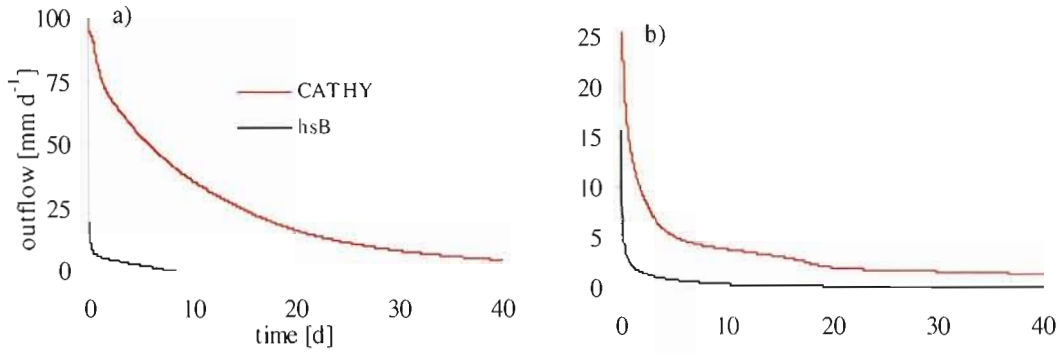

Figure 2.4 Calculated outflow rates of CATHY (red lines) and hsB (black lines) for (a) 5% and (b) 0.2% hillslope inclination.

Figure 2.5 shows that nodal leakage rates along the hillslope can vary up to two orders of magnitude and that spatial differences become negligible with decreasing aquitard conductivity. The magnitude of leakage rates is controlled by the actual hydraulic heads in the unconfined aquifer, which are affected by the boundary conditions in the CATHY model. We note, for instance, that at the downslope end return flow towards the unconfined aquifer occurs. Use of a spatially averaged leakage rate in hsB therefore has an impact on the simulated water table. Both models are highly sensitive to the aquitard's hydraulic conductivity and thickness.

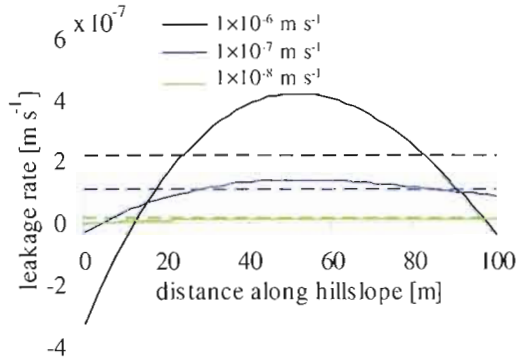

Figure 2.5 Spatially averaged (dashed lines) vs spatially distributed (solid lines) leakage rates calculated by CATHY at t = 5 days for different aquitard conductivities.

2.4 Conclusions and outlook

Extension of the hsB model to allow for leakage provides the opportunity to apply this approach in real world catchments with layered unconfined/confined units. Results from this work are encouraging but indicate the need to investigate, through use of the CATHY benchmark model, corresponding parameterization techniques (aquitard K) as well as initial and boundary conditions. These issues are the subject of ongoing work.

In a next step, a Darcy-type aquifer will be added below the aquitard in the hsB model, leading to the direct calculation of leakage flows between the phreatic aquifer and the deep aquifer. Depending of the conceptualization of the deep aquifer, it might be important to account for spatially discretized leakage rates in hsB.

Further applications will focus on idealized hillslopes (straight, concave, convex) as well as on a local scale real hillslope and regional scale catchment, leading to a complete leaky hsB model.

Preface to Chapter III

In chapter III, leakage is evaluated in a hillslope hydrological context in order to gain a more complete understanding of this process, including its spatial and temporal variability, the dependencies on hillslope and aquifer parameterization, and the influence of boundary conditions. The aim is to provide guidelines with respect to an eventual coupling, based on the leakage concept, between the hsB model and a groundwater flow model. This chapter is based on the paper "Broda, S., Paniconi, C., Larocque, M. (2009). Numerical investigation of leakage in sloping aquifers. *Hydrological Processes*, submitted in April 2010."

CHAPTER III

NUMERICAL INVESTIGATION OF LEAKAGE IN SLOPING AQUIFERS

Abstract A sloping aquifer resting on impermeable bedrock is a common paradigm in hydrological modeling. The underlying assumption of this paradigm is examined in this study of leaky hillslope systems. Leakage is simulated with a three-dimensional finite element Richards equation model for a 100 m synthetic hillslope composed of an unconfined and confined aquifer separated by an aquitard. The simulations examine different configurations of aquifer and aquitard properties (hydraulic conductivity, aquitard thickness), hillslope geometry (uniform, convergent, divergent), hillslope inclination (0.2, 5, and 30%) and boundary conditions (Dirichlet, seepage face), as well as the interplay between leakage, water levels, and outflow. The results show that leakage generally percolates in both directions, with downward (positive) leakage in upslope portions of the aquifer and upward (reverse or negative) leakage in downslope regions. Geometry is found to be a main determinant of the partitioning of leakage along a hillslope, with for instance upward leakage in large portions of convergent slopes but only in a restricted downslope region for divergent slopes. In steep hillslopes, the reverse leakage that occurs downslope as a result of quick upslope drying represents a major component of the water budget. Outflow boundary conditions also exert a major control on the volume and direction of leakage, with the placement and extent of Dirichlet or seepage face nodes along the outflow face being particularly important factors. A dimensional analysis is used to synthesize the main findings and to highlight the differences in response between leaky and non-leaky hillslope conceptualizations. Leakage is also examined for a larger scale aquifer system, in a preliminary assessment of the importance of this exchange process for river basin models that are based on extensions of simple hillslope conceptualizations.

3.1 Introduction

The gaining recognition of hillslopes as fundamental units in watershed hydrology has led to hillslope-based models being used as building blocks for larger scale river basin models (e.g., *Yang et al., 2002*; *Matonse and Kroll, 2009*). At the hillslope scale, models based on the Boussinesq equation are commonly used because of their relative simplicity and low dimensionality, their amenability to analytical solutions and, their adaptability to complex plan and profile morphologies (e.g., *Beven, 1981; Troch et al., 2003; Daly and Porporato, 2004; Hilberts et al., 2004; Basha and Maalouf, 2005; Chapman, 2005; Harman and Sivapalan, 2009b*). The basic conceptualization for these models is that of an unconfined aquifer or soil mantle resting on sloping impermeable bedrock. The assumption of zero flow across the base of these units, while appropriate for many applications, has evident limitations, especially at larger scales when the interactions between different components of a flow system play a greater role. It is thus important to examine the behavior of hillslope systems when the no-flow assumption is relaxed to allow leakage to an underlying aquifer, and to explore the geological, hydrological, morphological, and climatic conditions under which the leakage process is important.

The concepts of leakage and leaky layers have been extensively studied in classical hydrogeology, particularly in relation to aquifer pumping test analyses. *Jacob (1946)*, *Hantush (1949; 1960)* and *Hantush and Jacob (1954; 1955)* published fundamental papers on plane and radial steady and non-steady flow in pumped infinite and finite leaky aquifers. The theory was extended by *Neuman and Witherspoon (1969a; 1969b)* to take into consideration previously neglected effects of storage in the aquitard and drawdown in the unpumped aquifer. *Hemker (1984)* presented a combined analytical-numerical solution technique for steady flow in leaky aquifer systems with an arbitrary number of aquifers, applicable to flow problems with more complex boundary conditions. A generalized semi-analytical solution for a leaky and finite aquifer system was presented by *Zhou et al.* (2009). Leakage has also been investigated in the context of transient multilayer aquifer modeling *(Herrera, 1970; Cheng and Morohunfola, 1993; Gambolati and Teatini, 1996)*, landfill percolation *(Jayawickrama et al., 1988; Foose et al., 2001)*, urban water management *(Karpf and Krebs, 2005)* and coastal aquifer tidal response *(Jiao and Tang, 1999)*.

In hillslope hydrology the underlying hypotheses in Boussinesq-based models have been studied by many researchers. Most of these studies however have retained the impermeable bedrock assumption. For example, *Rastogi (1988)* looked at the effect of slope angle on horizontal and vertical flow, while *Paniconi et al. (2003)* and *Rocha et al. (2007)* investigated the impacts of hillslope geometry, inclination, and soil parameters on the storage and outflow response of Boussinesq models. The effects of boundary conditions were examined by *Franke and Reilly (1987) and Oliver and Christakos (1996), while Harman and Sivapalan (2009a; 2009b)* assessed the effects of temporal variability of recharge and lateral variations in hydraulic conductivity on hillslope flow. Extensions of Boussinesq models have been presented by *Hilberts et al. (2007), Hantush (2005),* and *Kacimov et al. (2004),* who coupled a Boussinesq model to, respectively, the unsaturated zone, surface routing, and a root water uptake submodel. Finally, *Clark et al. (2008)* assessed some of the field evidence for the validity of Boussinesq and other hillslope models.

Tromp-*van Meerveld et al. (2007)* demonstrated experimentally the influence of leakage to bedrock on the subsurface stormflow response and overall water balance using a sprinkler setup at the Panola Mountain Research Watershed. In a subsequent modeling study on the same watershed, *Tromp-van Meerveld and Weiler (2008)* concluded that bedrock leakage was necessary to simulate adequately the long-term subsurface flow response at the small watershed or hillslope scale. However, only a handful of studies have examined leakage in a hillslope or Boussinesq context. *Koussis et al. (1998)* included a leakage term in a version of Boussinesq's equation that was linearized and converted to a form amenable to Muskingum-Cunge solution techniques. *Broda et al. (2008)* modified the hillslope-storage Boussinesq model *(Troch et al., 2003)* to include a leakage term and explored the sensitivity of this model to a range of constant and variable leakage rates. *Cloke et al. (2003)* found that, in modeling hillslope-river interactions, including recharge to the riparian zone from the bedrock aquifer (with flow towards this aquifer originating at the foot of the hillslope) improved simulated heads significantly. *Hopp and McDonnell (2009)* ran synthetic three-dimensional simulation experiments based on the Panola catchment and confirmed that bedrock permeability can play a key role in subsurface flow response. For a sloping two-layer system, *Ahuja and Ross (1983)* assessed analytically the effects on hillslope flow of a constant leakage towards the underlying base material.

These studies underline the importance of considering leakage in hillslope groundwater hydrology and the need to improve our understanding of the factors that influence this flow process. A detailed investigation of leakage is important to the continuing evolution of simple, parsimonious models based on Boussinesq and similar conceptualizations that are used to simulate flow and transport processes at the hillslope and watershed scales. The objective of this paper is to explore, via detailed numerical simulations, how leakage behaves in complex hillslopes and how it is affected by a variety of factors. Leakage is simulated with a three-dimensional finite element Richards equation model of synthetic sloping aquifer systems composed of an unconfined and a confined aquifer separated by an aquitard. The simulations examine different configurations of aquifer and aquitard properties, hillslope geometry, and boundary conditions, as well as the interplay between leakage, water levels, and outflow. The analysis is intended to provide insight into conditions under which leakage becomes an important component of a hillslope's dynamics and water budget.

3.2 Methodology

The model used in this study is the three-dimensional finite element subsurface flow module (*Paniconi and Putti, 1994)* of the coupled catchment hydrological model described in *Camporese et al. (2010).* Only a brief description is provided here. The model solves the three-dimensional Richards equation:

$$\eta(\psi)\frac{\partial \psi}{\partial t} = \nabla \cdot (K_s K_r(\psi)(\nabla \psi + e_z)) \tag{3.1}$$

where $\eta = S_w S_s + \theta_s (dS_w / d\psi)$ [L^{-1}] is the general storage term, S_w [-] is the water saturation, S_s [L^{-1}] is the aquifer specific storage coefficient, ψ [L] is the pressure head, e_z [-] is the vector $(0,0,1)^T$, K_s [LT^{-1}] is the saturated hydraulic conductivity, and $K_r(\psi)$ [-] is the relative hydraulic conductivity. In this study, the *Brooks and Corey (1964)* relationships were used for the saturation–pressure and conductivity–pressure relationships:

$$\begin{aligned} S_e(\psi) &= (\psi_c / \psi)^{\beta}, && \psi < \psi_c \\ S_e(\psi) &= 1, && \psi \geq \psi_c \end{aligned} \tag{3.2}$$

$$\begin{aligned} K_r(\psi) &= (\psi_c / \psi)^{2+3\beta}, && \psi < \psi_c \\ K_r(\psi) &= 1, && \psi \geq \psi_c \end{aligned} \tag{3.3}$$

where the effective saturation S_e [-] is defined as $S_e = (\theta - \theta_r)/(\theta_s - \theta_r) = (S_w\theta_s - \theta_r)/(\theta_s - \theta_r)$ and where θ [-], θ_r [-] and θ_s [-] are the volumetric, residual, and saturated moisture contents, respectively. β [-] is a constant representing the pore size distribution index and ψ_c [L] is the capillary fringe height.

The basic configuration for the layered hillslope aquifer simulated in this work is shown in Figure 3.1. The total soil or sediment thickness of 10 m consists of an unconfined aquifer of 2 m thickness, a semi-permeable aquitard of uniform thickness between 0.2 m and 0.8 m (for different test cases), and a confined aquifer of uniform thickness between 7.8 m and 7.2 m. Uniform, convergent, and divergent plan shapes are simulated, as well as three different slope angles representing gentle (0.2%), moderate (5%), and steep (30%) hillslope inclinations.

The 10 m total thickness is discretized into 20 layers and the surface into 201 (x direction, along the length of the hillslope) by 7 (y direction, along the width) nodes, producing a numerical grid of 201x7x21 = 29547 node points. The hillslope crest, the lateral divides, and the bottom of the discretized domain are set as no-flow boundaries. The outflow face of the hillslope is modeled with different types of boundary conditions (Dirichlet and seepage face), extending over different portions of the aquitard and aquifer faces.

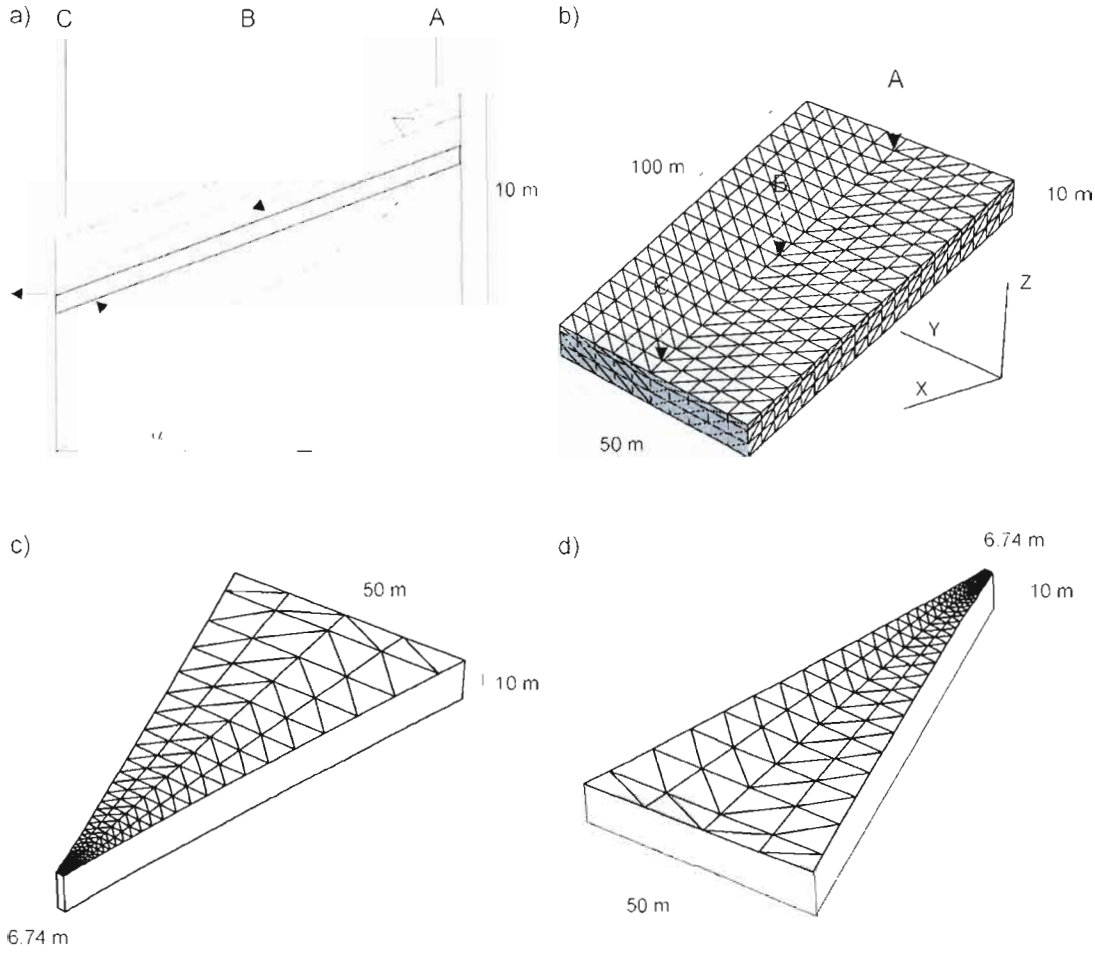

Figure 3.1 (a) Vertical cross section of the layered hillslope aquifer showing, from top to bottom, the unconfined aquifer, the aquitard (shaded layer), and the confined aquifer; (b,c,d) Plan shapes and dimensions of the uniform (b), convergent (c), and divergent (d) hillslopes (not to scale). The labels "A", "B", and "C" show, respectively, the upslope, midslope, and downslope points used for the leakage outputs.

The base case used as a reference point for all subsequent test cases has a moderate slope (5%), a hydraulic conductivity of 10^{-5} m s^{-1} for both the unconfined and confined aquifers, a conductivity of 10^{-7} m s^{-1} for the aquitard, and thicknesses of 0.6 m and 7.4 m, respectively, for the aquitard and confined aquifer. A Dirichlet boundary condition at atmospheric pressure head (ψ =0) is imposed at the seven nodes running along the top of the aquitard (i.e., at the bottom of the unconfined aquifer). This corresponds to the typical boundary condition used in

single-layer, non-leaky sloping aquifer models. The rest of the downslope face is considered impermeable. The base case configuration is summarized in Table 3.1.

Table 3.1 Summary description of the base case configuration.

Plan form geometry	straight
Hillslope length	100 m
Hillslope width	50 m
Hillslope thickness	10 m
Aquitard thickness b	0.60 m
Hillslope inclination a	5%
Aquifer saturated conductivity K_s	10^{-5} m s^{-1}
Aquitard saturated conductivity K_s'	10^{-7} m s^{-1}
Saturated moisture content or porosity θ_s	0.35
Pore size distribution index β	1.20
Residual moisture content θ_r	0.0
Capillary fringe height ψ_c	-0.45 m
Unconfined aquifer specific storage S_s	10^{-2} m^{-1}
Aquitard specific storage S_s	10^{-2} m^{-1}
Confined aquifer specific storage S_s	10^{-4} m^{-1}
Outflow boundary condition	prescribed head (y=0) at the aquitard/unconfined aquifer interface

In addition to varying, as mentioned, the hillslope geometry (plan shape), the slope angle, the relative thicknesses of the aquitard and confined aquifer, and the outflow boundary conditions, the saturated hydraulic conductivity (K_s) of the unconfined and confined aquifers (same K_s value) is also varied for different cases, from 10^{-3} to 10^{-6} m s^{-1}. The aquitard saturated conductivity (K_s') varies from 10^{-6} to 10^{-9} m s^{-1}. A series of nine test cases is considered, each focusing on a different factor or set of parameters that influence leakage. For each case, the parameter values altered with respect to the base case are summarized in Table 3.2. The nine test cases cover a representative range of hillslope configurations and parameterizations. A dimensional analysis that highlights the differences in response between leaky and non-leaky hillslope conceptualizations is also presented.

For test cases 1 to 8, no atmospheric forcing (rainfall or evaporation) is imposed on the surface of the hillslope and the simulations represent pure drainage for a 50-day period. The initial condition used for all simulations is that of a water table in the unconfined aquifer at a depth of 1 m from the surface and a vertically hydrostatic head profile through the entire domain established from this water table position. The rainfall (or recharge) surface boundary condition used in case 9 consists of two 10-day recharge pulses and no atmospheric forcing for the rest of the simulation. Finally, for all test cases the hillslope length is 100 m and the maximum width is 50 m (see Figure 3.1), except for case 6 where a length of 1 km and a width of 500 m are used.

Table 3.2 Summary description of the ten test cases.

Case 1	Influence of aquifer saturated conductivity: $K_s = 10^{-3}$, 10^{-4}, 10^{-5}, and 10^{-6} m/s
Case 2	Influence of aquitard saturated conductivity: $K_s' = 10^{-6}$, 10^{-7}, 10^{-8}, and 10^{-9} m/s
Case 3	Influence of aquitard thickness: b = 0.2, 0.4, 0.6, and 0.8 m
Case 4	Influence of slope angle: a = 0.2, 5, and 30%
Case 5	Influence of plan shape: convergent and divergent shapes as shown in Figure 1
Case 6	Influence of hillslope length: 1 km hillslope
	Influence of outflow boundary condition:
Case 7	Dirichlet BC along different portions of the outflow face
Case 8	Seepage face BC along different portions of the outflow face
Case 9	Seepage face BC along the unconfined aquifer and aquitard outflow face and Dirichlet BC along the confined aquifer outflow face
Case 10	Influence of surface boundary condition: recharge of 5 mm/d during the first 10 d and between days 20 and 30

The model outputs examined are the hydrographs computed at the outflow boundary, the storage profiles corresponding to the water table levels in the unconfined aquifer, and the leakage rates along the hillslope either at specified times or as a function of time at upslope, midslope, and downslope positions on the hillslope (labels "A", "B", and "C" in Figure 3.1). The storage and leakage profiles are taken along a longitudinal transect cutting through the middle of the hillslope.

Figure 3.2a shows the outflow hydrographs and storage profiles for the base case simulation in the unconfined aquifer. The water table drops fairly slowly in the upslope portion of the hillslope, and only begins to "slide down" the hillslope (complete vertical desaturation) after about 20 days. The storage levels increase downslope, generating water table peaks that exceed the initial water table height at approximately 8 m from the outlet. Figure 3.2b plots in vertical cross section the total heads for the longitudinal transect through the center of the hillslope at t=10 d, when the upslope region of the unconfined aquifer is already quite desaturated. The influence of the lower permeability aquitard is evident from the refracting contour lines at the aquifer/aquitard interface. In the central portion of the hillslope, flow in both aquifers is generally parallel to the hillslope base. At the downslope portion, upward flow occurs and the confined aquifer feeds the unconfined aquifer.

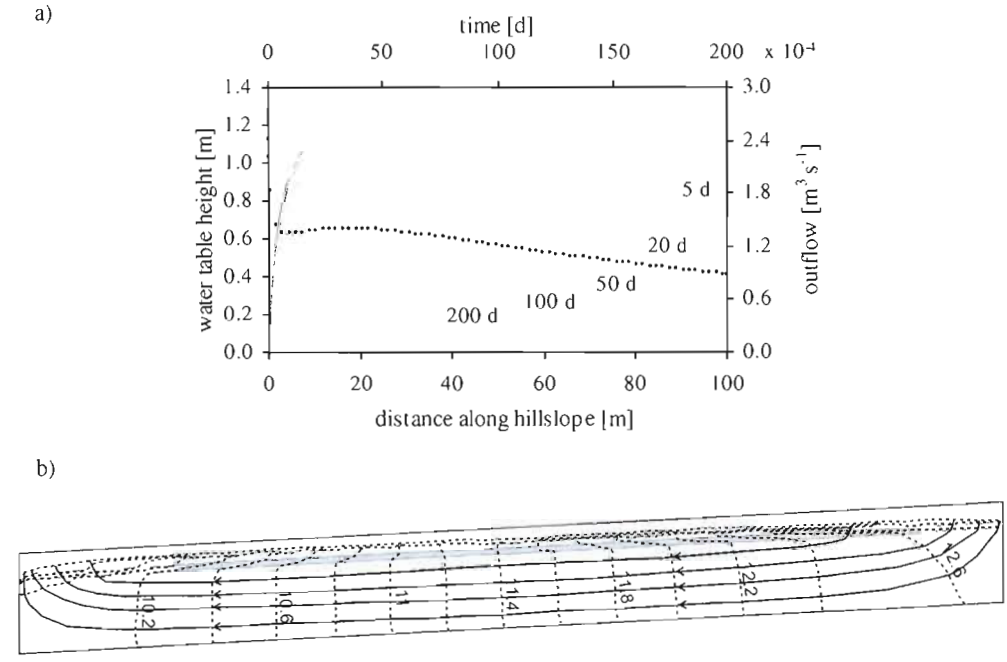

Figure 3.2 (a) Storage profiles vs. distance (solid lines) in the unconfined aquifer and outflow vs. time (dotted line) for the base case simulation; the dashed line shows the initial water table height; (b) contour map of total heads and flow lines for a vertical cross section along the length of the hillslope at t =10 d.

3.3. Results and dicussion

3.3.1 Hydraulic Properties

3.3.1.1 Leakage calculation methods and influence of aquifer conductivity (Case 1)

This first test case, which examines the influence of aquifer hydraulic conductivity, is also used to present and compare three possible methods of calculating leakage rates in a numerical model. The first method simply takes the vertical component of the Darcy velocity vector at the nodes located at the bottom of the aquitard layer. This gives a direct representation of the water flux entering the confined aquifer from the overlying aquitard, i.e., fed by the unconfined aquifer. Note that "vertical" here refers to the downward direction and not to the direction perpendicular to the inclination of the sloping aquifer. This convention makes the first method consistent with the other two methods. Also, as in standard practice, leakage is taken to be positive in the downward direction. In the second method, the leakage is given by the Darcy flux computed from the difference between the nodal head values at the top and bottom of the aquitard:

$$L = K_s' \frac{h_2 - h_1}{b} = C(h_2 - h_1) \tag{3.4}$$

where L [LT^{-1}] is the leakage rate, b [L] is the thickness of the aquitard, h_2 and h_1 [L] are the heads at the top and bottom of the aquitard, respectively, and $C = K_s'/b$ [T^{-1}] is the conductance (*Delleur, 1999*) or specific leakage (*Hantush and Jacob, 1955*).

By convention, leakage calculated according to the second method is set to zero once the water table in the unconfined unit reaches the bottom of the aquifer. Equation (3.4) would be one way of introducing a leakage term in a large scale (watershed) model that is built on extensions of simple hillslope modeling paradigms, and it is similar to the leakage expression used in *Koussis et al. (1998)*. The third method is based on equation (3.4) but it incorporates unsaturated zone transmission of water, replacing K_s' by $K_r'K_s'$, where K_r' is the relative hydraulic conductivity of the aquitard evaluated at the top of the aquitard. It relaxes the assumption of zero leakage when the unconfined aquifer becomes unsaturated (in vertical profile).

Figure 3.3 compares the leakage rates calculated using methods 1 and 3 for a range of aquifer conductivity values applied to the base case configuration. The largest disparities between the direct computation of leakage (method 1) and the difference formula (method 3) occur for highly conductive soils ($K_s = 10^{-3}$ or 10^{-4} m s^{-1}) at the upslope point (Figure 3.3a) and at early times. These differences are much smaller at later times and for aquifers of lower permeability ($K_s = 10^{-5}$ or 10^{-6} m s^{-1}). The differences are also much less significant for the highest conductivity aquifer at the midslope (Figure 3.3b) and downslope (Figure 3.3c) points. As expected, the magnitude of leakage is also smaller at these points compared to early-time upslope leakage. The upward (negative) leakage (see also Figure 3.2b) that predominates downslope (i.e., confined aquifer feeding unconfined aquifer), as well as the transition from positive to negative leakage at the midslope point, are a direct consequence of the inclination of the aquifer system and the placement of the outflow boundary conditions. These factors are explored in more detail later.

The differences in leakage rate calculated via the direct and difference formula methods, particularly significant for highly permeable aquifers (relative to the aquitard) at early time and in upslope regions, suggest that when pressure head gradients are strong the limitations of an approximate calculation as represented by commonly used formulae such as equation (4) ("corrected" in method 3 for unsaturated zone transmission) can become important. Compared to method 1, which gives the leakage rate at a point computed using the full Richards equation, methods 2 and 3 apply a difference formula across a layer (aquitard). In addition to possible inaccuracies when pressure varies greatly through the layer, an expression such as equation (3.4) does not consider storage effects in the layer. As storage and gradient effects are minimized, methods 1 and 3 should converge. This was indeed verified when comparing the methods for a simulation using a very thin aquitard (0.01 m). Method 1 is also subject to accuracy constraints, dictated by the vertical resolution of the grid used at the aquitard/aquifer interface, but this is readily alleviated by grid refinement. A simulation with a 40-layer grid did not appreciably change the overall results, hence the grid effect is considered to be negligible for the purposes of this study. The limitations of methods 2 and 3, on the other hand, are of a physical nature, dictated by aquitard thickness and storage properties, for instance.

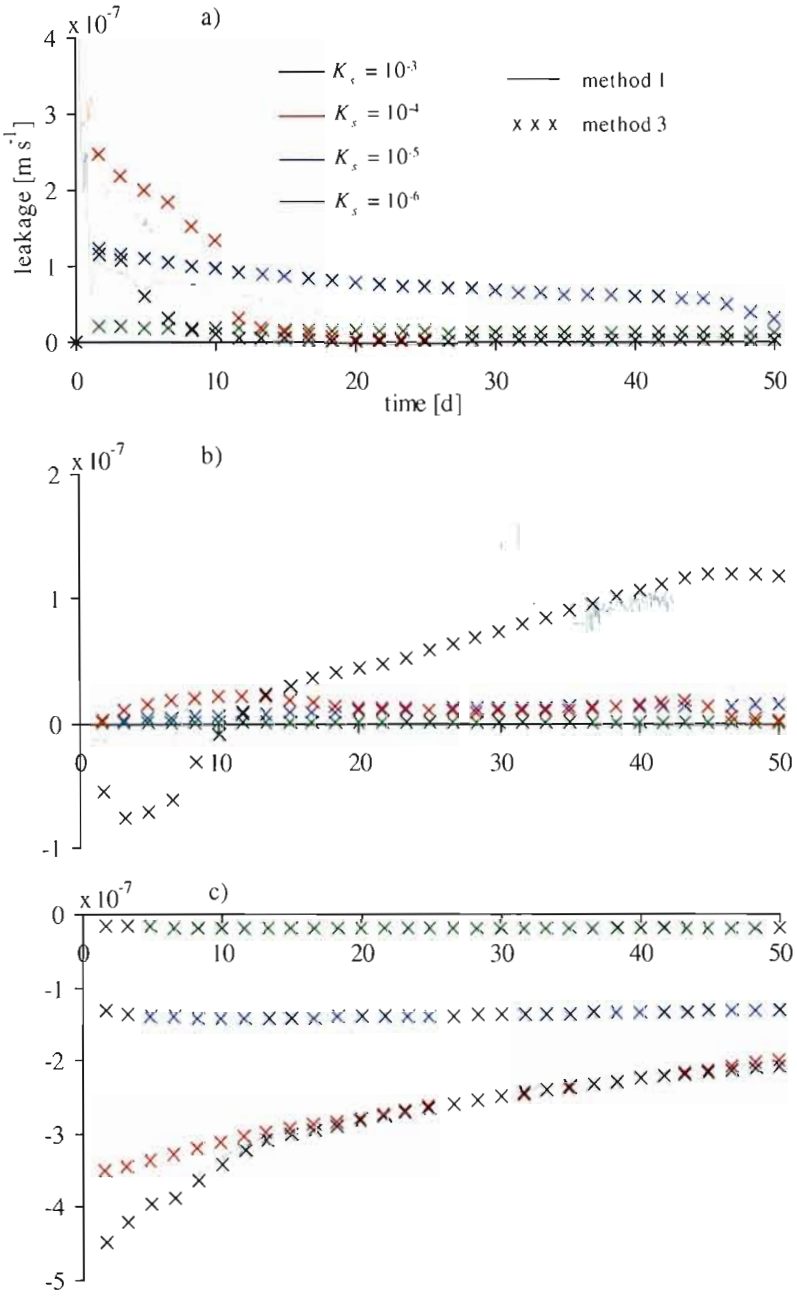

Figure 3.3 Influence of aquifer conductivity on leakage, with comparison of different methods of calculating the leakage rate. Leakage calculation methods 1 and 3 are compared at (a) the upslope point ("A" in Figure 3.1), (b) the midslope point ("B" in Figure 3.1), and (c) the downslope point ("C" in Figure 3.1).

The leakage rates for method 2 match those of method 3 very closely, except when the unconfined aquifer becomes unsaturated. This occurs earlier for the high-K_s cases (at 1.2, 6.5, and 24.5 d for K_s = 10^{-3}, 10^{-4}, and 10^{-5} m s^{-1}, respectively for the upslope point), after which time leakage remains zero for method 2. This illustrates the limitation of the zero leakage assumption used in method 2 and the importance of unsaturated zone transmission of water from the unconfined aquifer and aquitard to the confined aquifer.

It is interesting to observe in Figure 3.3a that the highest leakage rates during the peak response period are not obtained for the most permeable aquifer (K_s=10^{-3} m s^{-1}) but rather for the K_s=10^{-4} m s^{-1} aquifer. The K_s=10^{-3} m s^{-1} aquifer will certainly be the fastest to drain, but it also has the largest permeability contrast with the aquitard (at 10^{-7} m s^{-1}), thus there is proportionately greater flow towards the outlet that occurs within the unconfined aquifer rather than leaking across the aquitard. A final observation to make for this first test case concerns the high degree of spatial and temporal variability that characterizes leakage behaviour in a sloping aquifer. This is a much more complex dynamics than that which occurs in more classical, horizontal aquifer systems. This complexity must be kept in mind as hillslope and watershed models increasingly seek more complete representations of subsurface flow processes.

In the remaining test cases the third leakage calculation method will be used , i.e., equation (3.4) with unsaturated zone correction. This method is consistent with the direct, Richards equation method (in the limit as aquitard thickness goes to zero), it is the type of approach that is probably most practical in simple, parsimonious hillslope or watershed-scale hydrological models, and it is more general than the commonly used equation (3.4).

3.3.1.2 Aquitard conductivity (Case 2)

In this test case the aquifer hydraulic conductivity is kept fixed at K_s=10^{-5} m s^{-1} and the influence of varying the aquitard conductivity K_s' is investigated. Figure 3.4a shows that percolation towards the confined unit in the upslope portion increases as K_s' increases and that at the downslope point upward leakage also increases in magnitude as K_s' increases. The leakage rate is much less variable in time in the downslope portion than upslope, particularly for high aquitard conductivity values. It was also observed (not shown here) that the water

table in the unconfined aquifer drops in the hillslope at a much faster rate as K_s' is increased. The early-time water table (and hence pressure head) buildup upslope in the unconfined aquifer is greater at higher K_s'.

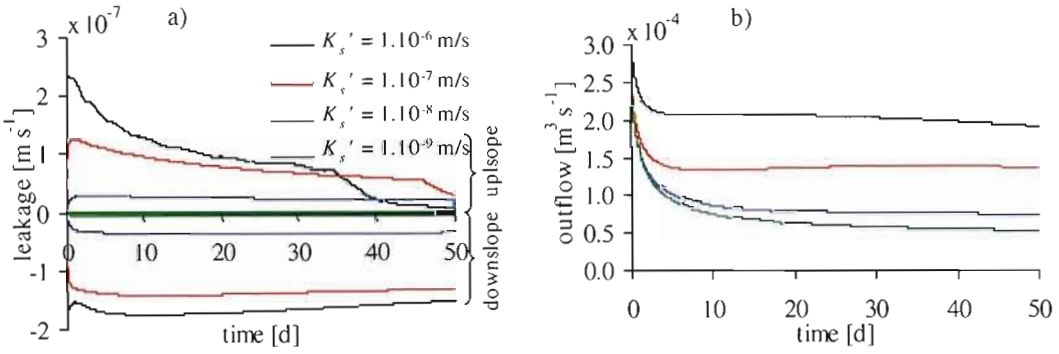

Figure 3.4 Influence of aquitard conductivity on (a) leakage rates at the upslope point (positive values) and downslope point (negative values) and on (b) outflow.

These results suggest a positive feedback between the unconfined and confined aquifers when they become more connected via increased aquitard conductivity, with a reinforcing effect on peak-time upslope leakage through higher K_s' and higher head gradient (see equation (3.4)). The differences in response seen in Figure 3.4a also imply that, when the aquitard is relatively permeable, the leakage process and the water in the confined aquifer have a significant impact on drainage for sloping aquifers. This is confirmed in Figure 3.4b, where outflow rate and volume vary significantly with aquitard permeability, despite all other parameters kept equal for all simulations. These results underscore the need to carefully scrutinize the "impermeable base" assumption often used in hillslope hydrological models, and the importance of seeking as reliable an estimate as possible of the hydraulic conductivity of the geological unit separating an unconfined aquifer from deeper formations.

3.3.1.3 Aquitard thickness (Case 3)

The impact of aquitard thickness b on leakage rates is evaluated in Figure 3.5, which shows decreasing leakage with increasing b, as expected from equation (3.4). Connectivity

between confined and unconfined aquifers increases as aquitard thickness decreases, with effects similar to those described for test case 2. For thin aquitards the role of aquitard storage becomes less important, with positive ramifications for leakage estimation, as discussed in test case 1.

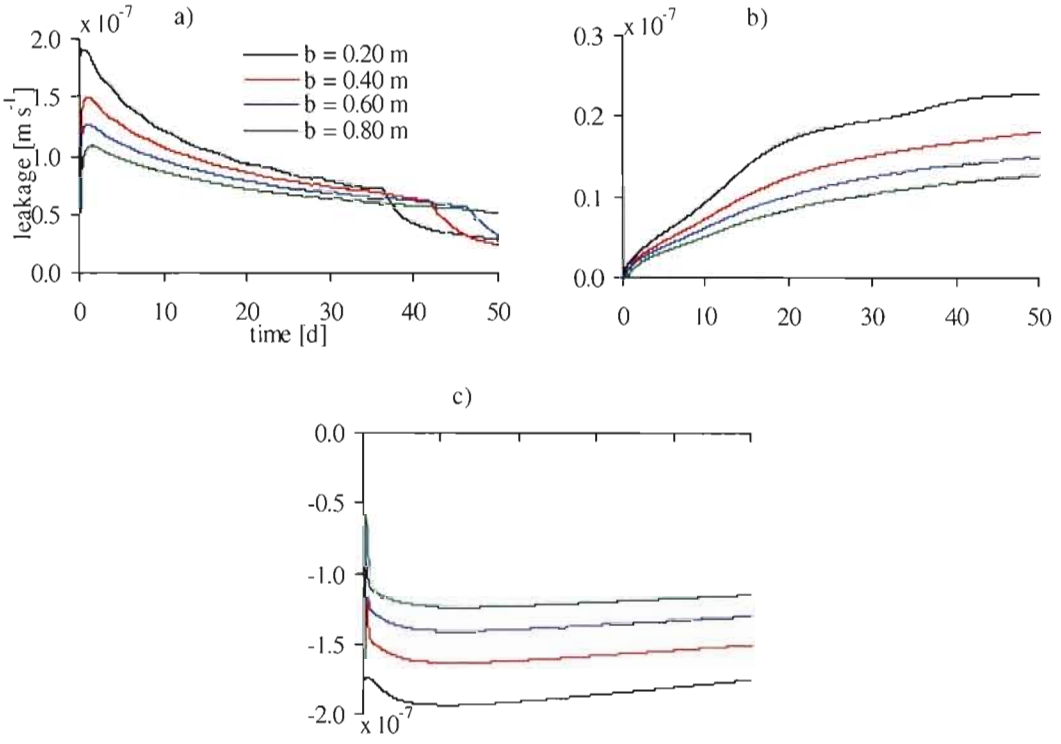

Figure 3.5 Leakage rates at the upslope (a), midslope (b) and downslope (c) points for different aquitard thicknesses.

3.3.2 Geometry

3.3.2.1 Hillslope inclination (Case 4)

Figure 3.6a shows leakage rates calculated at the upslope and downslope points for different slope angles. Unsurprisingly, hillslope inclination has a strong impact on leakage behavior. The water table drops very quickly in steep hillslopes, resulting in rapid drainage of the upslope region, as reported also by *Rastogi (1988)* and *Paniconi et al. (2003)*, and even partial desaturation of the confined aquifer.

The outflow dynamics shown in Figure 3.6b underline the rapid drainage response of steep hillslopes. While for the 0.2 and 5% case outflow decreases in time, the 30% case depicts a significant increase of outflow at early times, caused by the strong role of the unsaturated zone in delaying transmission of water to the outlet up to a maximum value. It also shows the contribution of deeper formations in maintaining high outflow rates throughout the drainage event in a layered and interconnected aquifer system.

Figures 3.6c and 3.6d show the cumulative outflow and leakage volumes, with the leakage volume separated into positive (downward) and negative (upward) components. This provides further evidence of the degree to which a confined aquifer can contribute to a catchment's water balance as hillslope inclination increases, with reverse leakage far exceeding percolation for the 30% slope angle (Figure 3.6d). The percolation volume in this case reaches a maximum at about 15 d and remains constant thereafter, i.e., leakage to the confined aquifer becomes negligible. This can also be seen in comparing the positive and negative portions of Figure 3.6a for the 30% case. For both the 5% and 30% cases, Figures 3.6c and 6d show that exchanges through leakage can amount to a considerable volume of water, comparable to or exceeding the amount of groundwater that flows in the unconfined aquifer and away from the hillslope.

This test case provides a more quantitative illustration of the balance and transition between positive leakage (percolation) and negative or reverse leakage seen also in previous tests where the spatial leakage patterns were plotted. It should be noted that in real catchments, the transition between percolation and reverse leakage will not be as neatly delineated (for instance into upslope, midslope, and downslope behavior), owing to local variations in hillslope inclination, aquitard properties, and other heterogeneities.

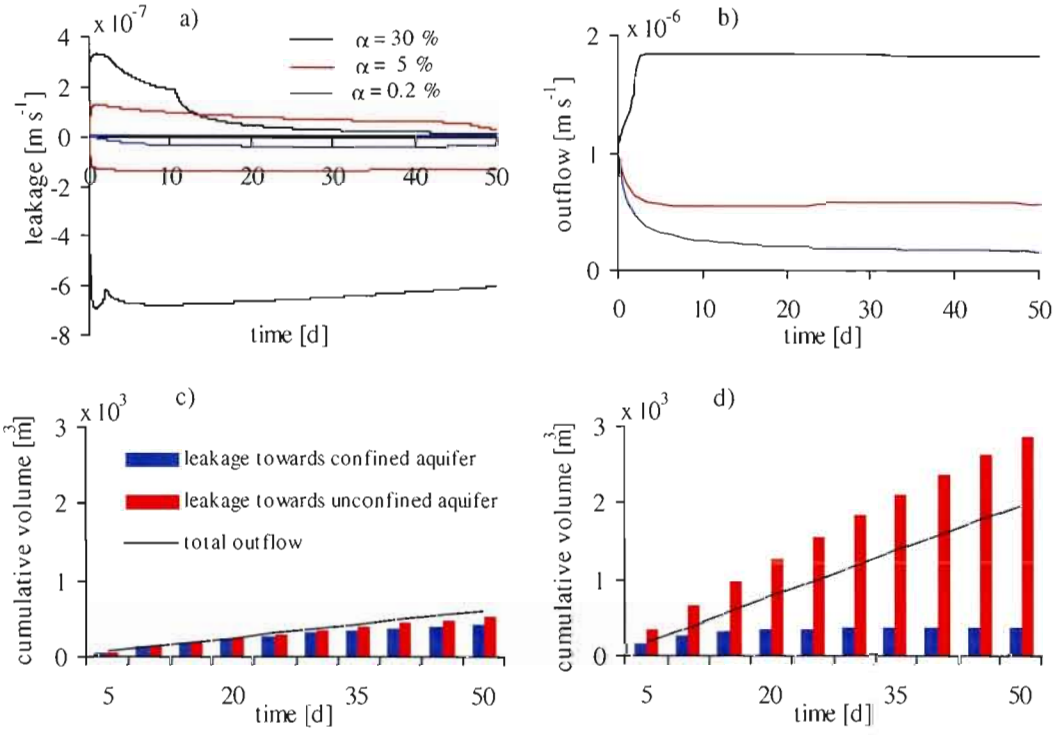

Figure 3.6 Effect of slope angle on (a) leakage rates at the upslope point (positive values) and downslope point (negative values) and on (b) outflow. Cumulative leakage and outflow volumes for the (c) 5% and (d) 30% slope cases.

3.3.2.2 Hillslope plan form shape (Case 5)

In Figure 3.7 total heads in the unconfined and confined aquifers and leakage rates are plotted along the hillslope at t=10 d for the three plan shapes shown in Figure 3.1. The convergent hillslope, by virtue of its converging flow paths and constricted outlet, creates a bottleneck near the outlet that results in high water tables (Figure 3.7b) and eventually even surface runoff (*Paniconi et al., 2003).* This causes reverse leakage along a greater portion of the hillslope compared to the uniform and divergent hillslopes (Figure 3.7d).

Generally, hillslope planform shape has a greater effect on the heads in the confined aquifer with an up to twofold head difference compared to the unconfined aquifer. Heads in the

confined aquifer can therefore exert a significant control on the partitioning of leakage into up- and downwelling areas along the hillslope.

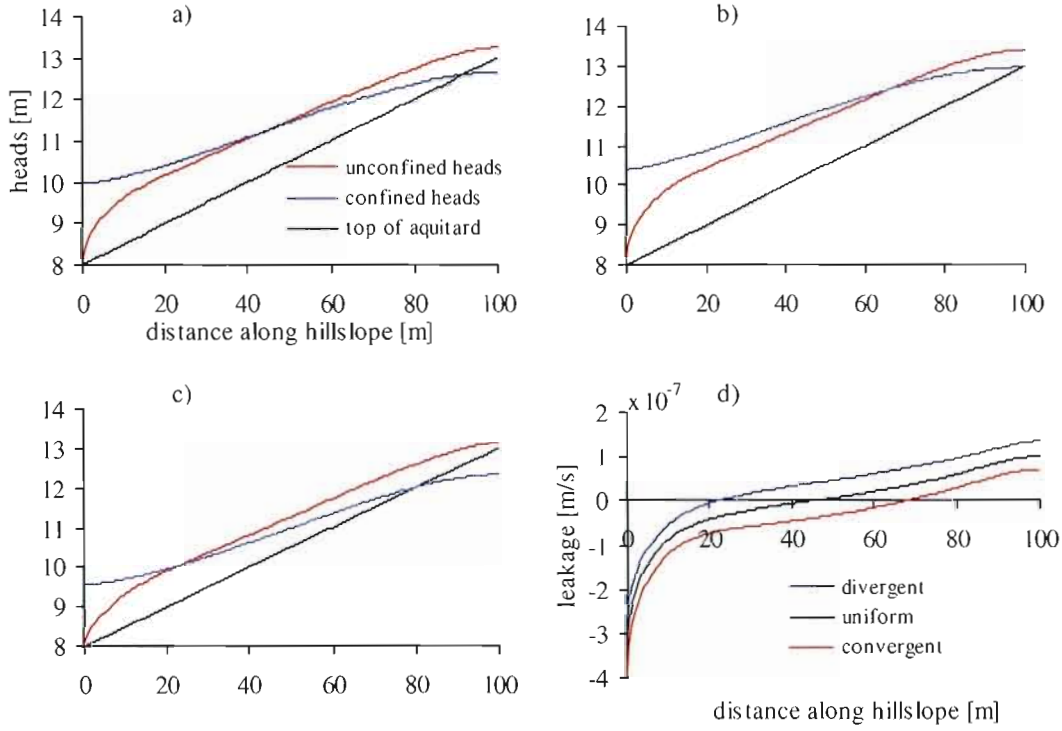

Figure 3.7 Heads in the unconfined and confined aquifers, with the elevation of the top of the aquitard as a reference for the uniform (a), convergent (b), and divergent (c) hillslopes. Leakage rates along the hillslope (d) for the uniform, convergent, and divergent hillslopes at $t = 10$ d.

3.3.2.3 Hillslope length (Case 6)

We examine in this test case the effect of hillslope length on leakage. This is particularly important if hillslope models are to be used as building blocks for larger scale hydrological models. For this test the hillslope length was extended to 1 km and the simulation time to 1000 d. The leakage and water table results presented in Figure 3.8 show more dramatically some of the trends observed for the base case. Upslope leakage is initially

very high but drops quickly as groundwater flow travels in the unconfined aquifer. Pressure heads build up downslope of the drainage front while a relatively steady midslope region is observed. Reverse leakage occurs downslope and varies more gradually than in the upslope region. Leakage magnitudes are approximately an order of magnitude smaller than those of the base case.

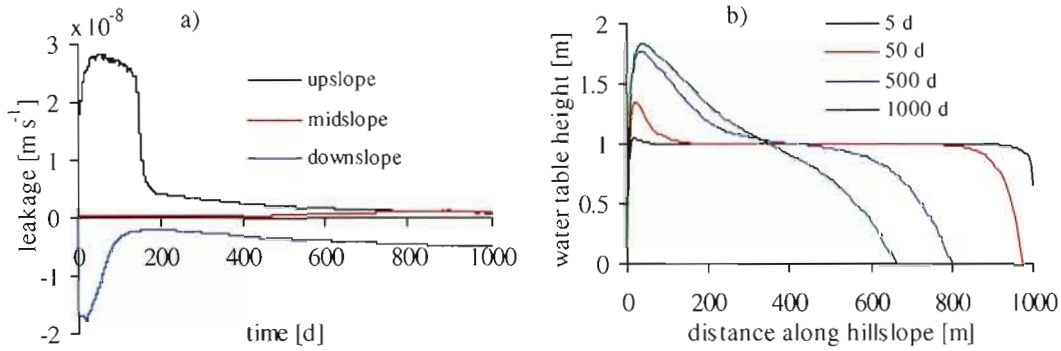

Figure 3.8 Results for a 1 km hillslope: (a) leakage rates at the upslope, midslope, and downslope points; (b) unconfined aquifer storage profiles at different times; the initial water table position is at 1 m height.

3.3.3 Boundary conditions

Boundary conditions (BCs) can exert a high degree of control on the dynamics of a groundwater system (e.g., *Franke and Reilly, 1987*; *Oliver and Christakos, 1996*). The BCs imposed at the outflow face of a hillslope model can be of different types, and the type and configuration imposed will strongly influence leakage processes, outflow rates, and pressure head distributions. The most common outflow face BC types are prescribed pressure head (Dirichlet condition) and seepage face. The configuration includes selecting the extent of the outflow face that is to be designated as a Dirichlet or seepage face BC, i.e., to what depth below the land surface or along which portion of the face will the BC be attributed. The extent of the Dirichlet or seepage face boundary is an especially important parameter in layered sloping aquifer systems, as will be evident from the results described below.

In the following two sections, note that in the finite element numerical model, unless explicitly assigned, all boundary nodes of the discretized hillslope (and thus also the outflow face) are by default treated as no-flow boundaries.

3.3.3.1 Dirichlet BCs (Case 7)

Five different prescriptions of Dirichlet boundary condition along the outflow face were investigated, beginning with the base case configuration, where atmospheric pressure head (ψ=0) is applied at the 7 nodes along the aquitard/unconfined aquifer interface (i.e., at a depth of 2 m below the surface of the hillslope). This Dirichlet strip is then successively extended to a depth of 2.4, 2.6, 3.4, and 10 m. At 2.4 m the Dirichlet face extends partly into the aquitard, at 2.6 m the entire aquitard outflow face is a Dirichlet BC, at 3.4 m the BC extends partly into the confined aquifer, and at 10 m the Dirichlet BC is assigned to the entire aquitard and confined aquifer outflow face. In all cases the Dirichlet BC face is in vertical hydrostatic equilibrium, with a prescribed head of ψ=0 at 2 m depth, thus mimicking the presence of an open body of water in contact with the sloping aquifer, with the depth of water corresponding to the extension of the Dirichlet BC face.

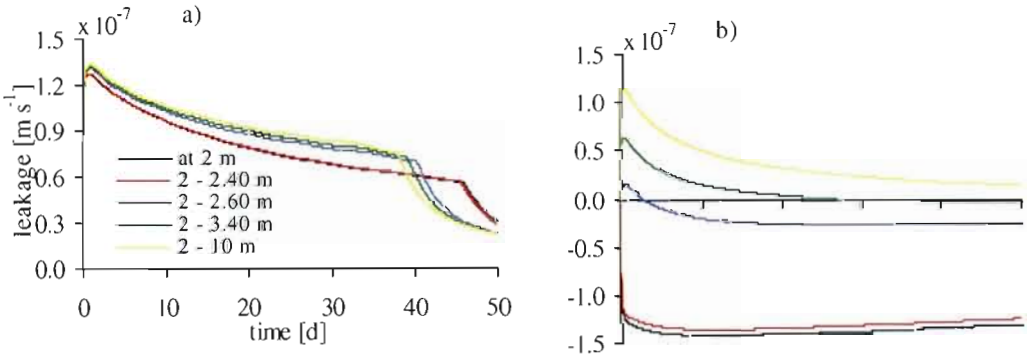

Figure 3.9 Leakage rates at the upslope (a) and downslope (b) points for five different prescriptions of Dirichlet boundary condition along the outflow face.

Figure 3.9 shows that as the Dirichlet BC face extends further into the aquitard, downslope leakage becomes smaller. When the Dirichlet BC comprises the entire aquitard outlet, the leakage is even positive for a brief period early in the simulation. This decrease in upward leakage is expected since water is no longer forced to drain towards a single strip of nodes

along the aquitard/unconfined aquifer interface. As the Dirichlet face extends into the confined aquifer as well, leakage becomes predominantly and eventually entirely positive. At play here, in combination with the extended Dirichlet face, is the impediment to vertical flow posed by the aquitard. In terms of upslope behavior, Figure 3.9 shows that as the Dirichlet face extends deeper into the aquifer system, the leakage rates remain generally higher and desaturation occurs earlier.

In Figure 3.10 outflow rates and water table profiles are shown for three of the five Dirichlet BC cases. As expected, the largest outflows (Figure 3.10a) are obtained for the longest outflow face. This is also seen in the calculated storage profiles (Figure 3.10b), where the lowest water tables are obtained when the Dirichlet BC extends along the entire aquitard and confined aquifer outflow faces. This in turn results in higher downward leakage. A strong impact on the resulting flow response was also reported by *Franke and Reilly (1987)*, who concluded that BC selection can define a particular groundwater flow system. The influence of the extent of the Dirichlet face is supported by *Oliver and Christakos (1996)*, who reported that knowing the exact location of the boundaries is generally indispensable, as uncertainties in model results related to boundary location can become even more dominant than those imparted by imperfect knowledge of hydraulic conductivity. In a more recent study, *Harman and Sivapalan (2009a)* found that the importance of BC effects also depends on the saturated thickness of the hillslope flow system.

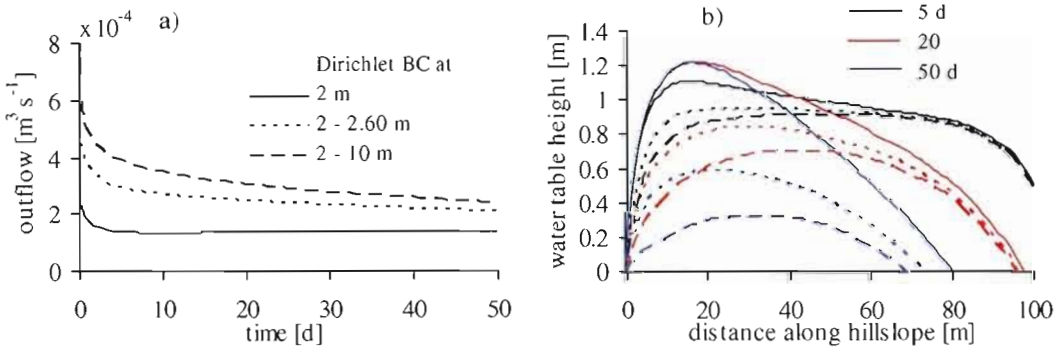

Figure 3.10 Outflow (a) and unconfined aquifer storage profiles at different times (b) for three different prescriptions of Dirichlet boundary condition along the outflow face.

3.3.3.2 Seepage face BCs (Case 8)

Three seepage face BC configurations were used: along the entire unconfined aquifer outflow face, along the entire unconfined aquifer and aquitard outflow faces, and along the entire outflow face, comprising both aquifers and the aquitard. Leakage behavior at the downslope point (Figure 3.11a) is similar to what was observed in the Dirichlet BC experiments: negative leakage diminishes and eventually reverses as the extent of the seepage face reaches further downward. This is also seen in the spatial distribution of leakage at t=10 d plotted in Figure 3.11b. As before, leakage at the upslope end is less affected by the extent of the outflow boundary condition.

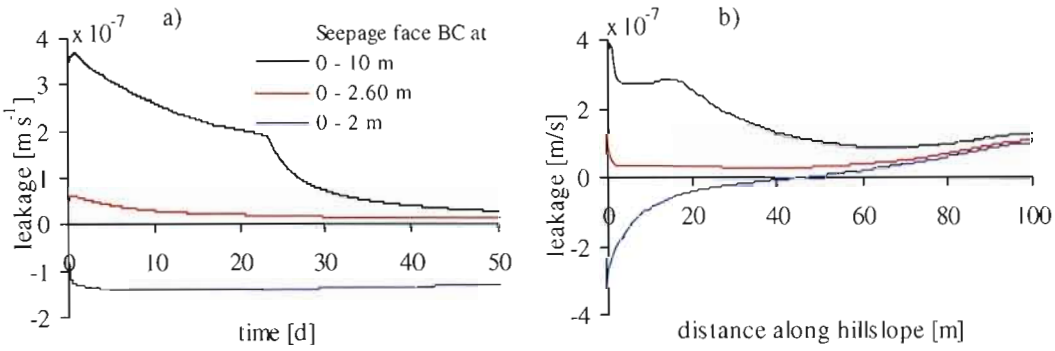

Figure 3.11 Leakage rates against (a) time (at the downslope point) and (b) distance (at t = 10 d) for three different prescriptions of seepage face boundary condition along the outflow face.

In Figure 3.12 the behavior of the exit point is examined for the three seepage face BC configurations. The exit point along a seepage face is where the water table intersects the outflow face: above the exit point all nodes are no-flow BCs and below it all nodes are prescribed head BCs. The position of the exit point is updated at each time step in the numerical model using an iterative procedure. As can be seen in the figure, there are some numerical oscillations in the updating procedure, but overall the exit point gradually drops as drainage proceeds. After 100 d the exit point has not yet reached the bottom of the unconfined aquifer (at z=8 m) for the two cases where the seepage face extends along the entire unconfined aquifer and along the entire unconfined aquifer plus aquitard, whereas it

has already dropped below the bottom of the unconfined aquifer for the case where the entire outflow face is treated as a seepage face BC. For all three cases, the very gradual drop of the exit point (and hence of the water table near the outlet) indicates that the near-outlet dynamics of a sloping aquifer are quite different from the Dirichlet BC case, where instead the imposition of a prescribed head at the base of the unconfined aquifer causes an immediate (and discontinuous) jump in near-outlet water table height from its initial position to zero.

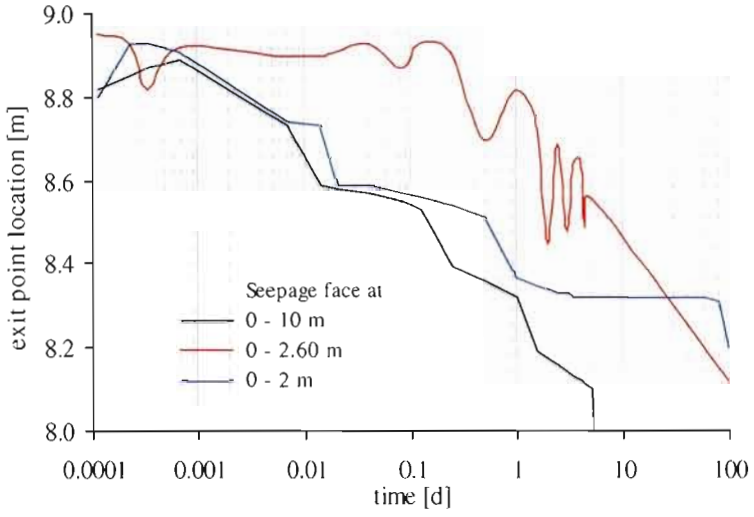

Figure 3.12 Behavior of the exit point for the three different seepage face boundary conditions.

3.3.3.3 Recharge (Case 10)

In this test case a constant recharge of 5 mm/d was applied as a surface boundary condition in two 10-d intervals, at the start of the 50-d simulation and again between days 20 and 30. In Figure 3.13 the resulting upslope and downslope leakage rates can be compared for three uniform hillslopes (0.2, 5, and 30% slope angles) and between the recharge and drainage-only (test case 4) simulations. As hillslope inclination decreases the impact of recharge on leakage increases. This is due to more important vertical flow in gently sloping aquifers as compared to more lateral flow along the aquitard/unconfined aquifer interface for steeper hillslopes. However, in terms of magnitude, downslope leakage and early-time

upslope leakage remain largest for the steepest hillslopes, as was the case for the drainage-only simulations, owing to the strong contributions of pressure head buildup and confined aquifer flow. Lag periods at the start and end of recharge events are also discernible in Figure 3.13, especially for the gentler slopes. These can be attributed to unsaturated zone transmission times. The increase in leakage associated with recharge is consistent with increased storage in the upper aquifer reported by *Harman and Sivapalan (2009b)* for a heterogeneous hillslope subjected to periodic recharge episodes. Finally, it can be seen how recharge events delay desaturation at the upslope point in steep (30%) hillslopes and prevent desaturation in hillslopes of moderate (5%) inclination.

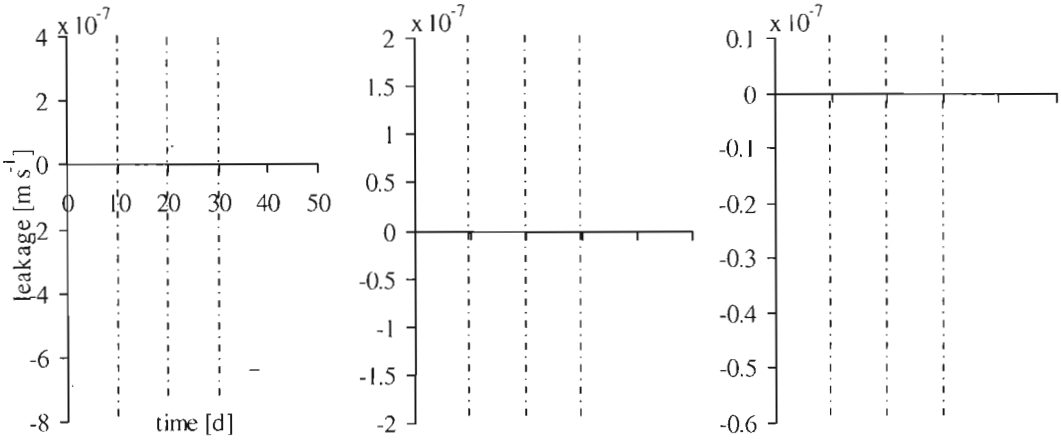

Figure 3.14 Influence of recharge on leakage rates at the upslope point (positive values) and downslope point (negative values) for slope angles of 30% (left), 5% (middle), and 0.2% (right). A recharge of 5 mm/d is applied during the first 10 d and between days 20 and 30. The lines in red show the drainage-only results presented in Figure 3.6.

3.3.4 Dimensional analysis

In order to generalize some of the results presented in the previous sections, a dimensional analysis was conducted based on the dimensionless kinematic time τ [-] and the dimensionless outflow ϕ [-] parameters used by Hilberts et al. (2004) as adapted from Ogden and Watts (2000):

$$\tau = \frac{tK_s\alpha}{fL} \quad ; \quad \phi = \frac{Q_{cum}(t)}{V_i} \tag{3.5}$$

where V_i [L^3] is the initial volume of water stored in the hillslope and $Q_{cum}(t)$ [L^3] is the cumulative flow volume at the outflow face up to time t:

$$Q_{cum}(t) = \int_0^t Q(t)dt \tag{3.6}$$

The flow variable ϕ represents the fraction of the total initial soil water storage that has drained from the hillslope up to kinematic time τ. Based on these relationships, a hillslope will drain most rapidly with large soil conductivities and hillslope inclinations or small drainable porosities and hillslope lengths.

The results of the analysis are shown in Figure 3.14 for varying hillslope inclination (5% and 30%), planform geometry, and aquitard conductivity. At the lowest aquitard conductivity (K_s'=10^{-12} m s^{-1}), the results essentially collapse onto a single profile, in line with the results reported by Hilberts et al. (2004) for unconfined aquifers on a sloping impermeable bed (the much lower ϕ values, or fraction of total stored water that drains, for the results in Figure 3.14 compared to Hilberts et al. (2004) are due to the extra storage provided by the confined aquifer in our setup, which contributes little to drainage when the aquitard has a very low permeability). The deviations from ideal behavior in terms of the dimensionless variables defined in equation (3.5) augment as K_s' increases, and these deviations are greatest for the steepest hillslope and for the convergent hillslope. In Hilberts et al. (2004), slight deviations for steeper slopes and more convergent planforms are attributed to the different balance between convection- and diffusion-driven flow between a Richards equation model and a Boussinesq equation model (or even a kinematic wave model, for which the relationships in equation (3.5) are ideally applicable) and to unsaturated or capillary effects that are absent in the latter two models compared to a Richards model. In addition to these effects, the absence of a leakage factor in expressions (3.5) also has a clear impact in the higher deviations observed here as K_s' increases.

Notwithstanding these "nonideal" conditions, Figure 3.14 clearly shows, as K_s' increases, the increasing availability for drainage of initially stored water in the confined aquifer unit, especially for the steepest hillslope. For this hillslope, only 16% of total initial storage is drained when $K_s'=10^{-12}$ m s^{-1}, whereas about 75% gets drained when interaction (leakage) between the unconfined and confined aquifers is augmented.

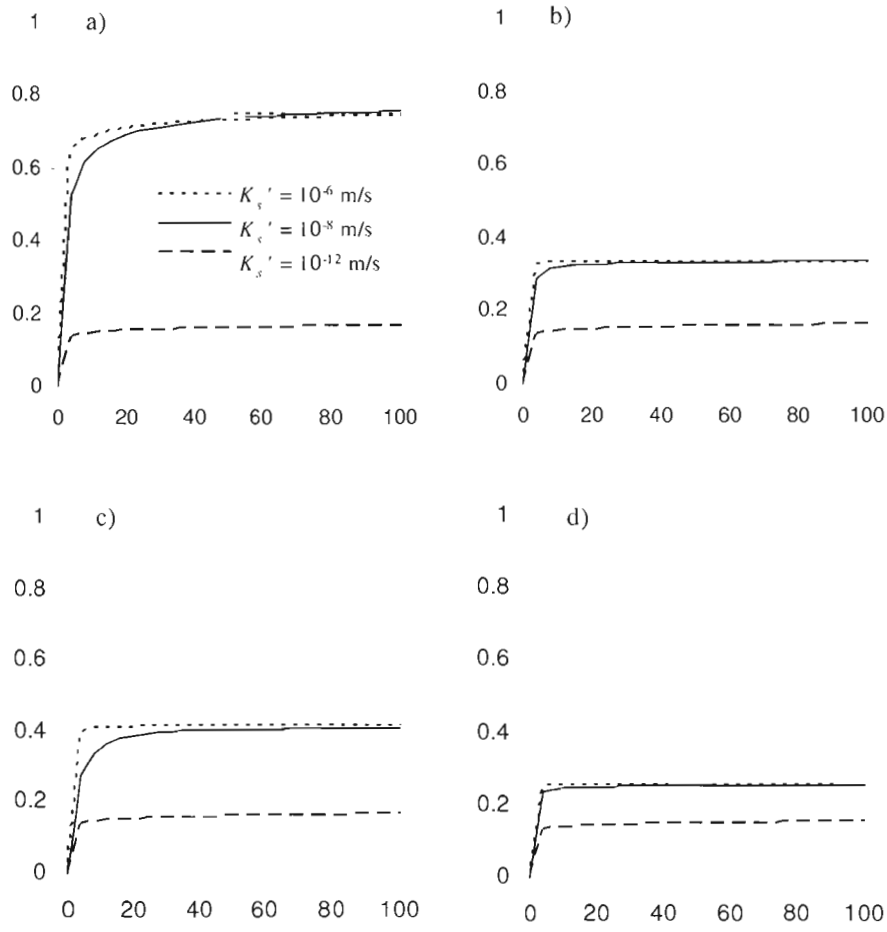

Figure 3.14 Influence of aquitard conductivity on the dimensionless hydrograph for a uniform hillslope of a) 30% and b) 5% inclination and for hillslopes of 5% inclination with c) convergent and d) divergent planform geometries.

In terms of the influence of hillslope geometry on the flow response under varying aquitard conductivities, Figures 3.14c and 3.14d show a higher drained fraction for the convergent hillslope compared to the divergent hillslope for the leaky cases ($K_s'=10^{-8}$ and $K_s'=10^{-6}$ m s^{-1}).

This might appear counterintuitive, and serves again to bring to light important differences in dynamics between single-layered and multi-layered aquifer systems. On analysis of the early time drainage behavior, it is seen that drainage is faster and greater in the divergent hillslope (as would be expected for a single unconfined aquifer). After τ=0.55, the convergent slope overtakes slightly the divergent one. The much larger fraction of initial storage contained in the upslope portion of the layered aquifer system for a convergent planform is responsible for this effect.

3.4 Conclusions

Incorporating leakage as a coupling term between a hillslope model and a groundwater flow model can be performed numerically, but the process itself is very difficult to observe and characterize in field studies. In this work, the driving forces influencing leakage in a hillslope hydrological context have been explored, including hydraulic properties, geometry, and boundary conditions. In addition to the expected high impact of aquifer and aquitard properties, slope angle and geometry are shown to exert strong controls on leakage processes. The results show how leakage can be positive or negative at different points along the hillslope and at different times during a drainage or recharge event, with upward (negative) leakage predominantly observed at the downslope portion of a hillslope. Geometry and boundary conditions at the outflow face were also shown to drive the partitioning of the hillslope into up- and downwelling leakage areas, with convergent hillslopes containing the largest portions of upward directed leakage. An important finding from this study is that the effect of leakage should not be neglected in steep slopes where reverse leakage volumes can contribute significantly to a hillslope's total outfow.

The results have generally demonstrated the significant volume of leakage within a hillslope relative to the overall water budget, even for a larger scale aquifer system (1 km hillslope). This supports findings from previous studies where leakage was considered a key process in understanding hillslope hydrology, and it challenges the adequacy of the commonly applied assumption of zero flux across the hillslope bottom. The contribution of the confined aquifer

to hillslope outflow was also shown to be significant, depending on how the boundary condition at the outflow face is treated numerically.

Further exploration of leakage processes at larger scales is needed and could be undertaken through modeling (including intercomparison studies) and field work (e.g., tracer experiments). Some of the important parameters examined in the test cases reported here are not easily estimated in the field. Aquifer stratigraphy, aquifer and aquitard hydraulic conductivities, and boundary conditions at the stream–aquifer interface are especially difficult to quantify. Continuing research on aquifer characterization is therefore also needed. A better understanding of the processes involved in the interconnections between soil and bedrock units, along with more representative models to simulate these processes, will also have implications on, for instance, hillslope stability and contaminant transport studies.

Preface to Chapter IV

In the following chapter, the findings of chapter III are transferred to a leakage-based coupling framework combining the hsB model and an analytic element-based groundwater flow model. The goal of this study is to demonstrate the coupled model's capability to reproduce water tables, outflows, and leakage rates obtained with a benchmark model. Tests are conducted on hypothetical single hillslopes and on a synthetic catchment. This chapter is based on the paper "Broda, S., Larocque, M., Paniconi, C., (2010). A low-dimensional hillslope-based catchment model for layered groundwater flow. *Journal of Hydrology*, to be submitted in December 2010."

CHAPTER IV

A LOW-DIMENSIONAL HILLSLOPE-BASED CATCHMENT MODEL FOR LAYERED GROUNDWATER FLOW

Abstract Despite the strong interaction of surface and subsurface waters, groundwater flow representation is often oversimplified in hydrological models. The challenge in coupling surface water and groundwater flow lies in the development of computationally efficient yet accurate models. In this work, a novel hillslope-based catchment model representing layered groundwater flow is presented and compared to results of a three-dimensional finite element Richards equation model. The proposed model consists of the hillslope-storage Boussinesq model (hsB), representing rapid shallow groundwater flow, and an analytic element-based model (AE), representing deep regional groundwater flow. The two models are iteratively coupled via a leakage term based on Darcy's law. A series of tests on single hillslopes and a synthetic two-hillslope (open-book) catchment is presented. The impact of soil parameterization (three different hydraulic conductivities), hillslope planform geometry (uniform, convergent, divergent), as well as hillslope inclination (0.2%, 5%, and 30%) under drainage and recharge events is examined by means of calculated heads, hydrographs, and exchange fluxes between the hsB and AE models. On the single hillslopes, good matches are obtained for most configurations, with the most significant differences in outflows and heads observed for the 30% slope and for hillslopes with convergent geometry. Cumulative flow volumes for the two-hillslope catchment are overestimated by approximately 1-4%. Heads in the confined and unconfined aquifers are adequately reproduced for both portions of the catchment. Response to recharge events is largely dependant on the drainable porosity parameter used in the hillslope model.

4.1. Introduction

The availability and quality of water resources can be compromised, sometimes irreversibly, by natural and anthropogenic factors including land use and climate changes. A better understanding of the interactions between surface and subsurface components of the hydrological cycle is needed to improve the reliability of simulation models and ensure sustainable water resources management. Although strong interactions between surface and subsurface waters are generally acknowledged, resource management has traditionally focused on surface water, soil water and groundwater as separate entities (Sophocleous, 2002; Winter *et al.*, 1998), and operational hydrological models often lack a complete representation of the hydrologic cycle.

Low flow periods are critical in operational watershed management from both ecological and socio-economic perspectives. During these periods, shallow (e.g., Arnold *et al.* 2000; Arnold and Allen, 1996) and deep (e.g., Le Maître and Colvin, 2008; Nastev *et al.*, 2005) groundwater flow can contribute significantly to streamflow. Among the ecological effects of low flow reduction are increased sedimentation and consequent alterations in stream morphology (Thompson, 2006), changes in the distribution and abundance of stream biota (Bradford and Heinonen, 2008; Dewson *et al.*, 2007; Brunke and Gonser, 1997), and increased stream water temperature caused by winds, bank storage, spring seepage and solar radiation (Smakhtin, 2001). Socio-economically, low flow reduction can adversely impact hydropower generation (Maurer *et al.*, 2009; Eckardt and Ulbrich, 2003). Global warming is expected to limit groundwater availability in the low and medium latitudes (Herrera *et al.*, 2008; Chen *et al.*, 2004; Eckhardt and Ulbrich, 2003), leading to baseflow reductions (Scibek and Allen, 2006; Yusoff *et al.*, 2002) and adversely impact groundwater quality (Bloomfield *et al.*, 2006). The development of appropriate tools for mapping recharge patterns and predicting low flow events is therefore crucial for designing sustainable water management strategies.

Various approaches for coupling groundwater models with surface flow models exist. These can be grouped into four categories: 1) fully-coupled, distributed surface water and groundwater models, e.g., HydroGeoSphere (Therrien *et al.*, 2005) and CATHY (Camporese

et al., 2010); 2) loosely coupled groundwater and surface water models, e.g., SWAT/MODFLOW (Sophocleous and Perkins, 2000); 3) extensions of existing surface water or land use models to include some representation of groundwater flow, e.g., ANSWERS (Bouraoui *et al.*, 1997); and 4) extensions of existing groundwater models to include some representation of surface water flow, e.g., MODFLOW/WhaT (Thoms and Johnson, 2005). Although fully-coupled models represent the entire water cycle, they are generally not applicable for water management purposes at large river basin scales due to intense parameter and computational requirements. Models in the other categories simplify and/or neglect compartments of the hydrological cycle, including the interactions between surface water and groundwater bodies. These models are thus inadequate when reliable assessments of climate change impacts on recharge dynamics and low flow regimes are of interest. There is a need for parsimonious, physically-based models that can accurately reproduce catchment scale hydrological processes including the interactions between surface flow, soil water, and groundwaters.

The objective of this work was to develop a new and computationally efficient hillslope-based model for shallow subsurface and deep groundwater flow. This model has the potential to be used in many surface flow models to improve the representation of aquifer flow, without the computational burden of fully-coupled models.

In recent scientifc literature, there is an increasing recognition of hillslopes as fundamental building blocks in watershed hydrology (e.g., Matonse and Kroll, 2009). This makes a hillslope-based computational unit appealing for incorporation into larger scale river basin models (Yang *et al.*, 2002). The interactions between shallow aquifers and deep aquifers were found to be important in several hillslope scale studies (Hopp and McDonnell, 2009; Tromp-van Meerveld and Weiler, 2008; Cloke *et al.* 2003) to understand long-term subsurface flow response. Hillslope processes are commonly simulated by means of the Boussinesq equation (e.g., Brutsaert, 1994), applicable to single layer flow systems representing a sloping unconfined aquifer on an impermeable base.

Models based on the analytic element (AE) method are tailored for simulating local problems within regional scale aquifers (Haitjema, 2005; Strack, 1989). These models are simple,

parameter sparse and computationally efficient. However, they are limited to single horizontal aquifers under steady state conditions.

In this work the hillslope-storage Boussinesq (hsB) model for transient shallow subsurface flow and the AE GFLOW model for steady-state deep regional groundwater flow are coupled via a leakage term that acts across a hypothetical aquitard. Tests are conducted on single hillslopes of varying inclination and planform geometry and on a synthetic watershed. Outflows, heads, and exchange fluxes between the subsurface aquifer and the deep aquifer are compared to the results from a fully-coupled three-dimensional (3D) Richards equation-based benchmark model.

4.2. Model description

The conceptual representation of the system under study includes an unconfined hillslope aquifer which carries groundwater flow towards a river or stream located downgradient. Underlying this unconfined aquifer is a deep regional-scale aquifer. The hillslope aquifer feeds the deep regional-scale aquifer with leakage through a resistance layer that forms the lower boundary of the hillslope. Both aquifers are connected at the downgradient stream. The hillslope aquifer is represented with the hsB model while the deep aquifer is represented with the AE model.

The hillslope-storage Boussinesq model was introduced by Troch *et al.* (2003). It provides a low-dimensional, computationally efficient representation of shallow groundwater flow in hillslopes of arbitrary geometry (Paniconi *et al.*, 2003). Hilberts *et al.* (2004) generalized the model formulation to handle non-constant bedrock slopes, while Hilberts *et al.* (2005) incorporated a storage-dependent drainable porosity to partially account for unsaturated zone effects. Broda *et al.* (2008) relaxed the no-flow condition at the bottom of the hillslope to incorporate a leakage term, allowing bi-directional vertical exchanges through a hypothetical aquitard. The hsB version from Troch *et al.* (2003) with the incorporated leakage term is used in this paper. Subsurface flow in hsB is described as follows:

$$f\frac{\partial S}{\partial t} = \frac{K\cos\alpha}{f}\frac{\partial}{\partial x}\left[\frac{S}{w}\left(\frac{\partial S}{\partial x} - \frac{S}{w}\frac{\partial w}{\partial x}\right)\right] + K\sin\alpha\frac{\partial S}{\partial x} + fNw - fLw \qquad (4.1)$$

where $S = S(x,t) = wf\bar{h}$ is the subsurface water storage [L^2], $\bar{h} = \bar{h}(x,t)$ [L] is the water table height averaged over the width of the hillslope, $w(x)$ [L] is the hillslope width function, f [-] is the drainable porosity, t [T] is the time, K [LT^{-1}] is the hydraulic conductivity, N [LT^{-1}] is the recharge, x [L] is the distance to the outlet along the hillslope, α [rad] is the angle that the sloping aquifer bottom makes with the horizontal, and L [LT^{-1}] is the leakage flux.

Heads in the deep regional-scale aquifer located below the hillslope are required to calculate the leakage flux. The leakage is calculated based on Darcy's law and uses the concept of flow through a resistance layer:

$$L = -K_s'\frac{h_2 - h_1}{b} = C(h_2 - h_1) \qquad (4.2)$$

where b [L] is the thickness of the aquitard, h_2 and h_1 [L] are the heads in the hillslope aquifer and the deep aquifer, and $C = Ks'/b$ [T^{-1}] is the conductance (Delleur, 1999) or specific leakage (Hantush and Jacob, 1955).

By applying this leakage, the no-flow boundary at the bottom of the hsB model is replaced by a Cauchy boundary. Conceptually, this layer can be seen as an aquitard limiting vertical flow towards the deeper aquifer. In the hsB/AE model, the aquitard thickness b is not incorporated as an aquitard per se, therefore storage properties in this unit are not considered.

The deep groundwater flow model which receives this leakage is the GFLOW analytic element model (Haitjema, 1995). This AE model simulates steady state flow in a single heterogeneous aquifer using the Dupuit-Forchheimer approximations (2D horizontal flow model). The analytic element method is useful in describing regional scale groundwater flow with local refinements (Strack, 1989; De Lange, 1996; Hunt, 2006; Kraemer, 2007). The method generates a continuous groundwater flow field by the superposition of closed-form analytical functions (analytic elements) which describe each feature individually to obtain a

full description of the area of interest. For example, wells are represented by Thiem's equation, which is the solution for a point sink in the horizontal plane. Streams and lake boundaries are represented by strings of line-sinks which are point sinks integrated along a line element. These line-sinks extract (or infiltrate) the water that enters or leaves the stream or lake, respectively. Zones of differing aquifer properties are modeled with polygons of line-doublets or double layers. Reference is made to Haitjema (1995) or Strack (1989) for further reading on this topic.

The AE model can receive different areal recharge rates in different zones. These "recharges" zones are used to assign the leakages from the hsB model to the underlying AE model, thus connecting the two models. Since the AE model is a steady state model, the actual transient flow system can only be represented as a series of instantaneous steady state solutions for the instantaneous leakage rates (recharge rates in the AE model) in the coupled hsB/AE model. The use of successive steady state solutions to represent transient flow is acceptable if the AE model (lower aquifer) responds relatively fast to transient forcing. For the cases presented in this thesis this is generally the case as long as the lower aquifer remains everywhere confined. The low storage coefficient for confined flow ensures a relatively rapid response of the lower aquifer to temporal changes in recharge.

The two models are coupled in a "pseudo transient state". Coupling of the hsB and AE models is based on the selection of a common time step Δt_c (the coupling time step). During this period the following steps are performed: 1) hsB is run in transient state to calculate heads and outflows, 2) the AE model is run in steady-state using initial heads, 3) leakage is calculated for this common time step using the steady-state heads from the AE model and the hsB heads at the end of t_c. This procedure is repeated until head variations between two iterations in the AE model are smaller than a pre-selected convergence criterion. A flow chart of the iteration scheme is depicted in Figure 4.1.

Outflows, leakages, and heads from the hsB/AE model are compared to those of the CATHY model (CATchment HYdrology), a three-dimensional finite element subsurface flow model (Paniconi and Putti, 1994; Camporese *et al.*, 2010) which is used as a benchmark in this study. This model solves the three-dimensional Richards equation:

$$\eta(\psi)\frac{\partial \psi}{\partial t} = \nabla \cdot (K_s K_r(\psi)(\nabla \psi + e_z)) \tag{4.3}$$

where $\eta = S_w S_s + \theta_s (dS_w / d\psi)$ [L^{-1}] is the general storage term, S_w [-] is the water saturation, S_s [L^{-1}] is the aquifer specific storage coefficient, ψ [L] is the pressure head, e_z [-] is the vector $(0,0,1)^T$, K_s [LT^{-1}] is the saturated hydraulic conductivity, and $K_r(\psi)$ [-] is the relative hydraulic conductivity. In this study, the Brooks and Corey (1964) relationships were used for the saturation–pressure and conductivity–pressure relationships:

$$\begin{aligned} S_e(\psi) &= (\psi_c / \psi)^{\beta}, && \psi < \psi_c \\ S_e(\psi) &= 1, && \psi \geq \psi_c \end{aligned} \tag{4.4}$$

$$\begin{aligned} K_r(\psi) &= (\psi_c / \psi)^{2+3\beta}, && \psi < \psi_c \\ K_r(\psi) &= 1, && \psi \geq \psi_c \end{aligned} \tag{4.5}$$

where the effective saturation S_e [-] is defined as $S_e = (\theta - \theta_r)/(\theta_s - \theta_r) = (S_w \theta_s - \theta_r)/(\theta_s - \theta_r)$ and where θ [-], θ_r [-], and θ_s [-] are the volumetric, residual and saturated moisture contents, respectively. β [-] is a constant representing the pore size distribution index and ψ_c [L] is the capillary fringe height.

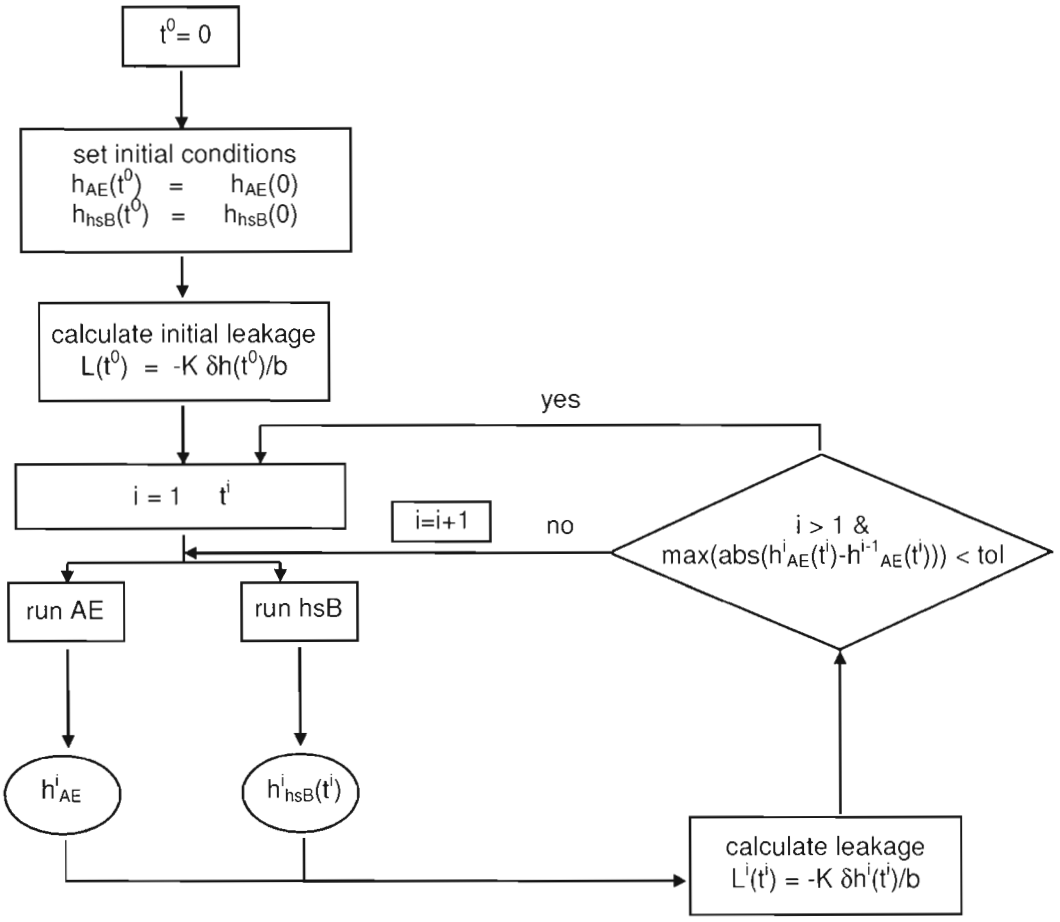

Figure 4.1 Flow chart of the coupling process between the hsB and AE models.

4.3. Experimental designs

4.3.1 Single hillslopes

The hsB/AE model is first tested on a set of single hillslopes with varying geometry, base inclination, and soil properties. Three planform geometries (uniform, convergent, divergent) and three hillslope inclinations (α=0.2%, 5%, and 30%) are used. The basic configuration for this setup is shown in Figure 4.2a. The hillslope aquifer has a thickness of 2 m while the GFLOW aquifer is 8 m thick. The hillslope length is 100 m for both units, with a $\Delta x = 0.5$ m. The hillslope width ranges from 50 m to 6.74 m, with the maximum width at

the outlet for the divergent slope and at the crest for the convergent slope (Figures 4.2d and 4.2e). While the hillslope aquifer can be sloping in hsB, the deep aquifer is constrained to be horizontal in the AE model. This has non consequence as long as the flow conditions in the lower aquifer remain confined. Our model setup for GFLOW is an infinite domain, in which regional and local ("nearfield") boundaries are defined and parameterized. Areal sinks (inhomogeneities) are used to model zones of different recharge (leakage) and hydraulic conductivity. In the surrounding infinite ("farfield") aquifer, a hydraulic conductivity orders of magnitude lower than the one applied within the inhomogeneities is used. The hillslope domain is therefore defined as a finite aquifer within an infinite domain.

Each tested hillslope experiment is represented in the benchmark model. The layered hillslope system has a total thickness of 10 m (Figure 4.2b) and is discretized with 20 layers. The surface is discretized into 101 nodes along the length of the hillslope (Δx = 1 m) by 7 nodes along the width of the hillslope (for the divergent hillslope Δy = 1.23 m at the crest and Δy = 8.33 m at the outlet). These 100 x 6 rectangular elements are subdivided diagonally to yield a surface grid of 1200 triangles. In vertical projection, each layer is discretized into 3600 tetrahedral elements, yielding a 3D grid with 72000 tetrahedral elements and 14847 nodes.

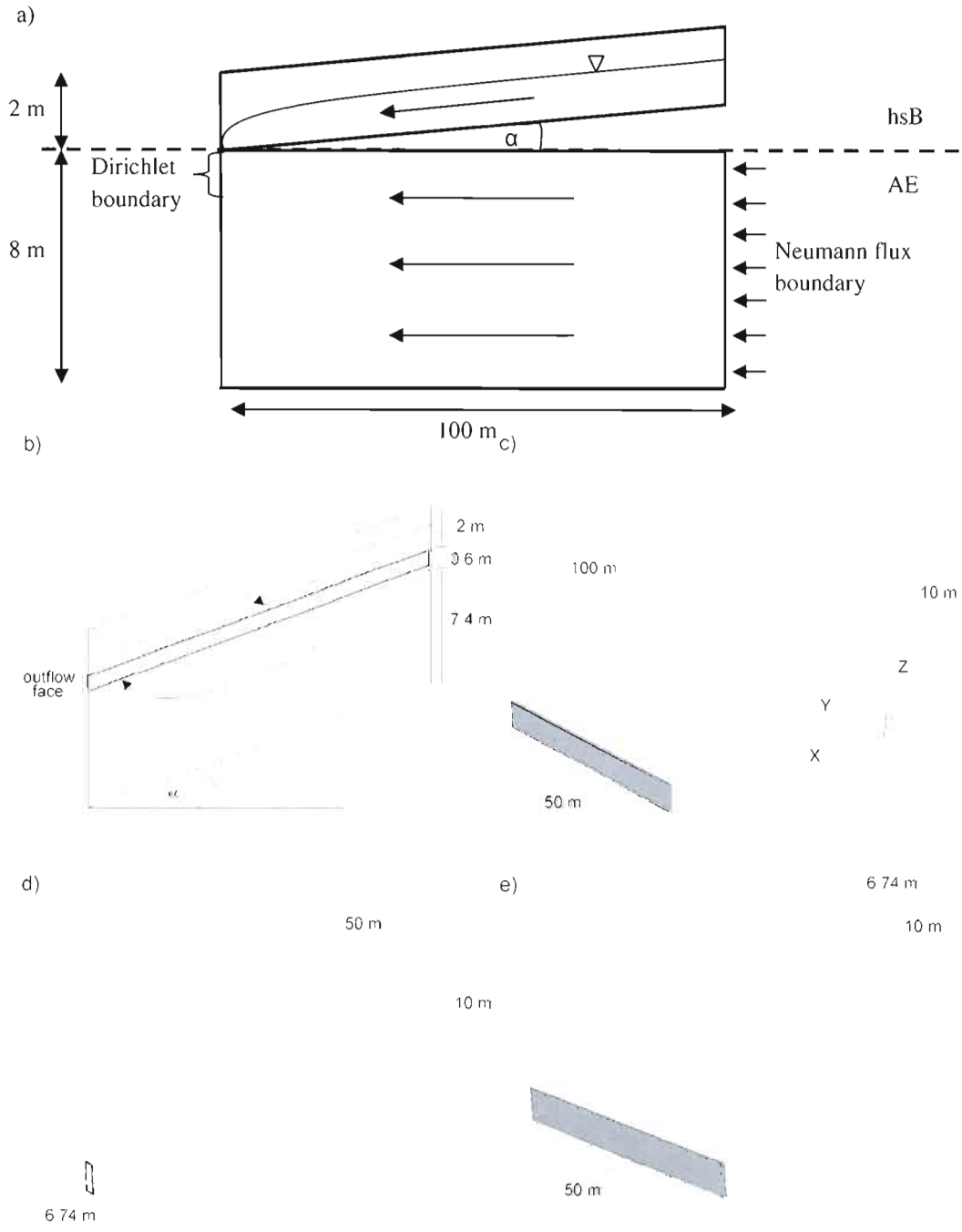

Figure 4.2 Vertical conceptualization of the single hillslope experiments (a) for the coupled hsB/AE model and (b) for the benchmark model; (c), (d) and (e) show the uniform, convergent, and divergent planform shapes, respectively.

The vertical extent of the CATHY model grid is set up to correspond to the conceptualization of the combined hsB/AE model. It is important to note that the aquitard layer is explicitly represented in the benchmark model. The total volume of the aquifer system in the benchmark model discretization is made equal to that in the hsB/AE model. Therefore the total thickness of the CATHY aquifer/aquitard system is kept constant along the hillslope, i.e., the base and the top of the modeled domain are parallel.

In both the hsB/AE and the benchmark models, the initial water table position in the hillslope aquifer is 1 m below the surface. This value was selected based on prelimiary tests in order to avoid occurrence of surface runoff, particularly in the 30% slope. In the deep aquifer, the initial hydraulic head distribution is vertically hydrostatic at a value of 8 m (the zero reference for the z coordinate is at the bottom of the confined aquifer). At the hillslope divide, a no-flow boundary is used in the hillslope aquifer and in the aquitard unit for the benchmark model. A Neumann flux boundary is used in the deep aquifer to represent groundwater flow from adjacent uphill hillslopes. This flux is equivalent to a groundwater flow gradient of 0.01% (fluxes are calculated using the experiment's aquifer conductivity and hillslope length).

The stream located downgradient in the hillslope is assumed to incise the aquitard unit for 0.6 m. To represent this, the water storage $S(x=0,t)$ for the hsB model is assigned a fixed value of zero (Dirichlet boundary condition) at the hillslope outlet. In the AE model, a head-specified line sink is placed at the outlet with a time-constant head set to 8 m. In the AE model, the Dupuit-Forchheimer assumption ignores resistance to vertical flow. A head of 8 m therefore represents a river cutting the entire deep aquifer, which would be unrealistic at the single hillslope scale. The AE model provides the possibility to account for the partial penetration of a shallow river by adding a resistance R [T] to the stream (Haitjema, 1995). Adding a resistance to the stream introduces two new parameters: the width W [L] and depth D [L] of the stream. The width is set to 0.5 m. The depth parameter refers to the distance between stream stage and the bottom of the stream resistance layer and is only relevant for losing streams. The depth is therefore set to 0.8 m, i.e. 0.6 m of stream depth + 0.2 m of a hypothetical resistance layer. Since the model setup prevents the occurrence of a losing stream, the only parameter which cannot be directly related to the benchmark model is the

resistance. This parameter is calibrated by means of the heads in the deep aquifer portion of the benchmark model. Since the stream penetration remains constant throughout the experiments, the resistance applies to the group of settings with the same aquifer conductivity; thus $R = 0.05$ d, 0.41 d, and 3 d for aquifer conductivities of 10^{-4}, 10^{-5} and 10^{-6} m s^{-1}.

In the benchmark model, the 0.6 m stream depth at the hillslope outlet is represented by means of a Dirichlet boundary applied from the bottom of the hillslope aquifer to the bottom of the aquitard (i.e., Dirichlet nodes at the outlet face from 2 m depth to 2.6 m depth, with a hydrostatic distribution of pressure heads from 0 m to 0.6 m). The AE model stream width of 0.5 m corresponds to half the distance between the Dirichlet node at the outflow face and its nearest neighbor node in the x-direction ($\Delta x/2$).

For the single-hillslope tests, a drainage scenario with zero infiltration in the hillslope aquifer and a recharge scenario with 5 mm/d of infiltration imposed on the hillslope aquifer are simulated for a 10-day period.

4.3.2 Open-book catchment

The hsB/AE model is also tested on a synthetic 1 km^2 "open-book" catchment consisting of two hillslopes of uniform planform geometries each 500 m long and 1000 m wide (Figure 4.3c). With this setup the coupled hsB/AE model will be applied for the first time on a multi-hillslope setup. Inclinations are set to 2.5 % and 5% and Δx to 1 m. The unconfined aquifer has a thickness of 2 m in both hillslopes and the deep aquifer has a thickness of 8 m (Figure 4.3a). As with the single hillslope experiments, the deep aquifer is horizontal with a hydraulic conductivity two orders of magnitude lower outside the inhomogeneities.

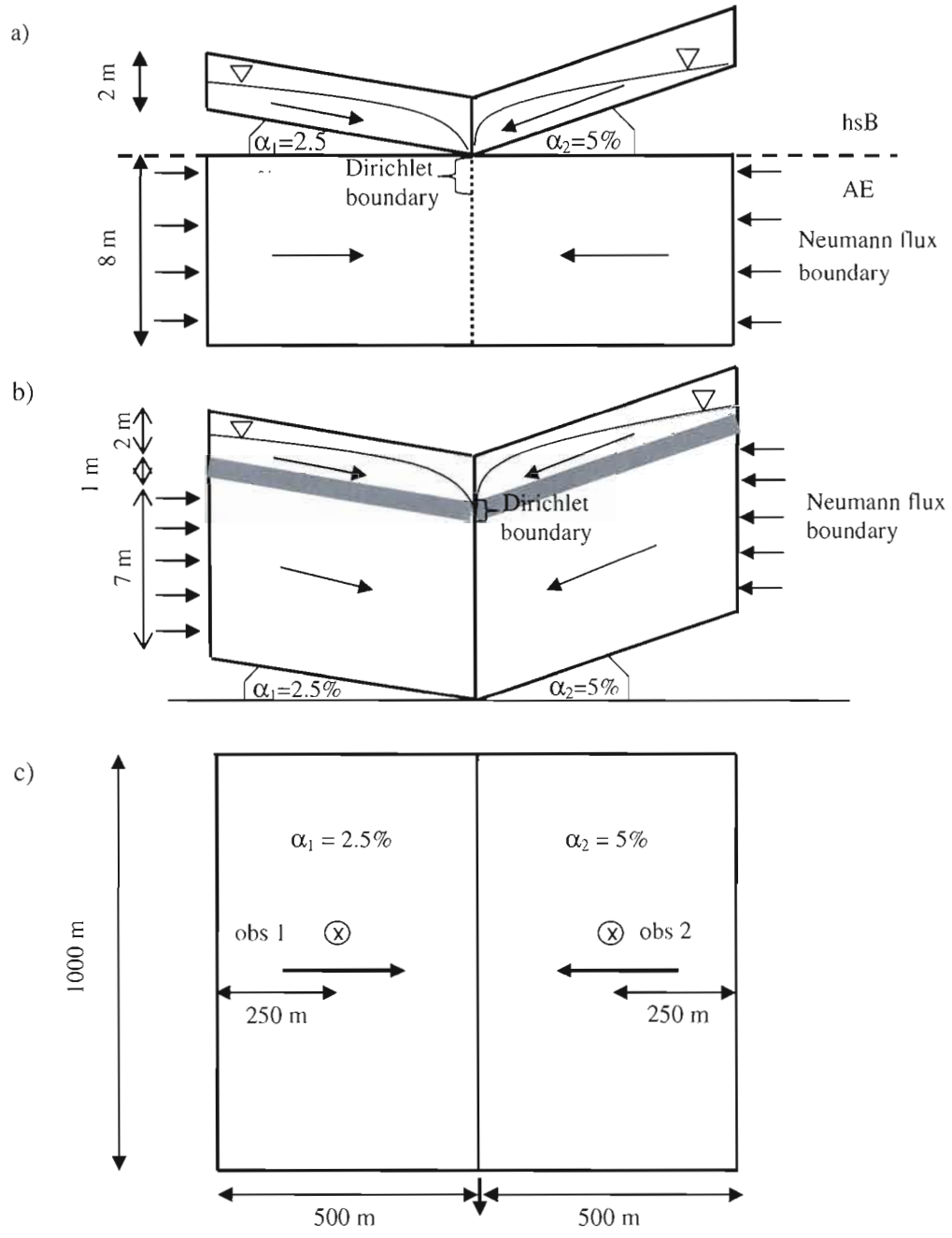

Figure 4.3 Representation of the open-book catchment: (a) vertical cross-section for the hsB/AE model, (b) vertical cross-section for the benchmark model, (c) plan view of the catchment; "obs1" and "obs2" are the observation wells; the black arrows reoresent the groundwater flow directions

The corresponding benchmark model has a total thickness of 10 m and is discretized into 40 layers. This catchment is represented by two standalone hillslopes in the benchmark model since each hillslope is an independent unit flowing into the stream channel. The subsurface flows computed at the Dirichlet outflow face for each of the two hillslopes are summed. For each hillslope, the surface is discretized into 1432 nodes with a varying Δx and Δy spacing between 100 m at the hillslope crests and 5 m at the stream boundary, producing an irregular numerical grid of 58712 nodes. As for the single hillslope experiments, the aquitard unit (of thickness $b = 1$ m in this case) is represented explicitely in the benchmark model (Figure 4.3b) while it is only conceptually included in the combined model (Figure 4.3a).

In contrast to the single hillslope experiments, the initial water table position in the hillslope aquifer however is 0.5 m below the surface, since prelimiary tests have indicated this value to be sufficient to avoinde the occurrence of surface runoff. In the deep aquifer, the initial hydraulic head distribution is vertically hydrostatic at a value of 8 m. At the hillslope divide, a no-flow boundary is used in the hillslope aquifer and in the aquitard unit for the benchmark model. As for the single hillslope experiments, Neumann flux boundaries at the upslope face of the deep aquifer provide a groundwater input corresponding to a flow gradient of 0.01%. For the virtual stream channel draining each hillslope, a Dirichlet boundary condition is applied from the bottom of the hillslope aquifer to the bottom of the aquitard (i.e., Dirichlet nodes ranging from 2 m to 3 m depth, with a hydrostatic distribution of pressure heads from 0 m to 1 m), thus incising the entire aquitard. In the combined hsB/AE model, all lateral divides of the hillslope aquifers are no-flow boundaries. At the downslope faces of the hsB hillslopes a zero storage condition (Dirichlet boundary condition) is applied. In the AE model, a head-specified line sink is positioned at the same elevation as the zero storage condition in the hsB hillslopes and set to 8 m. The width is set to 5 m (i.e., twice half the width of one element which runs along the stream boundary in the benchmark model), and the depth to 1.20 m (1 m stream depth + 0.2 m hypothetical resistance layer). The resistance R is calibrated for this setup to 4.2 d.

The simulations for the open-book catchment consist of a 10-day spin-up period of pure drainage followed by a 30-day simulation driven by three infiltration pulses of 25, 10, and

5 mm/d (from 10 to 11 d, 15 to 16 d, and 21 to 23 d, respectively) and zero infiltration for the remaining days.

4.3.3 Model parameters

On the single hillslopes, tests are conducted on aquifers with three different saturated conductivities K_s, ranging from 10^{-4} m s^{-1} (sandy loam) to 10^{-6} m s^{-1} (fine sand). The aquitard conductivities K_s' range between 10^{-7} m s^{-1} (silt) and 10^{-9} m s^{-1} (clay). Hydraulic conductivities are equal in the hillslope aquifer and the deep aquifer. The drainable porosity (f) is a dynamic parameter. Paniconi *et al.* (2003) adopted a mass balance-based matching procedure and defined the drainable porosity as the volume of water drained at steady state divided by the volume of soil initially saturated with this water in the benchmark model. They found that the values obtained are very close to the total porosity of the given soil. Thus, in this study, the same value was used for f in the hsB model and the saturated soil moisture content (θ_s) in the benchmark model. For each soil type, a separate set of Brooks-Corey parameters is used in the benchmark model, and a different value of f is used in the hsB model.

For the open-book catchment, the saturated hydraulic conductivity of the hillslope and the deep aquifer is set to 10^{-4} m s^{-1} and 10^{-5} m s^{-1}, respectively. A hydraulic conductivity of 10^{9} m s^{-1} is used for the aquitard. Table 4.1 summarizes the parameter values used in the single-hillslope and open-book experiments.

A convergence criteria of 0.01 m is used for the difference in calculated heads for the deep aquifer between successive iterations in the hsB/AE coupling scheme. In some cases (e.g., highly conductive aquifer material, steep slopes), numerical oscillations occurred during the iterative process and it was necessary to apply a relaxation factor (typically between 0.6 and 0.8 for the runs reported in this study).

Another important model parameter is the number of areal sinks (inhomogeneities) used to represent the surface boundaries in the AE model. For each inhomogeneity an individual leakage rate can be applied, hence one can account for locally up- and downward directed

flow. In a leakage study based on a 3D Richards equation model (Broda *et al.*, 2010), three distinct zones (up-, mid-, and downslope) were identified with characteristic leakage behavior. In the current study, the general hillslope setup is identical to the setup used by Broda *et al.* (2010). Based on these observations three sub-units were used in the current study.

Table 4.1 Soil parameters used in hsB, the AE model and the benchmark model.

Single hillslopes			
Aquifers			
Saturated conductivity K_s *[m* s^{-1} *]*	10^{-4}	10^{-5}	10^{-6}
Saturated moisture content or porosity θ_s *[-] /*			
Drainable porosity f [-]	0.25	0.35	0.45
Pore size distribution index β *[-]*	3.3	1.20	0.44
Residual moisture content θ_r *[-]*	0.0	0.0	0.0
Capillary fringe height ψ_c *[m]*	-0.25	-0.45	-0.9
Unconfined aquifer specific storage S_s *[*m^{-1}*]*	10^{-2}	10^{-2}	10^{-2}
Confined aquifer specific storage S_s *[*m^{-1}*]*	10^{-4}	10^{-4}	10^{-4}
Aquitard			
Saturated conductivity K_s' *[m* s^{-1} *]*	10^{-7}	10^{-8}	10^{-9}
Saturated moisture content or porosity θ_s *[-]*	0.42	0.495	0.5
Specific storage S_s *[*m^{-1}*]*	10^{-2}	10^{-2}	10^{-2}

Open-book catchment		
Aquifers		
Saturated conductivity K_s *[m* s^{-1} *]*	10^{-4}	10^{-5}
Saturated moisture content or porosity θ_s *[-] /*		
Drainable porosity f [-]	0.25	0.35
Pore size distribution index β *[-]*	3.3	1.2
Residual moisture content θ_r *[-]*	0.0	0.0
Capillary fringe height ψ_c *[m]*	-0.25	-0.45
Unconfined aquifer specific storage S_s *[*m^{-1}*]*	10^{-2}	10^{-2}
Confined aquifer specific storage S_s *[*m^{-1}*]*	10^{-4}	10^{-4}
Aquitard		
Saturated conductivity K_s' *[m* s^{-1} *]*	10^{-9}	
Saturated moisture content or porosity θ_s *[-]*	0.5	
Specific storage S_s *[*m^{-1}*]*	10^{-2}	

4.4. Results for the single hillslope experiments

4.4.1 Varying aquifer conductivity

Figure 4.4 shows the outflow hydrographs of the hsB/AE and benchmark models for three different soil types in a uniform aquifer with α=5% under free drainage conditions. The matches for all materials tested are very good, with the benchmark model producing slightly higher subsurface flow rates at early time, particularly for the medium conductivity soil (K = 10^{-5} m s^{-1}). This is attributable to additional water contained in the capillary and unsaturated zones for the benchmark model (Paniconi *et al.*, 2003). In the case of the more conductive aquifer material (K = 10^{-4} m s^{-1}), after approximately seven days a distinct bend in the hsB/AE outflows is observed. This can be attributed to numerical artefacts in the coupled model at late-time drainage, when the hsB hillslope is almost entirely drained causing small oscillations in the head calculations. Over the simulation period, the deep aquifer contributes in average 75% (for the case of K = 10^{-4} m s^{-1}), 70% (K = 10^{-5} m s^{-1}) and 50% (K = 10^{-6} m s^{-1}) of the total outflow.

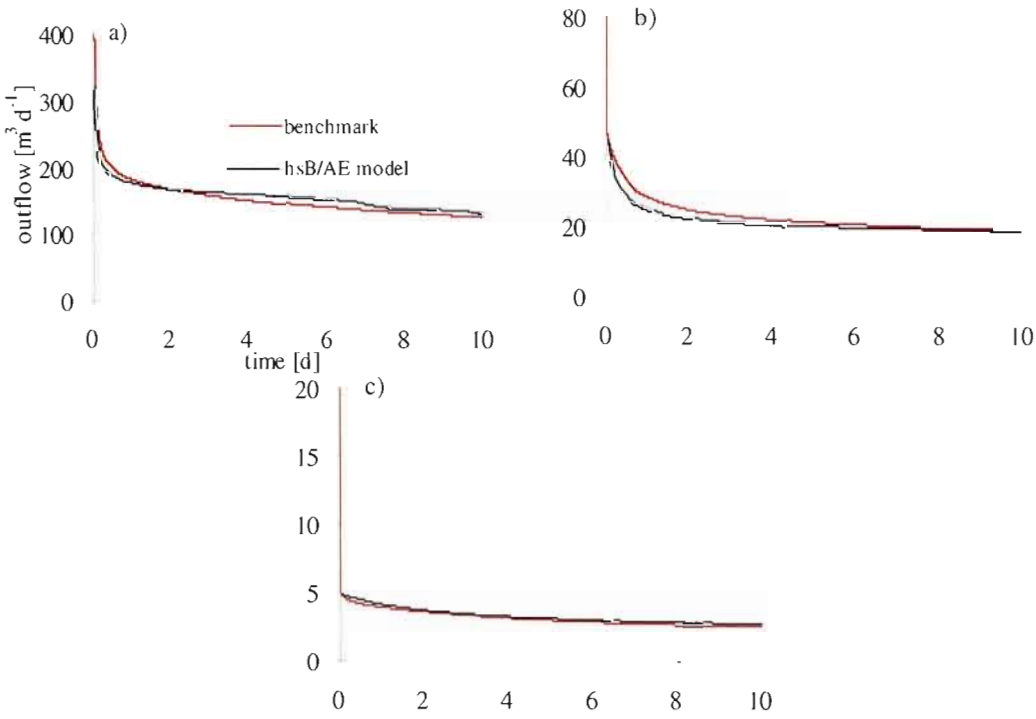

Figure 4.4 Outflow hydrographs for the hsB/AE and benchmark models for a drainage period of 10 days with an aquifer conductivity K of (a) 10^{-4} m s^{-1}, (b) 10^{-5} m s^{-1} and (c) 10^{-6} m s^{-1}.

The good correspondence between the hsB/AE and benchmark models can be further observed by examining the calculated heads and leakage rates along the hillslope x-axis. The leakage rates obtained with equation (4.2) are compared using the vertical component of the velocity vector computed by the benchmark model at the bottom of the aquitard layer at the end of the simulation period. Figure 4.5 confirms that the leakages are similar for the cases of $K = 10^{-6}$ and $K = 10^{-5}$ m s^{-1}, everywhere except at the hillslope extremities, where the boundary conditions have a strong influence. Close to $x = 0$ m, in the proximity of the Dirichlet boundary, the groundwater flux exhibit a distinct shift from positive to negative values, indicating reverse leakage, i.e., water from the deep aquifer into the hillslope aquifer. Larger deviations between leakage rates are observed upslope for the case of $K = 10^{-4}$ m s^{-1}. While leakage rates for the hsB/AE model drop suddenly to zero at about 15 m distance from the hillslope crest, unsaturated storage and nonzero relative conductivities contribute to maintain positive leakage in the benchmark model.

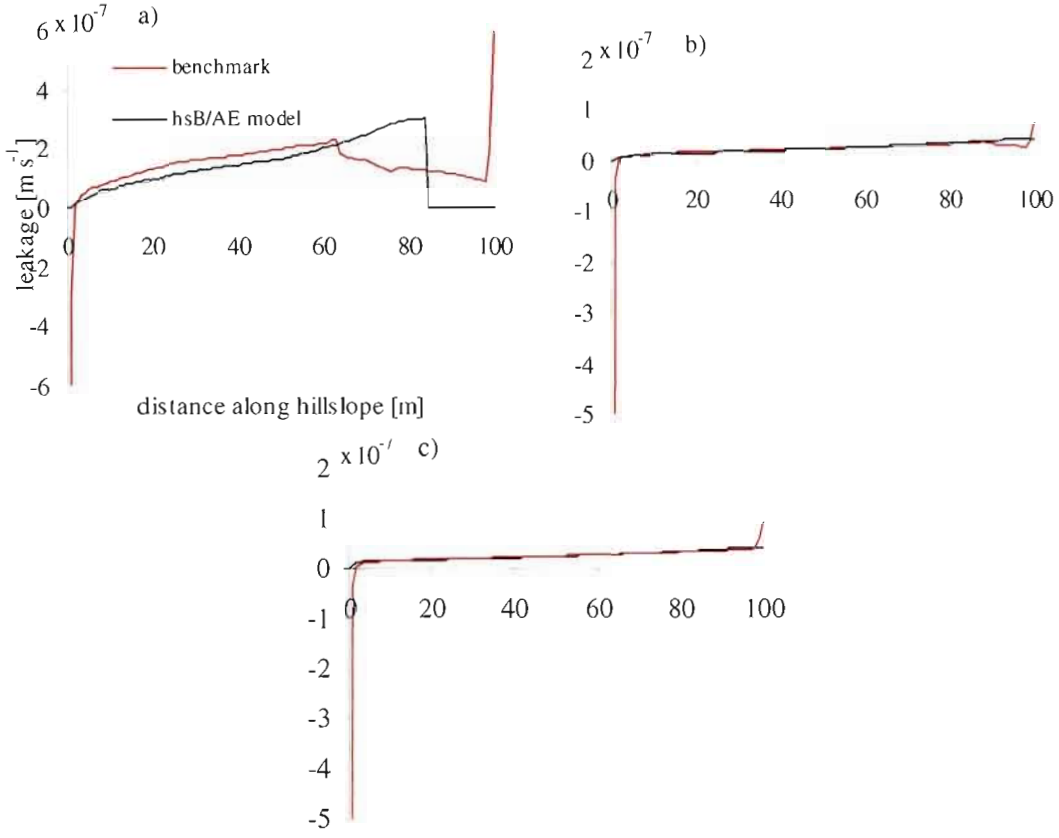

Figure 4.5 Leakage rates along the hillslope for the hsB/AE and benchmark models at t=10 d for an aquifer conductivity K of (a) 10^{-4} m s^{-1}, (b)10^{-5} m s^{-1} and (c) 10^{-6} m s^{-1}.

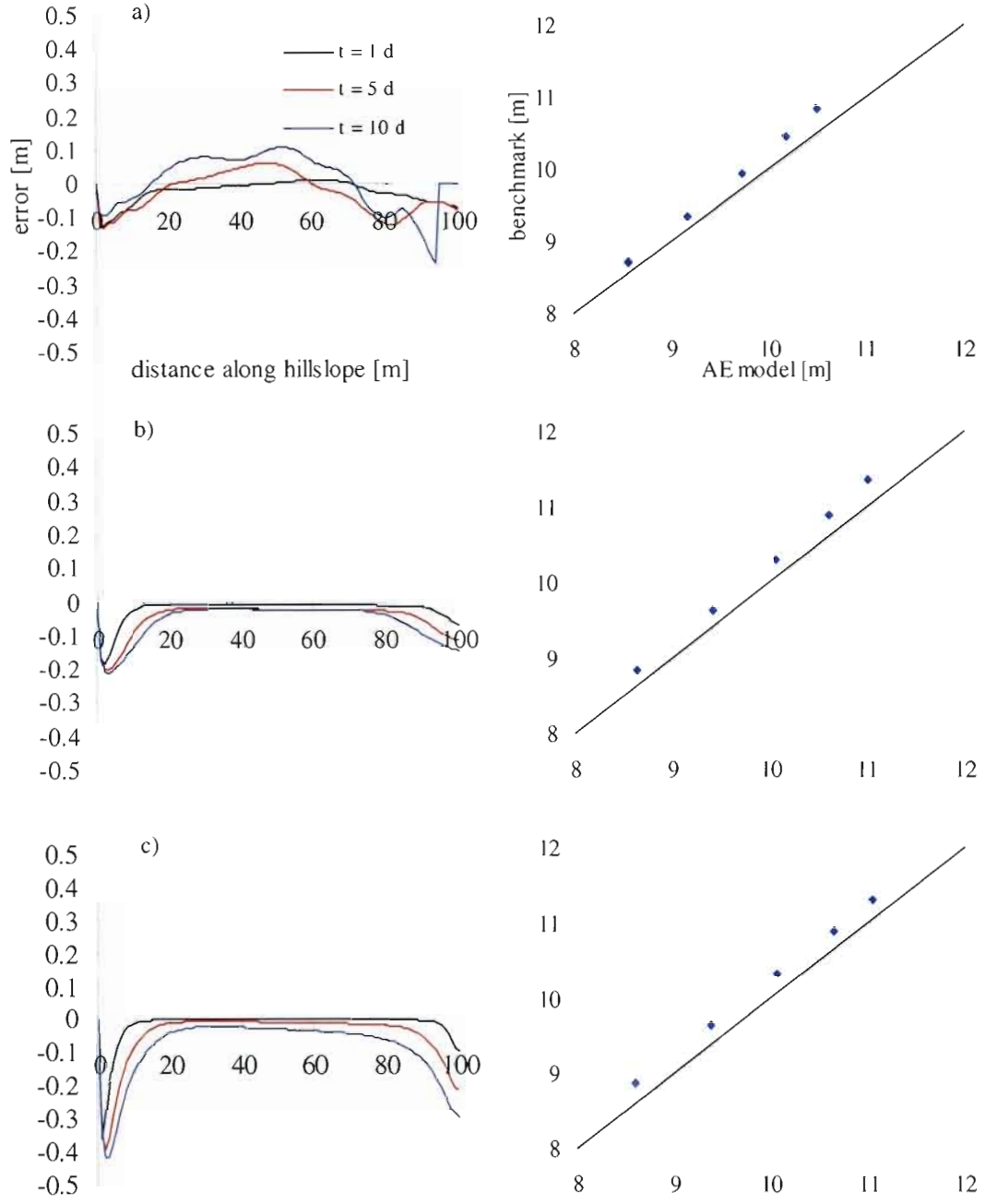

Figure 4.6 Errors in heads in the hillslope aquifer at t=1, 5 and 10 days (left) and in the deep aquifer (right) at the end of a 10 days drainage period with aquifer conductivities K of (a) 10^{-4} m s^{-1}, (b) 10^{-5} m s^{-1} and (c) 10^{-6} m s^{-1}.

This is confirmed in Figure 4.6, which shows the head deviations (benchmark-hsB/AE heads) in the hillslope aquifer at 1, 5 and 10 days and in the deep aquifer at 10, 30, 50, 70, and 90 m from the outlet. Deviations from the benchmark in the hillslope aquifer are largest in the proximity of the up- and downgradient boundaries for all times, ranging between 0.2 and 0.42 m. Elsewhere, heads are underestimated for $K=10^{-4}$ m s^{-1} and overestimated for $K=10^{-5}$ m s^{-1} and 10^{-6} m s^{-1} at late times, showing clear indication of the influence of the unsaturated zone in the benchmark model, which is in agreement with findings of Paniconi *et al.* (2003). In the deep aquifer, however, deviations increase slightly with distance from the outlet and range between 0.14 and 0.36 m. Heads in the deep aquifer are consistently underestimated in hsB/AE relative to the benchmark, which is a result of the slightly erroneous, partially lower leakage rates shown in Figure 4.5.

4.4.2 Varying hillslope inclination

In this set of tests the uniform hillslope base is inclined by 0.2%, 5%, and 30% while the aquifer and aquitard conductivities are set to 10^{-5} m s^{-1} and 10^{-8} m s^{-1} and a recharge event of 5 mm/d is applied.

Table 4.2 summarizes the impact of slope on the calculated heads, outflow, and leakage rates by means of the root mean square error (RMSE), maximum deviation, first, second, and third quartiles (Q_1, Q_2, Q_3) of the total deviation. The quartiles are calculated for the deviations along the hillslope for the transient heads in the hillslope aquifer and the leakage rates. The RMSE is calculated as follows:

$$RMSE = \sqrt{\frac{\sum_{i=1}^{j}(O_i - F_i)^2}{j}} \qquad 4.7$$

where O_i and F_i are the benchmark and calculated values, respectively, and j is the number of values.

The largest head deviations are observed for the 30% slope. This is especially critical in the deep aquifer where a maximum deviation of more than 11 m was simulated. For the 0.2 and 5% slopes, head deviations are small and increase only slightly in time in the hillslope aquifer. With the 30% slope the maximum deviations increase in time, indicating again the strong influence of the unsaturated zone in the benchmark solutions. Furthermore, for the 30% slope, the quartiles of the total deviations indicate a shift from over- to underestimation of heads (negative to positive quartiles) in time in the unconfined aquifer. The negative Q_1 values for the medium slope are attributed to the effects of the upgradient and downgradient boundaries, where heads are overestimated by the hsB model. With the 0.2% slope this overestimation can be observed at a small portion downgradient only and is not captured by Q_1.

The same trends can be observed for the errors in calculated outflows. The maximum deviation for the 30% slope exhibits an underestimation in the hsB/AE model of more than 18 $m^3 d^{-1}$ (approximately 20%). For this case, the head change convergence criterion needed to be relaxed from 0.01 m to 0.4 m in order to reach "convergence" at all. The resulting solution shows differences in heads (between benchmark and hybrid model) in the lower (GFLOW) aquifer that are an order of magnitude higher than for the medium and gently sloping cases (Table 4.2). The errors in the lower heads for the 30% case cause errors in leakage that can easily account for the 20% error in outflow stated above. Furthermore, the 30% slope case developed an unconfined zone in the GFLOW model at the up-gradient end of the model. This increases the storage capacity of the lower aquifer and makes it respond much slower to transient forcing. Consequently, the successive steady state GFLOW solutions become less valid in representing the transient flow in the lower aquifer, which may well explain the convergence problems and subsequent large errors in heads and flows. The development of transient AE models is thus of particular interest in order to capture general flow features for a broader spectrum of aquifers. The outflows in the 5% and 0.2% hillslope match remarkably well those produced by the benchmark model. A small offset can be observed at early times, indicated by the maximum deviations in Table 4.2. This can be related to the initial conditions(Hilberts *et al.*, 2005).

Table 4.2 Deviations in transient and steady state heads, outflows, and leakage rates in the hsB/AE model relative to the benchmark model for three different hillslope inclinations.

Inclination [%]	**0.2**			**5**			**30**		
Transient-state heads in the hillslope aquifer									
t [d]	1	5	10	1	5	10	1	5	10
RMSE [m]	0.04	0.07	0.10	0.04	0.06	0.07	0.12	0.09	0.18
Max. deviation [m]	-0.19	-0.21	-0.21	-0.19	-0.20	-0.19	-0.32	-0.32	0.30
Q_1 *[m]*	0.01	0.04	0.07	-4e-3	-3e-3	-0.02	-0.11	-0.02	0.07
Q_2 *[m]*	0.01	0.05	0.10	-8e-5	0.03	0.05	-0.10	0.02	0.16
Q_3 *[m]*	0.01	0.05	0.11	2e-3	0.04	0.06	-0.10	0.07	0.23
Steady-state heads in the deep aquifer									
RMSE [m]		0.11			0.25			6.85	
Max. deviation [m]		0.13			0.32			11.09	
Outflows									
RMSE $[m^3 d^{-1}]$		0.89			1.37			16.89	
Max. deviation $[m^3 d^{-1}]$		2.54			4.05			18.65	
Leakage rates									
RMSE $[10^{-7} m s^{-1}]$		0.08			0.16			1.35	
Max. deviation $[10^{-7} m s^{-1}]$		-0.13			-0.39			5.07	
Q_1 $[10^{-7} m s^{-1}]$		-0.08			-0.11			0.16	
Q_2 $[10^{-7} m s^{-1}]$		-0.01			0.03			0.81	
Q_3 $[10^{-7} m s^{-1}]$		0.06			0.14			1.67	

The leakage rates deviations confirm the poor match for the hillslope with a 30% inclination. In particular, localisation and timing of hillslope desaturation cannot be properly captured in the hsB/AE model for the steep hillslope. For the medium and gentle sloping aquifers, on the other hand, hsB/AE leakage rates match remarkably well the benchmark results, as can be seen from the low RMSE values in Table 4.2. The quartiles suggest a very slight over- and underestimation in comparison to the benchmark for the gentle and medium hillslopes, respectively.

4.4.3 Varying planform geometry

The hsB/AE model was also tested with different hillslope planform geometries. The aquifer and aquitard conductivities are set to 10^{-5} m s^{-1} and 10^{-8} m s^{-1} respectively. The inclination of the hillslope is 5% and simulations are conducted with the hillslope receiving an infiltration of 5 mm/d.

Using the same statistical measures as in the previous section, Table 4.3 shows that the maximum deviations in transient state heads in the hillslope aquifer for all three tested geometries are negative, except for the convergent slope at $t = 10$ d. These maximum deviations are found close to the outflow face, indicating a strong influence of the boundary conditions. This is confirmed by the lower quartiles Q_1, which indicate deviations much lower than the maximum deviations, hence the maximum errors occur on a very small portion of the hillslope. In general, heads in the divergent hillslope are slightly overestimated almost everywhere, while in the convergent hillslope calculated heads are mostly underestimated. For all geometries, the RMSE increases with time. In the deep aquifer a similar trend can be observed, with the largest deviations in the divergent aquifer, while heads in the uniform aquifer produce the best match with the benchmark. The maximum deviation for the combined model in the deep aquifer is observed upgradient and, as before, the heads in this aquifer are smaller in the hsB/AE model than in the benchmark.

Table 4.3 Deviations in transient and steady state heads, outflows, and leakage rates in the hsB/AE model relative to the benchmark for three different planform geometries.

Planform geometry	**uniform**			**convergent**			**divergent**		
Transient-state heads in the hillslope aquifer									
t [d]	1	5	10	1	5	10	1	5	10
RMSE [m]	0.04	0.06	0.07	0.05	0.10	0.20	0.07	0.11	0.13
Max. deviation [m]	-0.19	-0.20	-0.19	-0.15	-0.18	0.25	-0.27	-0.35	-0.39
Q_1 *[m]*	-4e-3	-3e-3	-0.02	0.02	0.06	0.10	-0.05	-0.07	-0.08
Q_2 *[m]*	2e-5	0.03	0.06	0.03	0.1	0.22	-0.03	-0.03	-0.02
Q_3 *[m]*	2e-3	0.04	0.06	0.04	0.12	0.24	-0.02	-0.01	1e-3
Steady-state heads in the deep aquifer									
RMSE [m]		0.25			0.47			0.45	
Max. deviation [m]		0.32			0.63			0.87	
Outflows									
RMSE $[m^3 d^{-1}]$		1.37			2.00			0.97	
Max. deviation $[m^3 d^{-1}]$		4.05			-3.53			2.14	
Leakage rates									
RMSE $[10^{-7} m s^{-1}]$		0.16			0.08			0.17	
Max. deviation $[10^{-7} m s^{-1}]$		-0.39			-0.20			0.49	
Q_1 $[10^{-7} m s^{-1}]$		-0.11			-0.06			-0.10	
Q_2 $[10^{-7} m s^{-1}]$		0.03			0.02			0.04	
Q_3 $[10^{-7} m s^{-1}]$		0.14			0.10			0.16	

The calculated outflows match relatively well but underestimate slightly the benchmark results for the uniform and divergent hillslopes. The maximum deviations in these two hillslopes occur at early simulation times and are therefore subject to the definition of the initial conditions. The largest RMSE are observed for the convergent aquifer system. It should be noted that the coupled model overestimates the outflows (negative maximum deviation) for this planform geometry which again reflects the role of water retention in the unsaturated zone for the benchmark model.

Leakage rates are well reproduced for all tested geometries. RMSE and maximum deviations are lowest for the convergent geometry. This is somewhat surprising given that heads and outflows were largest for this geometry. In examining the error patterns in detail, a distinct partitioning of the hillslope was found: there are areas where leakage rates are underestimated downgradient and overestimated upgradient by the same order of magnitude, producing some cancellation of errors. For the divergent hillslope, leakage rates are underestimated by the hsB/AE model over large portions of the aquifer, explaining the slight overestimation of heads in the shallow aquifer.

It should be noted that for all cases reported, the benchmark leakage rates show a distinct shift to negative values (reverse flow toward the hillslope aquifer) very close to the outflow face, a consequence also of how the boundary conditions are imposed (the position and extent of the Dirichlet face, for instance).

For all tests conducted, the hsB/AE model is computationally more efficient with respect to the 3D benchmark model. However, the computational efficiency, i.e. the number of iterations needed until the convergence criteria is achieved, is depending particularly on the conductivity of the deep AE aquifer. This is related to the increased sensitivity of such aquifers to small variations in leakage, which cause comparatively large variations in the heads used for the convergence check of the coupled model.

4.5. Results for the open-book catchment

Three different coupling time steps (t_c) are tested in the open-book catchment experiments, i.e., 5, 10, and 30 d. Figure 4.7 displays the outflow rates obtained by the hsB/AE model and the benchmark for t_c = 5 d (i.e. with the AE model run 30d / t_c = six times over the simulation period). Prior to the first recharge event, an almost perfect match is obtained by the hsB/AE model with respect to the benchmark. While the combined model responses immediately to the recharge event, a delay of approximately two days is observed with the benchmark, clearly showing the influence of the unsaturated conductivity on water transfer to the unconfined aquifer. This also explains the dampened response to the recharge event in comparison to the hsB/AE model. Furthermore, the differences in outflow between the two models slightly increase with each recharge event upcoming, with the hsB/AE model overestimating the outflow.

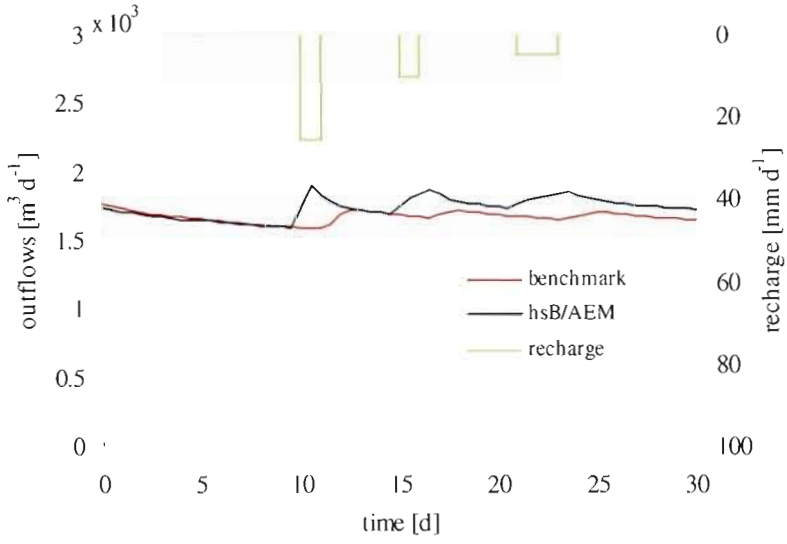

Figure 4.7 Simulated outflows from the hsB/AE and benchmark models for the open-book catchment. A coupling time step of t_c = 5 d is used for the hsB/AE model.

Table 4.4 shows that the cumulative volume error at the end of the simulation is 3.9%. The total outflow is partitioned into 70% from the hillslope aquifer and 30% from the deep aquifer, an indication of the importance of interactions between regional and local scale

aquifers in terms of streamflow contribution. Heads in the hillslope aquifer in both portions of the catchment match well those of the benchmark, with 0.11 m and 0.07 m underestimation respectively. In the deep aquifer, heads are overestimated by the combined model in the 2.5% slope section by a similar order of magnitude, as they are underestimated in the 5% slope section. AE models cannot account for topography, i.e., the top of the aquifer is horizontal. The consequence of this is that the flow regime may be treated as unconfined in areas where it is actually confined. This would lead to an overestimation of transmissivity, which could be compensated for by redefining the hydraulic conductivity in the inhomogeneity domains used to model different recharge or aquifer property zones. Another option would be to alter the bottom elevation within an inhomogeneity to represent a stepping aquifer bottom. This option would be useful in a regional scale domain with marked topography. The difference in heads is also captured by the leakage rates. While in the mildly inclined portion a shift from over- (lower quartile) to underestimating (higher quartile) the leakage can be observed, an overestimation in the 5% section is reported by all quartiles.

Contrary to the single-hillslope experiments where the heads in the deep aquifer are systematically underestimated, in the open-book catchment, over- and underestimations are observed. This can be explained by the assumption of equally spaced and numbered leakage zones along the hillslope. The open-book setup represents an experiment on a larger scale, hence it is suggested to carefully re-evaluate the three sub-block assumption.

Furthermore, and besides the impact of the steady state AE assumption, the errors in the deep aquifer can also be attributed to the calibration of the resistance term, which is somewhat biased since steady state heads in a model with no unsaturated zone are calibrated against benchmark heads which reflect the contributions of the saturated zone, the capillary fringe, and the unsaturated zone. The underestimated heads in the hillslope aquifer for the hsB/AE model can also be related to unsaturated zone processes (Hilberts *et al.*, 2005; Paniconi *et al.*, 2003).

Table 4.4 shows that the number of coupling time steps (t_c) has only a very limited influence on the quality of simulated heads, leakages and hence outflows. Although heads in the hillslope aquifer remain virtually unaffected, deviations in the deep aquifer are slightly variable with different coupling time steps, but no trend is observable. In this particular case,

distinct recharge events are applied within a distinct coupling period, hence the rising head in the unconfined unit could be captured more accurately for the leakage calculations if shorter t_c were used. When applying the coupled model to a real catchment, t_c should be carefully selected, to correspond for instance to recharge (spring and fall) and drainage (summer) seasons. On the other hand, since the aquitard is not represented physically in the hsB/AE model, the available water volume for drainage is overestimated. This is probably an additional factor that leads to overestimation of the outflows.

Table 4.4 Deviations in transient and steady state heads, leakage rates, and outflows relative to the benchmark model for the open-book catchment.

	2.5% slope			5% slope		
t_c [d]	**5**	**10**	**30**	**5**	**10**	**30**
Transient-state heads in the hillslope aquifer						
Max. deviation [m]	0.11	0.11	0.11	0.07	0.07	0.07
Steady-state heads in the deep aquifer						
Max. deviation [m]	-1.29	-1.27	-1.23	1.03	0.90	1.10
Leakage rates						
RMSE [10^{-9} m s^{-1}]	3.09	3.09	3.09	4.45	4.33	4.48
Max. deviation [10^{-9} m s^{-1}]	-8.45	-8.45	-8.46	-10.03	-9.94	-10.06
Q_1 [10^{-9} m s^{-1}]	-3.73	-3.73	-3.74	-5.15	-4.99	-5.16
Q_2 [10^{-9} m s^{-1}]	0.55	0.54	0.49	-3.71	-3.52	-3.76
Q_3 [10^{-9} m s^{-1}]	1.52	1.51	1.48	-2.61	-2.40	-2.68

Outflows			
t_c [d]	**5**	**10**	**30**
RMSE [$m^3 d^{-1}$]	98.3	100.0	98.6
Max. deviation [$m^3 d^{-1}$]	311.6	310.3	301.4
Cum. volume error [%]	-3.9	-3.7	-3.9

Similarly to the single-hillslope tests, the drainable porosity for the hsB model was assumed to be equal to the porosity used in the benchmark model. However, it can be expected that drainable porosities will be lower than the benchmark porosities, particularly in less conductive aquifer material, and different under recharge conditions. In a final set of tests, a

range of drainable porosity values was used (f = 0.1, 0.2, 0.25, 0.3, and 0.4). Figure 4.8 shows the hydrograph results for these different f values. With a low f of 0.1 the model response is most prominent, with highest peak flows after the first recharge event and flows remaining high throughout the simulation. It can be expected that with longer drainage periods between each recharge event, all hydrographs will converge to one curve. The effect on cumulative total outflows at the end of the simulation in comparison to the benchmark model supports this hypothesis. With f = 0.2 the coupled model overestimates the total volume by 1.2%, which reduces significantly the already small error of 3.9% obtained for the value of f (0.25) used in the previous open-book simulations. Consequently, drainable porosity should be considered as an additional fitting parameter, particularly in light of the complex interplay between the amount and duration of infiltration events, aquifer properties and hillslope geometry which influences the value of this parameter.

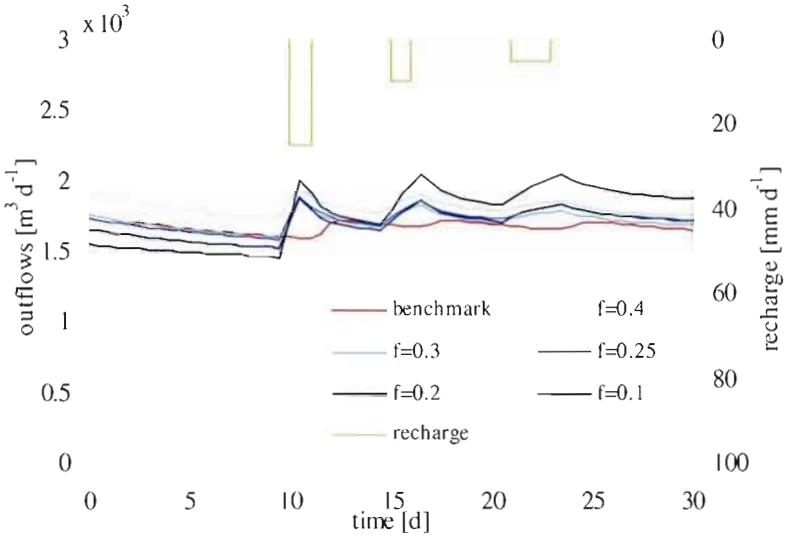

Figure 4.8 Influence of the drainable porosity f on outflows calculated by the hsB/AE model for the open-book catchment.

4.5 Conclusions

This study presented a new catchment model that combines a hillslope-based conceptualization for shallow subsurface flow with a steady state representation of deep regional scale groundwater flow. In comparison to a benchmark numerical model, the coupled model was able to successfully reproduce outflow, leakage, and head responses for a range of aquifer properties, planform geometries and hillslope inclinations. The computational effort is negligible compared to the detailed 3D benchmark model and largely depends on the number of iterations needed until a common solution is found for both aquifer systems. Generally, the hsB/AE model is computationally superior with respect to the benchmark model and most efficient for more conductive aquifers, while more iterations are needed for deep aquifers of low conductivity.

The largest discrepancies between the proposed hsB/AE model and the benchmark model were obtained for steep (30%) slopes and for hillslopes of convergent planform geometry. These differences are mainly attributed to physical-hydrological differences between the benchmark and hsB/AE model and to the steady state, horizontal flow limitation of the AE model. Recent developments in transient flow versions of AE-based models (e.g., Kuhlman and Neuman, 2006, 2009) could be incorporated in future versions of the hsB/AE code. A transient AE model would improve the numerical performance (convergence, etc) of the hsB/AE model and also make it more widely applicable (for instance to nonuniform recharge simulations). Another improvement to the hsB/AE model would be to extend the hsB model to a partial representation of the unsaturated zone (e.g., Hilberts *et al.*, 2007).

The proposed model has the potential to improve subsurface flow representation in hydrological models where surface–subsurface interactions, local aquifer–regional aquifer interactions, and low flows play a key role in watershed dynamics.

CHAPTER V

APPLICATION OF THE hsB/AE MODEL TO THE ALLEN RIVER CATCHMENT, SOUTHERN QUEBEC

5.1 Introduction

The hsB/AE model representing layered groundwater flow is capable of simulating hydraulic heads, leakage, and outflow rates compared to the three-dimensional benchmark model (Broda *et al.*, 2010). These numerical experiments were conducted under well defined but hypothetical configurations of domain discretization, boundaries, and aquifer parameters. The full potential of the hsB/AE model can be further tested by simulating hydrodynamic processes, including baseflow contributions to streamflow, for a real catchment. The importance of validating distributed, physically-based models against observation data for actual catchments is evident, and the literature is replete with examples that show how such exercises can serve to highlight the complexities of the processes being studied. This in turn spurs further model development, in a continuous effort to improve our understanding of hydrological dynamics. As examples, Werner *et al.* (2006) applied MODHMS (Panday and Huyakorn, 2004) on an Australian catchment and were unable to reproduce baseflows obtained with three different hydrograph separation techniques. The degree of spatial discretization limited the model's capacity to simulate local scale processes like bank storage. Gauthier *et al.* (2009) reported that a significantly accurate representation of the system heterogeneity is required to obtain adequate simulation results. Particularly, surficial deposits and bedrock conductivity zones were found to be crucial to matching observations.

The application of detailed models to real world catchments requires many parameters and the acquisition of field data (both parameters and state variables such as heads and flow rates) is time intensive and costly. Increasing parameter density also often implies increasing

calibration difficulties. Furthermore, computer codes need to be accurate and robust, but also as efficient as possible in order to manage the computational burden associated with distributed or integrated process-based models. As an example of the numerical challenges that can arise with such models, LaBolle *et al.* (2003) reported on the numerical instabilities related to differences in time scales between streamflow and groundwater flow components.

In this chapter, the coupled low-dimensional hsB/AE model is applied to a small catchment in southern Quebec in order to i) examine the model's applicability to real conditions; ii) assess its ability to reproduce observed flows; and iii) provide insight on the groundwater contributions to streamflow for this study catchment.

5.2 Study site

The selected site for the hsB/AE application is the Allen catchment. This catchment is part of the transboundary Chateauguay river watershed located in southernwestern Quebec and northeastern New York State (Figure 5.1). The site has been selected for this study because it is a well-studied headwater catchment with a short but good record of streamflow and precipitation data. Recently, the Allen River catchment has been the subject of a number of hydrogeological studies on: the hydrological role of a peatland (Fournier, 2008; 2007), peat thickness estimation (Rosa *et al.*, 2008) and recharge estimation (Gagné, 2010). The site hosts the Covey Hill Natural Laboratory (Larocque *et al.*, 2006) which instrumented for long term hydrological and ecosystemic surveys. The catchment covers an area of 30 km^2 and its topography ranges from 340 m to 85 m. Covey Hill is considered an important recharge area for the regional Chateauguay River watershed (Croteau, 2006). The eastern part of the hill is drained via the Allen River, which contributes to the des Anglais River, one of the main tributaries of the Chateauguay River. The climate is continental temperate with a mean annual temperature of 6.7 °C and average lows in January (-9.6 °C) and highs in July (20.6 °C). The mean annual precipitation is 929 mm with snow precipitation between November and March (Environment Canada, 2007). The Allen catchment represents the the model area.

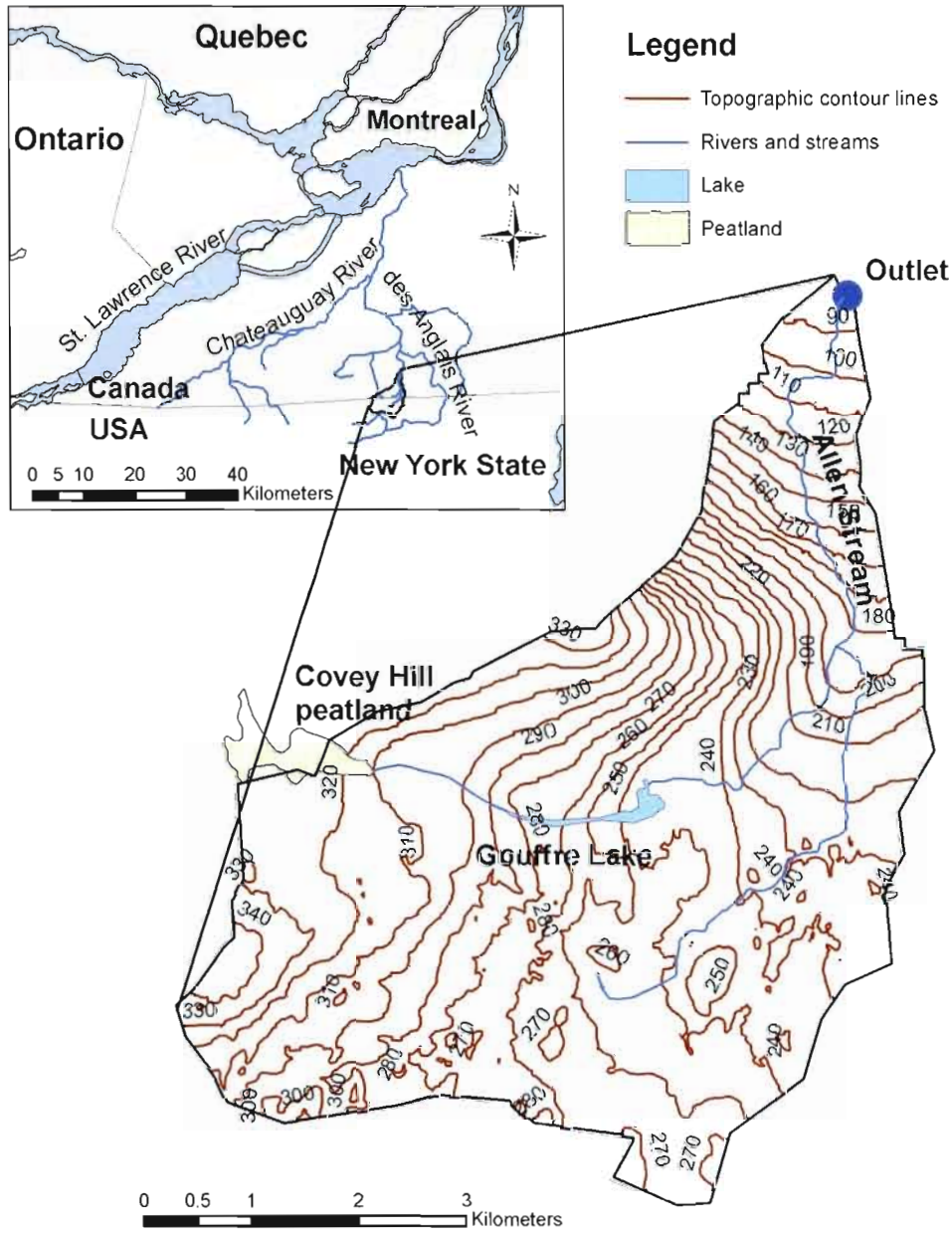

Figure 5.1 Localization of the Allen River catchment and map of surface water features and topographic contour lines.

The site description is extended to the area surrounding the Allen River catchment in order to include the entire simulated flow domain. This zone constitutes the farfield domain, which

contains hydrologic features that control flow in and out of the nearfield domain, with the Noire River in the north and northwest and the des Anglais River in the east and south.

Covey Hill is located on Cambrian sandstone of the Potsdam Group (Covey Hill Formation) divided into the basal Covey Hill Formation and the upper Cairnside Formation, deformed and fractured during the Appalachian orogen (Globensky, 1986). The Covey Hill Formation extends almost entirely into the farfield domain, while the Cairnside formation is present only in the eastern portion, from the foot of Covey Hill to the des Anglais River (Figure 5.2). The Havelock breccia follows the Havelock fault in the eastern part of the study area. The hydrogeological influence of this major structural feature is not well defined, as few data are available within its extent (Lavigne, 2006).

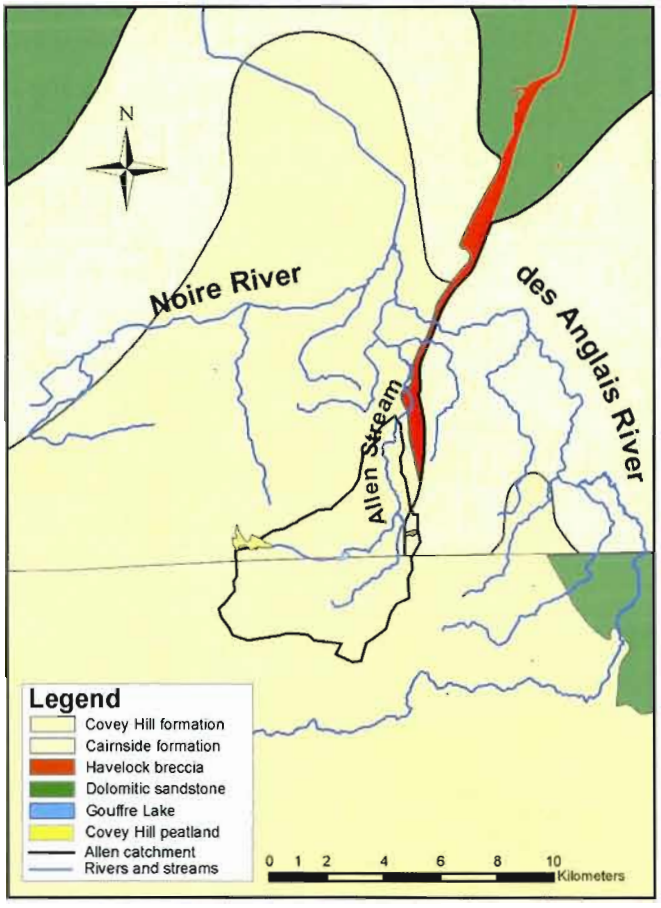

Figure 5.2 Bedrock geology of the study area (Coté *et al.*, 2006).

Surface deposits are practically absent at the hilltop. Elsewhere, the bedrock is overlain by Quarternary deposits of variable thickness, composed of gravel, sand, and sandy tills. The thickness of the sediments varies with altitude and with slope (Figure 5.3). Up to 10 m of sediments can be found south and west of the hill, whereas thin layers of sediments are found in the steepest portions of the hill, at altitudes ranging between 220 and 100 masl. Sediments increase in thickness up to 8 m at the northern foot of Covey Hill (Lasalle, 1981; Tremblay, 2008). Outside of the Allen River catchment, sediments are of similar composition and thicknes reaches 30 m at the domain edges, particularly in the east and west, and in the proximity of the des Anglais and Noire rivers.

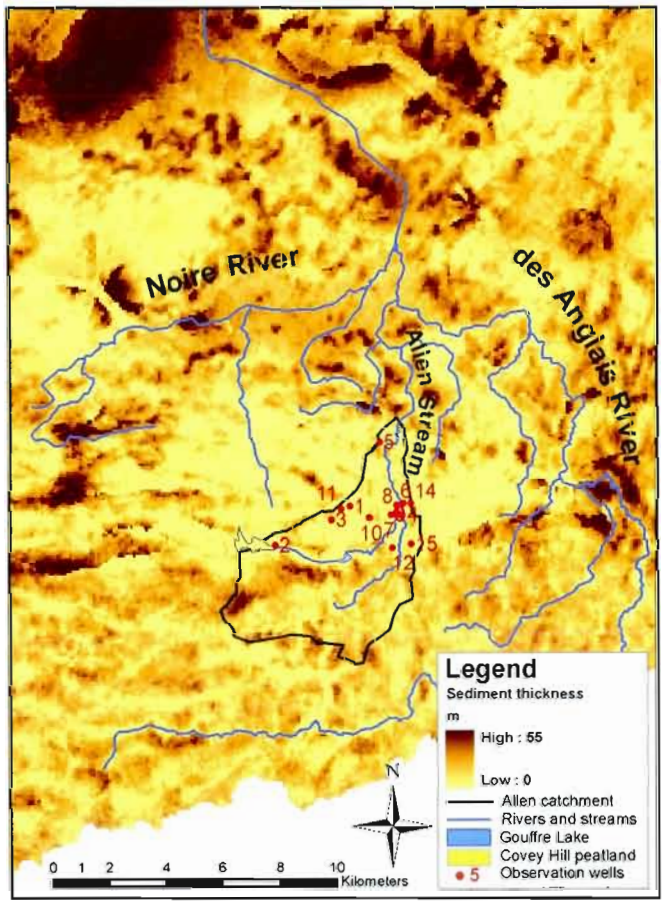

Figure 5.3 Thickness of Quaternary sediments at the study site (Coté *et al.*, 2006).

Groundwater flow occurs in the sandstone at a regional scale and in the Quarternary sediments at a local hillslope scale. The bedrock aquifer is generally unconfined over the study area. Flow occurs from south to north in the fractures and dissolution joints rather than in the sandstone porosity (Nastev *et al.*, 2004). Springs occur at mid-slope where saturated fractures meet topography principally in the northeastern face where the slopes are steepest (approximately 10% inclination). Slopes of this order of magnitude can also be found in the western portion of the study area, whereas in the rest of the domain the slopes vary between roughly 1% and 3% inclination. The bedrock water table depth varies between 2 and 15 m and flows generally radially with respect to the hilltop. Hence, groundwater flow gradients are largest in the steep portions of the domain. Low gradients can be found along the Noire River and the lower portions of the des Anglais river (see Figure 5.8).

An important surface water feature is the Covey Hill peatland with a surface area of 0.51 km^2, located west of the hilltop and partitioned into two drainage basins. The eastern part covers 0.35 km^2 and drains towards the Allen River (the western part drains towards the Outardes River). Heads in the peatland are lower than in the surrounding bedrock aquifer, indicating groundwater input from the aquifer to the organic deposits. Because the bedrock underlying the peatland is relatively impervious, however, it is assumed that no water is exchanged vertically between the organic deposits and the bedrock aquifer (Fournier, 2008). Another major hydrological feature is the groundwater fed Gouffre Lake, with a depth of approximately 50 m (Gagné, 2010). With the Allen catchment being a headwater catchment and major recharge area, there is minimal stream incision of the aquifer and streamflows are relatively low. Consequently, the aquifer is drained only nominally by the streams.

A total of 15 bedrock observation wells (private monitoring wells, Ministère du Développement durable, de l'Environnement et des Parc du Québec and Geological Survey of Canada piezometers and data from the Système d'Informations Hydrogéologiques [SIH; MDDEP, 2007]) are available (see Figure 5.7). Groundwater levels in the bedrock aquifer are measured using *Solinst* level loggers and vary during a hydrological year from 0.6 to 7.7 m. The smallest variations are observed in the wells located near the peatland. The larger variations are widely distributed over Covey Hill and there is no apparent link with location (Fournier, 2008; Gagné, 2010).

Hydraulic conductivities of the fractured bedrock are available from pumping tests performed in previous studies (Barrington *et al.*, 1992; Lavigne, 2006) and from slug tests performed in wells located near the peatland (Fournier, 2008). Available hydraulic conductivities range from $7x10^{-8}$ to $3x10^{-5}$ m s^{-1}. They are highly variable and correspond obviously to a wide range of fracture conditions; nevertheless the available measurements serve to define an interval of possible K values. The variation of K with depth is not known with precision but a decrease of two orders of magnitude was measured between two closely located wells at 3 and 15 m depth (Fournier, 2008) as well as between two 80 m wells at the top of the hill unit (Godin and Rouleau, 2006).

5.3 Data and methods

5.3.1 Input data

Daily rainfall from a rain gauge on Covey Hill, potential evapotranspiration calculated by means of a modified Penman method (Gagné, 2010) and streamflow data at the catchment outlet recorded using *TruTrack* loggers are available for the period of April to October 2008. The total precipitation for the studied period amounts to 652 mm and total evapotranspiration to 376 mm. The minimum, maximum and averaged streamflows at the catchment outlet are respectively, 0.05, 21.19 and 0.46 m^3/s.

Due to the absence of a land surface-atmosphere interface in the hsB/AE model, evapotranspiration is not represented. The precipitation time series must therefore be treated beforehand to provide the net precipitation on a daily time scale:

$$P_k^{net} = P_k \frac{\sum_{k=1}^{j} P_k - \sum_{k=1}^{j} ETP_k}{\sum_{k=1}^{j} P_k} \tag{5.1}$$

where P^{net}_k [mm d^{-1}] is the net daily precipitation for day k, P_k [mm d^{-1}] is the measured rainfall for day k, ETP_k [mm d^{-1}] is the estimated evapotranspiration for day k, and j is the

total number of days in the considered study period. On a yearly basis, the net precipitation is 44% of the total precipitation, where in October the P^{net}/P_k ratio is largest (0.83) and with 0.12 in August smallest (Figure 5.4). The net precipitation can be partitioned into surface runoff and soil infiltration. It therefore needs to be converted into the required recharge input for the hsB module. Because the hsB version used in the hsB/AE model does not represent the unsaturated zone, recharge is therefore equivalent to soil infiltration.

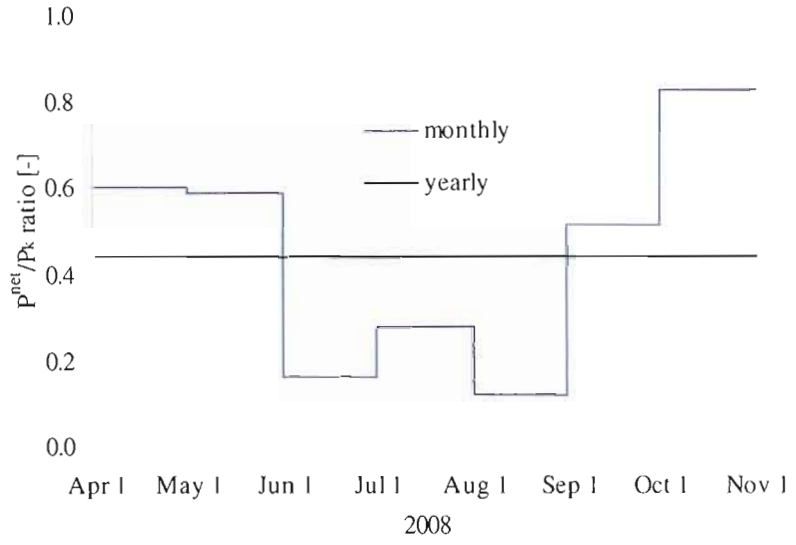

Figure 5.4 Ratio of net Precipitation to total precipitation based on monthly averages

Estimation of groundwater recharge, which can be highly variable in time and space, is a challenging problem in hydrogeology. Some of the complicating factors include the effects of land use changes, the problems associated with spatial extrapolation of point data, and the presence of localized or indirect processes. These can occur for instance in shallow aquifers when rising water tables induced by recharge create a local groundwater system with associated local seepage discharge, thereby reducing net recharge. Moreover, recharge that reaches the water table can subsequently be extracted by evapotranspiration (de Vries and Simmers, 2002). In the context of coupling hydrological models and groundwater flow models, even the definition of groundwater recharge may be ambiguous and can vary depending on scale and the specific aquifer under consideration (Barthel, 2006).

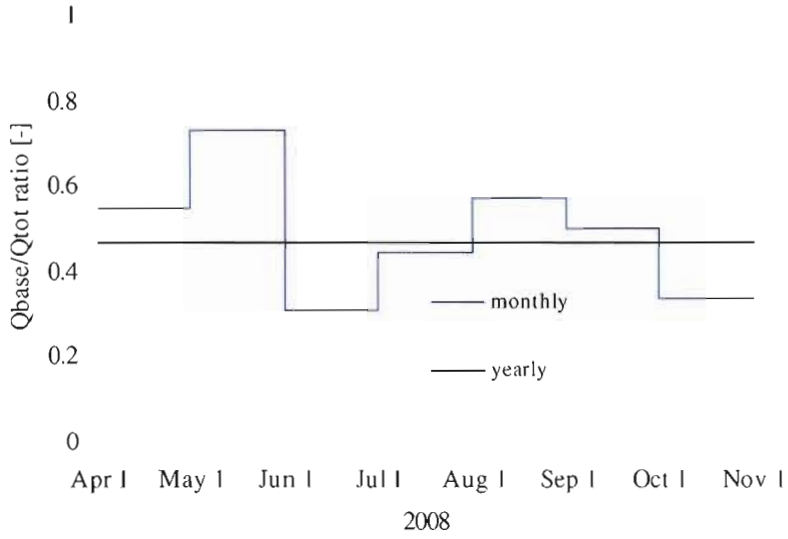

Figure 5.5 Ratio of baseflow to total flow based on monthly and yearly averages.

In this study, groundwater recharge is estimated based on the ratio of baseflow Q_{base} to total flow Q_{tot} of the Allen River at the catchment outlet and on recharge values reported in recent modeling studies of the Allen catchment or Chateauguay River watershed. Hydrograph separation using the Chapman method (Chapman, 1999) has been conducted by Gagné (2010). On a yearly and monthly basis, i.e., taking the average of the monthly ratios, the Q_{base}/Q_{tot} ratio is respectively 0.46 and 0.48. Figure 5.5 illustrates the temporal variability of the monthly Q_{base}/Q_{tot} ratio, clearly indicating recharge periods in April-May and August-September.

In the modeling study of Fournier (2008), the catchment was partitioned into recharge zones and calibrated recharge rates varied between 37 and 183 mm/year, corresponding to 13 and 64% of the net precipitation of 287 mm for the April–October 2008 period. In a modeling study carried out over the entire Chateauguay River watershed (Lavigne, 2006), groundwater recharge over the Allen catchment ranged between 0 and 400 mm/year, with an average of 86 mm/year or 30% of the net precipitation between April and October 2008. In the study conducted by Gagné (2010) groundwater recharge was estimated to be 162 mm/year, i.e., 56% of the net April–October precipitation.

Based on these findings, the groundwater recharge used in this study is defined to be 50% of the net precipitation P_{net}. This results in an infiltration or recharge estimate for the period from April to October 2008 equal to 22% of the total precipitation over the catchment, or 144 mm over this study period. Figure 5.6 visualizes the partitioning of daily rainfall events into actual aquifer recharge. Using a ratio averaged over the 7-month period probably underestimates recharge in the spring and fall and overestimates recharge in the summer. Furthermore, groundwater recharge is taken to be spatially homogeneous, which is a considerable simplification given that infiltration rates are expected to be highest in the hilltop portions of the catchment. The impact of these assumptions will be discussed later.

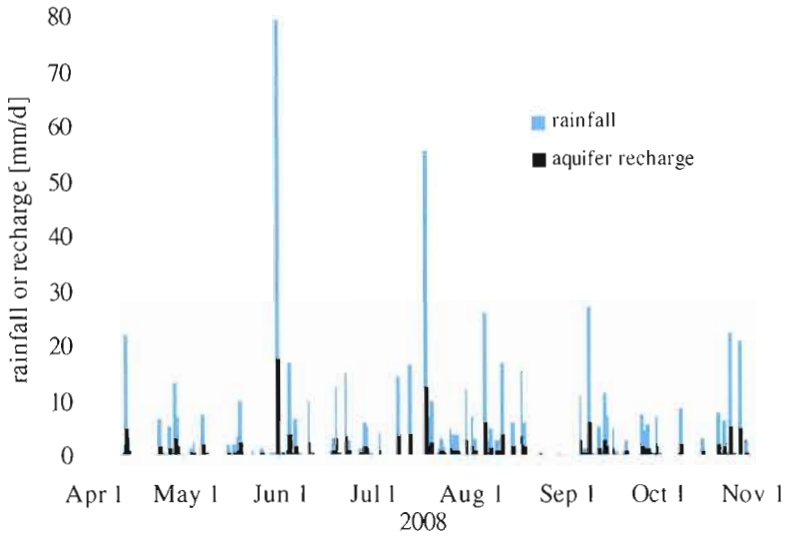

Figure 5.6 Daily observed rainfall and corresponding estimate of aquifer recharge.

The hsB/AE model is expected to simulate baseflow from the deep aquifer and shallow subsurface flow (interflow) from the hillslope, both contributing to the total input from the aquifer to the stream. Hence, compared to the observed streamflow hydrograph, the model results are expected to fall between the total outflow (which includes also any surface runoff contributions) and the estimated baseflow component. Figure 5.7 illustrates the full hydrograph at the outlet of the Allen catchment as well as the Chapman-based baseflow hydrograph. The peak baseflows in the spring and early summer are related to snow melt and

it is expected that they will not be easily reproduced with the hsB/AE model due to the absence of a snow melt and runoff representation. Furthermore, baseflow separation algorithms are generally somewhat subjective, since the baseflow dynamics largely depend on the selection of the baseflow index (Eckhardt, 2008), resulting in high frequency variability to smooth baseflow hydrographs. Although the large baseflow component during the spring period appears to be unrealistic, verifying credibility of the Chapman baseflows obtained by Gagné (2010) have nevertheless not been subject of this study and hence remain unaltered. However, other separation techniques should be tested as well, but is left to future research. In late summer and early autumn, however, baseflow constitutes most of the total outflow, thus this period should be more easily simulated with the coupled model representing layered groundwater flow.

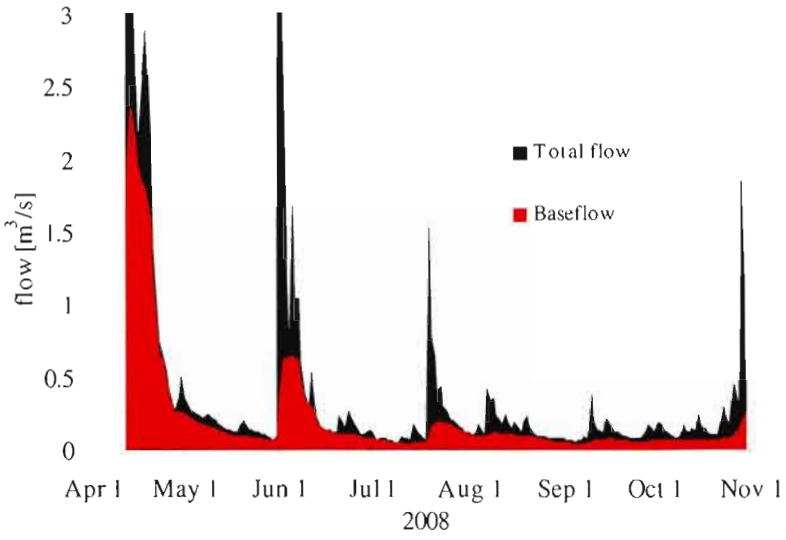

Figure 5.7 Total flow and estimated baseflow at the Allen River catchment outlet.

5.3.2 Hillslope delineation

GIS pre-processing is employed to partition the Allen watershed into hillslopes using ArcHydro tools and the "Editor" function in ArcGIS. The approach applied in this study was presented by Matonse and Kroll (2009) and is based on the methodology described by Fan

and Bras (1998). The hillslopes are classified as uniform, convergent, divergent, or a combination of these shapes, based on the general groundwater flowline patterns (Figure 5.8a). Hillslopes of similar geometry were combined to form larger hillslopes. "Natural" hillslopes then had to be converted into regular "numerical" hillslopes that define the individual recharge units in the hsB/AE model (Figure 5.8b). The regular planform shapes dictated by the hsB model are uniform, monotonically convergent, and monotonically divergent. In order to preserve the surface area of each hillslope, the hillslope length and width is calibrated and regular width functions are generated using intervals of $\Delta x = 50$ m.

An automated approach for hillslope delineation would greatly facilitate the application of the hsB-based modeling approach to a wide range of catchments. Accurate extraction and delineation of hillslopes based on digital elevation models (DEMs) or triangulated irregular networks (TINs) is an active topic of research (e.g., Bogaart and Troch, 2006; Noël *et al.*, 2010). A strong constraint in any automated algorithm would be the avoidance of overlaps and/or gaps between hillslopes. In hsB standalone applications at the catchment scale, this issue is not relevant, since lateral divides are taken to be no-flow boundaries and hence hillslope interconnectivity is not accounted for. Nonetheless, in the context studied in this thesis, these issues need to be resolved in order to avoid mass balance errors due to over/underestimation of aquifer surface areas and unwanted mixing of leakage fluxes across multiple hillslopes. Equally appealing in resolving this issue would be an extension of the hsB model to allow for entirely arbitrary geometries.

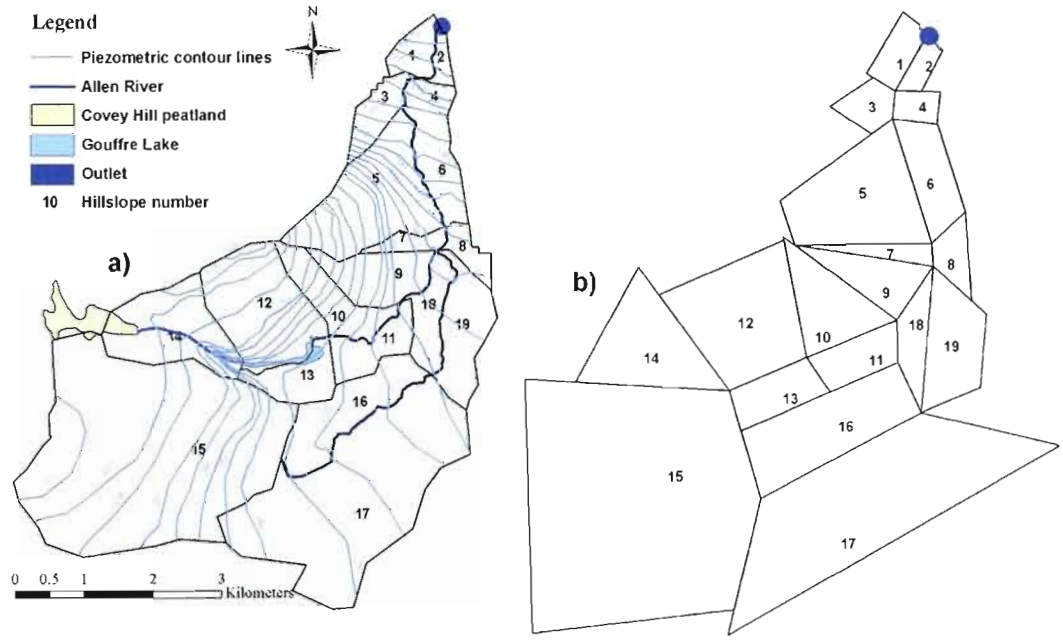

Figure 5.8 a) Naturally delineated hillslopes and b) regularly-shaped numerical hillslopes extracted from the Allen River catchment.

Table 5.1 provides a summary of the calibrated surface areas based on the width functions, deviations from actual surface areas, hillslope inclinations and Quaternary aquifer thicknesses for each hillslope. Slopes and thicknesses are obtained using statistical tools of ArcGIS. In total, 19 hillslopes are delineated, with a total surface area of 30.08 km^2. The total surface of the catchment is underestimated by 0.04 km^2 which is considered to be negligible. Although the total surface area of the catchment is preserved, the definition of the general flow direction within each each hillslope, hillslope inclination and aquifer thickness are subject to higher errors. The hsB approach is based on the assumption of width-averaged flow perpendicular to the outflow face. Hence, within each delineated numerical hillslope, groundwater flow is perpendicular to the stream draining the hillslope. For instance, groundwater flow in hillslope 6 is expected to be parallel to the stream according to the piezometric contour lines (Figure 5.8a), but assumes an orientation perpendicular to the stream in the model representation (Figure 5.8b). Only increasing the number of hillslopes in the domain can relax this inaccuracy. Slope angles and aquifer thicknesses are subject to

errors caused by the interpolation of point data information to the catchment scale. Furthermore, the thickness of the Quaternary deposits is considered to be highly variable in space (Tremblay, 2008) and this cannot be entirely accounted for in the hsB model which uses a constant thickness for each hillslope.

Table 5.1 Characteristics of the 19 hillslopes extracted from the Allen River catchment.

Hillslope #	Surface [km^2]	Calibrated surface [km^2]	Absolute difference [km^2]	Average slope [%]	Average thickness of Quaternary deposits [m]
1	0.45	0.43	0.02	2.4	3.5
2	0.19	0.20	0.01	2.2	3.5
3	0.55	0.56	0.00	5.1	3.5
4	0.27	0.27	0.00	2.9	3.5
5	2.40	2.40	0.00	8.1	2.0
6	0.80	0.76	0.04	3.0	2.0
7	0.24	0.24	0.00	5.8	2.0
8	0.28	0.30	0.02	2.9	2.5
9	1.01	1.00	0.01	7.0	1.6
10	0.93	0.95	0.02	5.5	4.0
11	0.68	0.65	0.03	2.8	2.8
12	2.21	2.24	0.03	4.8	3.8
13	0.71	0.69	0.03	2.7	2.8
14	1.77	1.81	0.03	3.1	3.0
15	8.80	8.79	0.02	3.2	8.0
16	1.45	1.47	0.02	2.7	6.5
17	5.56	5.49	0.07	2.3	6.6
18	0.66	0.64	0.01	3.5	1.7
19	1.14	1.20	0.06	2.8	3.8
all	30.12	30.08	0.04	3.8	3.5

5.3.3 Model parameterization

At the base of each outflow face of the 19 hsB hillslopes a zero storage boundary condition is applied. All other lateral divides are no-flow boundaries, hence hillslope interconnectivity is neglected. The topography of the studied domain, including also the farfield domain, ranges between 340 and 45 m. In this study, the aquifer in the AE model is

assigned a constant thickness of 340 m. The nearfield domain is defined by three inhomogeneities per hillslope, representing three distinct zones of constant recharge. In total, 57 inhomogeneities are applied. In the farfield, a recharge rate of 144 mm is used.

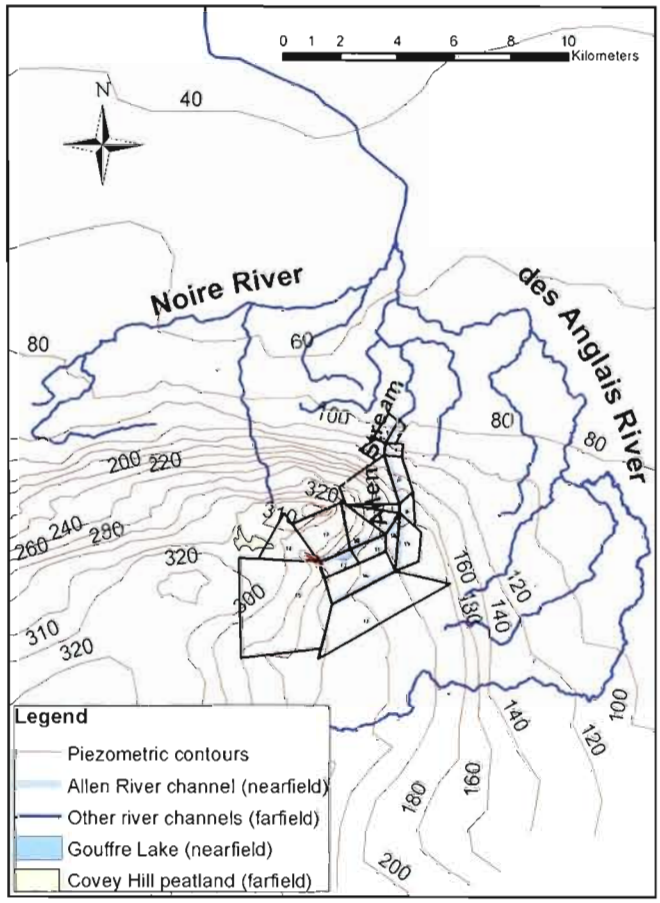

Figure 5.9 Nearfield and farfield boundaries for the Allen River watershed model.

The Allen River is represented in the AE model with head-specified line sinks having a width of 0.8 m and a depth of 0.5 m. The resistance R to vertical flow of the Allen Stream is a calibration parameter and will be discussed later on. The Covey Hill peatland, although in reality located with approximately 50% of its surface within the Allen catchment, is almost entirely located outside the nearfield domain. This is caused by the preservation of the surface area during the hillslope delineation process. The peatland is represented using a

farfield fixed head boundary. The Gouffre Lake is defined as a lake boundary of 50 m depth. In the farfield, a number of streams are defined as fixed head boundaries, hence fully penetrating the aquifer (Figure 5.9).

In this study, the routing of streamflow contributions from individual hsB hillslope elements to the catchment outlet was neglected. Given that the maximum length of the flow path along the stream channel is roughly 8 km, it is expected that the time of concentration is below the numerical time step of 1 d.

5.4 Results

The coupled hsB/AE model was run from April to October of 2008 (213 d), with a spin-up period of the same length to minimize the impact of the initial conditions. Given the relatively short input time series available, the length of the calibration period was limited as well. The steady state AE model was run just once within the simulation period, i.e., a coupling time step t_c of 213 d was used. Preliminary runs with smaller t_c values produced a negligible influence on the quality of the model results but increased the computational time.

5.4.1 Model calibration

A manual trial-and-error calibration was performed for the following parameters: hydraulic conductivities in the aquitard, hillslope and bedrock aquifer, drainable porosity, aquitard thickness, stream resistance, and initial soil moisture. The calibration was conducted to minimize errors between simulated and observed mean hydraulic heads in the bedrock aquifer and estimated baseflows at the Allen River outlet over the entire 213 d simulation period. The calibrated parameters are homogeneous over the entire study area. The best results were obtained from August to October, when streamflow response is less dominated by surface flow phenomena.

As can be seen in Figure 5.10, the model performs poorly for the spring and early summer months, due mainly to the absence of snow melt and surface runoff representation in the hsB/AE model. The difficulty during large baseflow periods is also due to the lack of a

soil component in the hsB/AE model that can accurately partition water between runoff, evapotranspiration, and interflow. Matonse and Kroll (2009) reported similar difficulties in simulating high flow events with an hsB-based model.

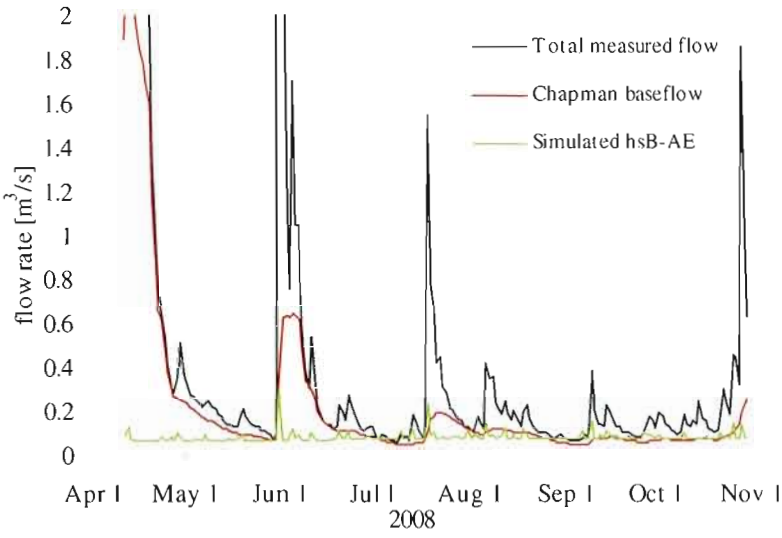

Figure 5.10 Simulated hsB/AE flows compared with total flows and Chapman baseflows for the April-October 2008 period.

The poor match against estimated baseflow in spring and early summer may also be partly due to uncertainties in the baseflow separation technique (Jones *et al.*, 2006). The Chapman method used here is based on removing, via a recursive one-parameter digital filter, the high-frequency quickflow signal from the low-frequency baseflow signal (Chapman, 1999; Smakhtin, 2001). One of the limitations or sources or uncertainty or error in the method is that streamflow contributions from bank storage, lakes, wetlands and snow are ignored. This uncertainty is particularly significant in the spring for the Allen catchment, when snowmelt is normally a significant contributor to streamflow. Additionally, the Chapman baseflow includes groundwater flow and interflow, and the latter is not represented in the hsB/AE model.

Because the computed heads in the bedrock aquifer represented by the AE model component are at steady state, these are compared to yearly averages of the observed heads. As can be

seen in Figure 5.11, the mean error (2.19 m) is relatively small and the computed heads are both under- and overestimated compared to the measured values (r^2 = 0.79). Close to the Allen River, heads are generally overestimated (e.g., observation wells 6 to 9), while further away they tend to be underestimated (e.g., observation wells 1, 3, 11). This can be explained in part by the large resistance applied to the river bed, reducing flow towards the stream and causing heads to build up. The underestimation of heads in the other regions can be related to the homogeneous representation of the deep aquifer. In particular, heads on the steep portions of Covey Hill are poorly reproduced. This portion of the domain is also the one where strong vertical gradients due to fracturing are observed (Gagné, 2010; Fournier, 2008; Nastev *et al.*, 2004). The introduction of variable conductivity zones would help improve the simulated results. The fact that recharge is applied homogeneously in the farfield also introduces bias in the model. Croteau (2006) described highly variable recharge zones throughout the basin. A spatial refinement of the annual recharge could potentially improve the results.

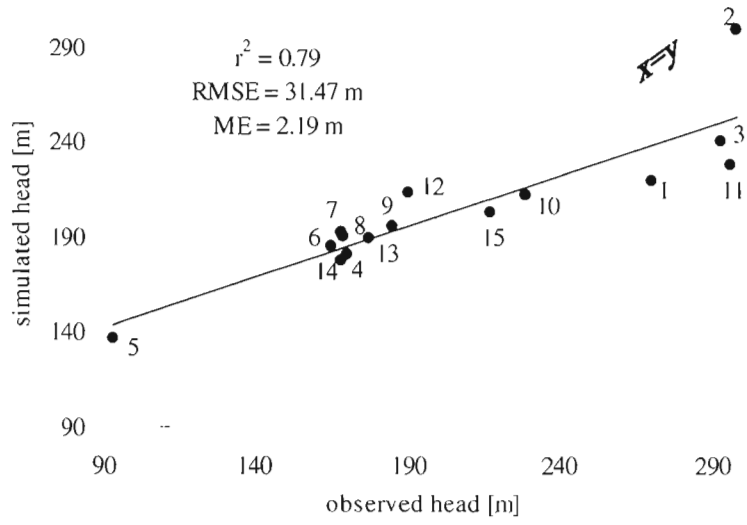

Figure 5.11 Scattergram of measured and simulated heads in the bedrock aquifer.

The calibrated parameter values are summarized in Table 5.2. The hydraulic conductivities used for the hillslope and bedrock aquifers are within the ranges reported by Croteau (2006)

and Lavigne (2006). A pronounced vertical anisotropy has been hypothesized for the Allen River catchment, in particular around Covey Hill, with horizontal to vertical conductivity ratios of 1000 (Fournier, 2010) and even 15000 (Lavigne, 2006). Since the resistance R in the Dupuit-Forchheimer-based AE model is accounting for 3D flow effects near a stream, the relatively large value for R (30 d) represents a very limited vertical flow exchange between the surface water and groundwater. The aquitard conductivity and thickness cannot be related to any field observations or literature data for the study site. These two parameters, which primarily control the convergence rate during the iterative coupling process between the hsB and AE models are therefore pure calibration parameters.

Table 5.2 Calibrated parameters for the Allen River catchment.

Parameter	**Calibrated value**
Hillslope hydraulic conductivity K_s *[m/s]*	2×10^{-5}
Drainable porosity f [-]	0.22
Initial soil moisture [-]	0.3
Bedrock hydraulic conductivity K_s *[m/s]*	5×10^{-6}
Aquitard hydraulic conductivity K_s' *[m/s]*	1×10^{-10}
Aquitard thickness b [m]	2
Stream resistance R [d]	30

5.4.2 Flows during the low flow period

The hsB/AE model simulates reasonably well the catchment response in the August to October period when the aquifer provides an important proportion of total flow.

Figure 5.12 shows the total measured outlet discharge, the estimated baseflow component, and the simulated hsB/AE discharge for the month of August 2008. This period is characterized by a number of recharge events in the first half of the month followed by a 10-day drainage period. Generally, the simulated flow underestimates the baseflow, with a relatively low RMSE of 0.024 m^3/s. A maximum deviation between hsB/AE flow and estimated baseflow of 0.049 m^3/s is observed during the peak rainfall event of 26 mm, where

the actual aquifer recharge is 5.8 mm. The impact of the recharge event is significant and the response of the hsB/AE model indicates a strong contribution from the hillslope aquifer. Flow dynamics caused by the recharge events are generally reproduced well according to the observed total flow data. Towards the end of the month, the simulated flow becomes larger than the baseflow and approaches the total measured flow. During this period, the total measured flow drops to 0.07 m^3/s, which is below the 10^{th} percentile of 0.08 m^3/s for total streamflow between April and October. Hence it can be assumed that the measured flow is almost entirely supplied by baseflow during this late-August period.

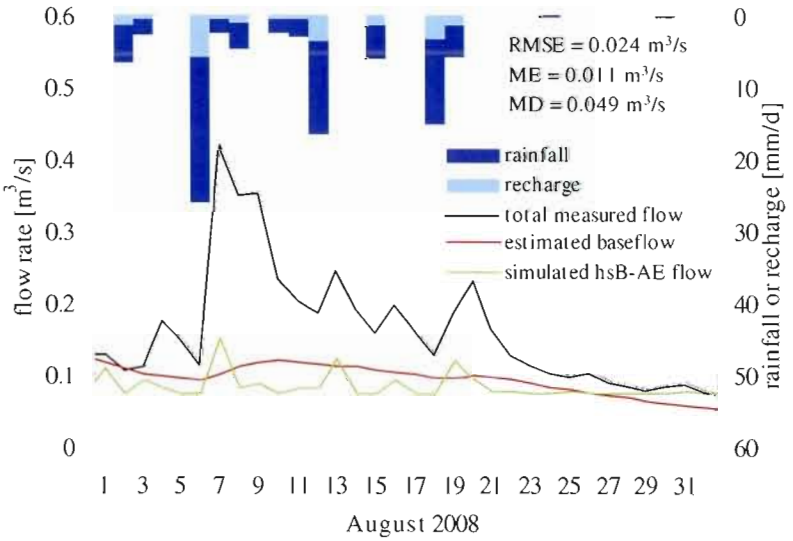

Figure 5.12 Simulated hsB/AE flow for August 2008 compared with total outlet discharge and estimated baseflow. A statistical summary of the comparison between hsB/AE and the estimated baseflow is also given (RMSE = root mean squared error; ME = mean error; MD = maximum deviation).

The drainage period extends into the month of September, for a total duration of 17 days. The RMSE and mean error for the entire month are reasonably small. The hsB/AE flow remain very close to the total measured discharge during this period (Figure 5.13). In the following period, the hsB/AE flow remains higher than the estimated baseflow. This can be attributed

to the steady state nature of the AE model, where contributions from the deep aquifer over a dry period are generally expected to be less than those during wet periods. The model response to recharge events is captured well, with the resulting hydrograph showing the influence of recharge on subsurface runoff. Possible improvements to the model in terms of recharge estimation include introduction of an atmosphere-soil module and use of a *P/ETP* ratio calculated over multiple years instead of over a single year, in order to capture interannual *P/ETP* variations.

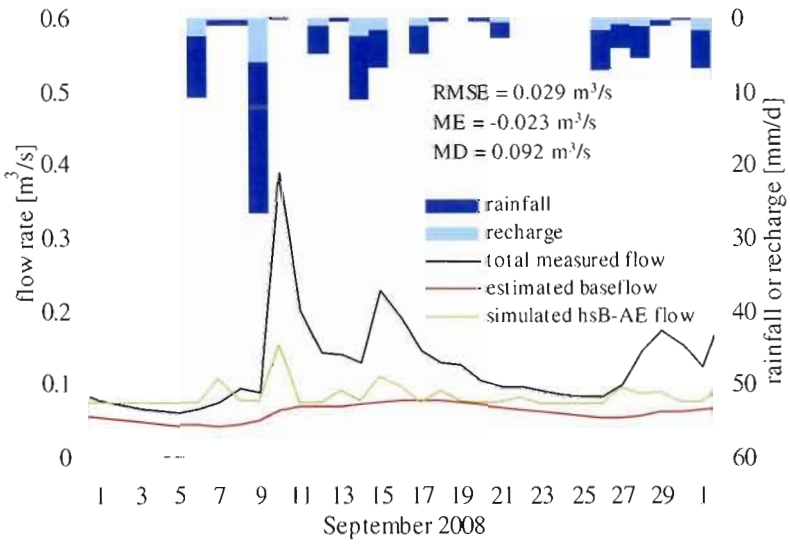

Figure 5.13 Simulated hsB/AE flow for September 2008 compared with total outlet discharge and estimated baseflow. The statistical measures are as defined for Figure 5.11.

October is characterized by increasing rainfall frequency and intensity towards the end of the month. The hsB/AE flow represents well the baseflow pattern until October 25 (Figure 5.14). The large rainfall events after this date are not well-captured in relation to total discharge due to the lack of a surface runoff component in the model. For the October 1-25 period the simulated flow is generally larger than the estimated baseflow. The relatively large RMSE (0.048 m^3/s) calculated over the entire month drops to 0.013 m^3/s when it is computed over

the period October 1-22. It should be noted that the measured hydrograph peaks that are seen in Figure 5.13 around October 13 and 15 do not correspond to rain events and are perhaps attributable to measurment errors or to the influence of a man-made static dam that controls flow into one of the lakes on the Allen River.

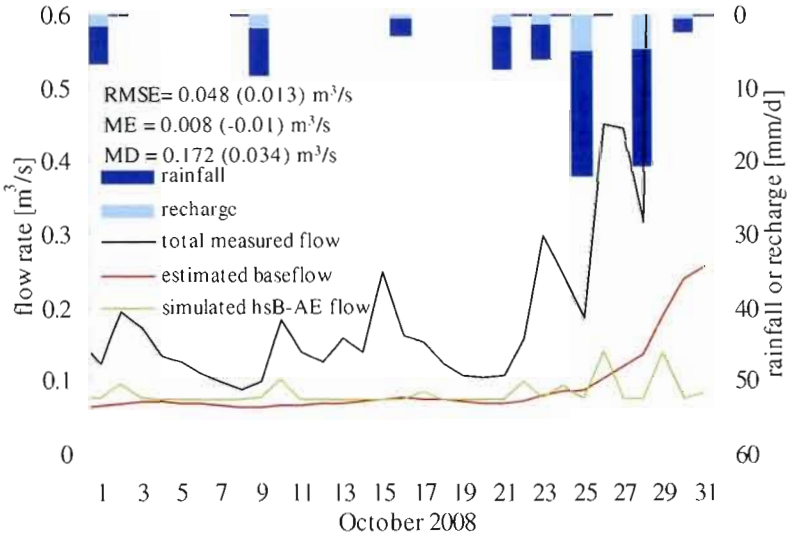

Figure 5.14 Simulated hsB/AE flow for October 2008 compared with total outlet discharge and estimated baseflow. The statistical measures are as defined for Figure 5.11 (the values in parentheses are for the period October 1-22).

For the period from August to October 2008, the total simulated hydrograph is partitioned into roughly 53% contributed from the hsB aquifer and 47% from the AE aquifer. Inter-monthly variations are small, with contributions from the hsB aquifer increasing to roughly 55%. Figure 5.15 compares the monthly ratio between estimated baseflow and total observed discharge with the monthly ratio between hsB/AE outflow and total observed discharge. This figure underscores the generally increasing importance of the baseflow contribution to streamflow as summer progresses, and the hsB/AE's model ability to partially capture this trend. Over the entire simulation period, the model-computed ratio is 0.34, which compares well with the ratio obtained in previous studies (e.g., 0.30 at the 90th percentile in Gagné, 2010) and reasonably well with the ratio based on the Chapman baseflow (0.48). For the

period between August and October, the model-computed ratio is 0.51 which compares very well with the ratio based on the Chapman method.

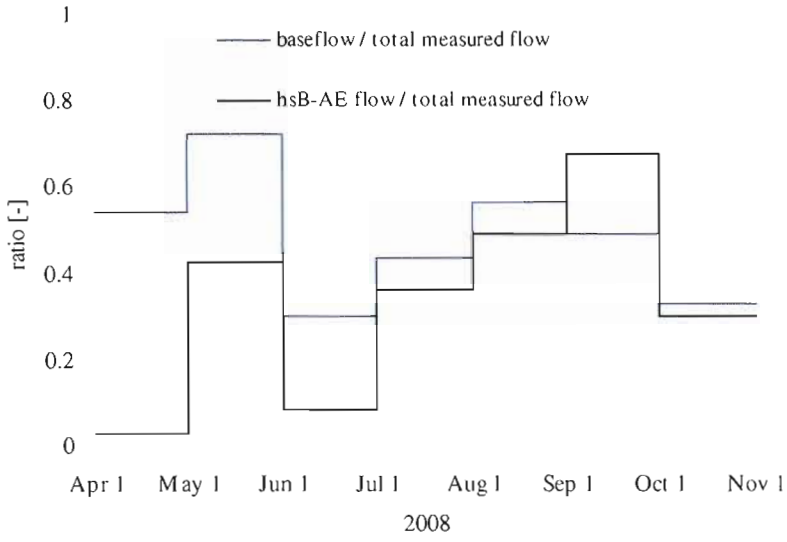

Figure 5.15 Ratios of estimated baseflow to total measured discharge and hsB/AE model-computed outflow to total measured discharge.

5.5 Conclusions

The main objective of this study was to apply the newly developed coupled hsB/AE model to a real catchment and examine the outflow behavior produced by this model in comparison to measured streamflow and estimated baseflow. The recharge input to the model was calculated from estimates of net precipitation and baseflow/streamflow ratios and from recharge rates obtained in previous studies. Simulated heads in the bedrock aquifer are overestimated in the proximity of the Allen stream, while they are underestimated at further distances. This is mainly attributed to the homogenous representation of the AE aquifer, i.e., constant aquifer thickness and conductivity throughout the entire domain and within a single hillslope and the lacking representation of resistance to vertical flow in the Dupuit-Forchheimer-based AE model. It is expected that these results could be improved by

introducing variable thickness and conductivity zones. Overall, the computed hsB/AE flows were shown to capture reasonably well the estimated baseflows during periods when baseflow dominates the hydrograph response (e.g., late August to late October). Due to the absence of snowmelt and surface runoff components in the model, the catchment response during spring discharge and extreme rain events is underestimated. Nonetheless, the model mimics quite well the timing and the rising and falling limbs of hydrograph peaks. Furthermore, results obtained in previous studies on this catchment (Fournier, 2010; Gagné, 2010), indicating a large baseflow contribution to streamflow, could be confirmed with the hsB/AE model.

Aquifer recharge is a critical input to the model. Currently based on a *P/ETP* ratio obtained over a single year, a more refined approach would be to use a ratio from a longer period and to include recharge estimation in the calibration procedure in order to relax arbitrary assumptions concerning net precipitation and other factors. The model calibration was conducted on aquifer and aquitard parameters as well as initial saturation of the hillslopes. Because sediment thickness in the Allen catchment has a high degree of spatial variability (Tremblay, 2008) and errors related to interpolation of point data information on sedimentary layering to the regional scale are significant, sediment thickness should become a calibration parameter as well. Generally, it was difficult to reproduce periods where total flow is dominated by surface flow phenomena. The incorporation of a soil-atmosphere interface for partitioning rainfall into runoff, evapotranspiration and aquifer recharge is expected to improve models performance during wet periods. Other areas of further research include automated width function generation.

CHAPTER VI

CONCLUSIONS

The objective of this thesis was to develop a low-dimensional yet accurate subsurface flow model for layered groundwater flow and to thoroughly test and verify it against a detailed numerical model and a real catchment. The new model consists of an extension of the hillslope-storage Boussinesq (hsB) model to allow for vertical exchange fluxes through a hypothetical semi-pervious unit at the hillslope bottom coupled with an analytic element-based model representing regional and deep groundwater flow. The combined hsB/AE model was first tested on numerical hillslopes and on an open-book catchment. The results were compared to those obtained with a fully-coupled finite element model based on the Richards equation (benchmark model). The new model was further tested in an application to a small headwater catchment in southwestern Quebec.

In chapter 2 the original hsB model was prepared for coupling with a groundwater flow model by allowing for vertical fluxes through a hypothetical aquitard at the hillslope bottom. A leakage term based on Darcy's law was incorporated by extending the mass balance and combining it with the Boussinesq equation. For preliminary testing, experiments on a numerical hillslope were conducted with the extended hsB and the benchmark model. Leakage rates at the bottom of the aquitard were used as input to the extended hsB model. This new hsB model simulated reasonably well heads and outflows, indicating the potential of the hsB model to simulate recharge to a deep semi-confined aquifer. The large spatio-temporal variability in leakage patterns and the high sensitivity to boundary conditions for the leakage process underlined the importance of investigating hillslope leakage in more detail.

Chapter 3 addressed these issues by means of a thorough study of leakage in a hillslope context. The benchmark model was used in these analyses, with numerical experiments

conducted for a 100 m synthetic hillslope composed of a layered aquifer system. The simulations examined the influence of different configurations of aquifer and aquitard properties, hillslope geometry (including length and inclination) and boundary conditions on leakage, water levels and outflow. The results showed that leakage generally percolates in both directions, with downward (positive) leakage in upslope portions of the aquifer and upward (reverse or negative) leakage in downslope regions. Geometry was found to be a main determinant of the partitioning of leakage along a hillslope, with for instance upward leakage in large portions of convergent slopes but only in a small downslope region for divergent slopes. In steep hillslopes, the reverse leakage that occurs downslope as a result of quick upslope drying represents a major component of the water budget. Outflow boundary conditions also exert a major control on the volume and direction of leakage, with the placement and extent of Dirichlet or seepage face nodes along the outflow face being particularly important factors.

In chapter 4 the understanding of hillslope leakage from chapter 3 was applied in combining the hsB model, representing shallow hillslope groundwater flow, with the AE model representing deep regional groundwater flow. A series of tests on single hillslopes and a synthetic two-hillslope (open-book) catchment was presented. The impact of aquifer parameterization, hillslope planform geometry and inclination under drainage and recharge events was examined. The results were compared to those of the benchmark model. On the single hillslopes, remarkable matches were obtained for all tested setups, with significant deviations observed only for the 30% slope and for hillslopes with convergent geometry. Results for the two-hillslope catchment were reasonable, with cumulative flow volumes underestimated by roughly 10-12%. The response to recharge events was found to largely depend on the selection of the drainable porosity used in the hillslope model. Based on these findings, it can be suggested that the drainable porosity be treated as a fitting parameter. Overall, the hsB/AE model was found to be computationally efficient and reasonably accurate, and suitable for application in hydrological contexts involving layered groundwater flow at the catchment and river basin scale with streamflow that has a strong baseflow component.

In chapter 5 the new model was applied to a real catchment. The selected Allen watershed is part of the Chateauguay regional transboundary watershed and is one of its main recharge areas. The model-computed discharge to the stream was compared to the total measured outlet streamflow and to baseflow estimated using the Chapman filter. Significant deviations from the baseflow hydrograph occurred during high flow periods, when recharge events are most pronounced and frequent and where total flow is dominated by surface flow phenomenas. The computed hsB/AE flows were shown to capture reasonably well the baseflow during periods when baseflow dominates the hydrograph response (e.g., late August to October).

Research on the new modeling approach presented in this thesis is naturally far from being complete. Additional effort should be put on further testing the current version of the hsB/AE model, as well as on improvement of the hsB and AE model components. As a next step in model improvement, the hsB/AE model should be incorporated into a land surface hydrological model, in order to have a complete representation of the water cycle. Additionally, tests should be performed with more realistic hillslope geometries, including profile curvature. One major limitation of the hsB/AE model is the steady-state AE component. A transient AE model is expected to improve model performance. Leakage rates would no longer need to be averaged over a pre-defined coupling time period, hence peak recharges to the deep aquifer could be better accounted for. Furthermore, the AE model can only account for a varying aquifer bottom, while the aquifer surface remains horizontal. An extension of the AE model to account for actual aquifer topography would be an innovation tailored to the coupling with hsB. Finally, a transient AE model would help improve numerical stability and efficiency since the number of iterations in the coupling procedure is expected to be reduced. An automated approcach for hillslope delineation as well as an extension of the hsB model to allow for entirely arbitrary geometries would greatly facilitate the application of the hillslope-based modeling approach. Given the highly variable thickness of hillslope aquifers over single hillslopes, it could be worth conducting a further extension of the hsB model to account for a spatially variable unconfined aquifer thickness.

In summary, the presented hsB/AE model is a parameter sparse and computationally efficient tool for simulating groundwater flow on local hillslopes coupled to a regional groundwater

system. Given the gaining popularity of fully integrated models operating at the watershed scale, the hillslope-based paradigm developed here provides a promising alternative to traditional modeling techniques. Finally, the extended hsB model that allows for vertical exchanges at the hillslope bottom makes the model readily available for coupling with other deep groundwater flow modules.

REFERENCES

Ahuja, L. R., Ross, J. D. (1983). Effect of subsoil conductivity and thickness on interflow pathways, rates and source areas for chemicals in a sloping layered soil with seepage face. *J. Hydrol.* 64: 189-204.

Anderson, E. I. (2005). Modeling groundwater-surface water interactions using the Dupuit-approximation. *Adv. Water Res.* 28: 315-327.

Arnold, J. G., Allen, P. M. (1996). Estimating hydrologic budgets for three Illinois watersheds. *J. Hydrol.* 176: 57-77.

Arnold, J. G., Allen, P. M., Bernhardt, G. (1993). A comprehensive surface-groundwater flow model. *J. Hydrol.* 142: 47-69.

Arnold J. G., Muttiah R. S., Srinivasan R., Allen P. M. (2000). Regional estimation of base flow and groundwater recharge in the Upper Mississippi river basin. *J. Hydrol.* 227: 21-40.

Barrington, S., Philion, H., Bonin, J. (1992). An evaluation of the water reserve potentials: the ecological region of the Covey Hill « Gulf ». Rapport du département de génie agricole, Faculté d'agriculture et de sciences environnementales, McGill University, Montreal, Qc, Canada.

Barthel, R. (2006). Common problematic aspects of coupling hydrological models with groundwater flow models on the river catchment scale. *Adv. Geosci.* 9: 63-71.

Basha, H. A., Maalouf, S. F. (2005). Theoretical and conceptual models of subsurface hillslope flows. *Water Resour. Res.* 41(W07018): doi:10.1029/2004WR003769.

Beven, K. (1981). Kinematic subsurface stormflow. *Water Resour. Res.* 17(5): 1419-1424.

Bixio, A., Orlandini, S., Paniconi, C., Putti, M. (2000). Physically-based distributed model for coupled surface runoff and subsurface flow simulation at the catchment scale. In: *Computational Methods in Water Resources, vol. 2, Computational Methods, Surface Water Systems and Hydrology*, edited by L. Bentley, J. F. Sykes, C. A. Brebbia, W. G. Gray & G. F Pinder, 1115–1122. A. A. Balkema, The Netherlands.

Broda, S., Paniconi, C., Larocque, M. (2010a). Numerical investigation of leakage in sloping aquifers. *Hydrol. Process.*, submitted.

Broda, S., Larocque, M., Paniconi, C. (2010b). Development of a new hillslope-based groundwater flow model: combining the hillslope-storage Boussinesq with an analytic element model. *J. Hydrol.*, in preparation.

Brooks, R., Corey, A. (1964). Hydraulic properties of porous media. *Hydrol. Pap.* 3. Colorado State University, Fort Collins, CO, USA

Brouyère, S., Carabin, G., Dassargues, A. (2004). Climate change impacts on groundwater resources: modelled deficits in a chalky aquifer, Geer basin, Belgium. *Hydrol. J.* (12): 123-134.

Brunke, M., Gonser, T. (1997). The ecological significance of exchange processes between rivers and groundwater. *Freshwat. Biol.* 37: 1-33.

Camporese, M., Paniconi, C., Putti, M., Orlandini, S. (2010). Surface–subsurface flow modeling with path-based runoff routing, boundary condition-based coupling, and assimilation of multisource observation data. *Water Resour. Res.* 46(2): W02512, doi:10.1029/2008WR007536.

Chapman, T. (1999). A comparison of algorithms for stream flow recession and base flow separation. *Hydrol. Process.* 13: 701-714.

Chen, Z., Grasby, S. E., Osadetz, K. G. (2004). Relation between climate variability and groundwater levels in the upper carbonate aquifer, southern Manitoba, Canada. *J. Hydrol.* 290(1-2): 43-62.

Clark, M. P., Rupp, D. E., Woods, R. A., Tromp-van Meerveld, H. J., Peters, N. E., Freer, J. E. (2008). Consistency between hydrological models and field observations: linking processes at the hillslope scale to hydrological responses at the watershed scale. *Hydrol. Process.* doi: 10.1002/hyp.7154.

Cloke, H. L., Renaud, J.-P., Claxton, A. J., McDonnell, J. J., Anderson, M. G., Blake, J. R., Bates, P. D. (2003). The effect of model configuration on modelled hillslope–riparian interactions. *J. Hydrol.* 279: 167-181.

Cooper, D. M., Wilkinson, W. B., Arnell, N. W. (1995). The effects of climate changes on aquifer storage and river baseflow. *Hydrol. Sci. J.* 40(5): 615-631.

Coté, M.-J., Lachance, Y., Lamontagne, C., Nastev, M., Plamondon, R., Roy, N. (2006). Atlas du bassin versant de la rivière Châteauguay - Territoire, Eau souterraine, Aménagement. Ministère du Développement Durable, de l'Environnement et des Parcs, Québec: 57 p.

Croteau, A. (2006). Détermination de la distribution spatiale et temporelle de la recharge à l'aquifère régional transfrontalier du bassin versant de la rivière Châteauguay, Québec et Etats-Unis. MSc thesis. Université du Québec INRS ÉTÉ : 346 p.

Daly, E., Porporato, A. (2004). A note on groundwater flow along a hillslope. *Water Resour. Res.* 40(W01601): doi:10.1029/2003WR002438.

De Lange (1996). NAGROM, a groundwater model for national groundwater management and regional and local studies. *Eur. Water Pollut. Contr.* 6(5): 63-67.

De Vries, J. J., Simmers, I. (2002). Groundwater recharge: an overview of processes and challanges. *Hydrol. J.* (10): 5-17.

Delleur, J. W. (1999). The Handbook of Groundwater Engineering. 992 pp., CRC Press, Boca Raton, Fl, USA.

Dewson, Z. S., James, A. B. W., Death, R. G. (2007). A review of the consequences of decreased flow for instream habitat and macroinvertebrates. *J. N. Am. Benthol. Soc.* 26(3): 401-415.

Eckhardt, K. (2008). A comparison of baseflow indices, which were calculated with seven different baseflow separation methods. *J. Hydrol.* 352: 168-173.

Eckhardt, K., Ulbrich, U. (2003). Potential impacts of climate change on groundwater recharge and streamflow in a central European low mountain range. *J. Hydrol.* 284(1-4): 244-252.

Environment Canada. (2007). Moyenne climatique de la station Hemmingford Four Winds Quebec, 1961-2006.http://www.climate.weatheroffice.ec.gc.ca/climateData/dailydata

Fan, Y., Bras, R.L. (1998). Analytical solutions to hillslope subsurface storm flow and saturation overland flow. *Water Resour. Res.* 34(4):921–927.

Foose, G. J., Benson, C. H., Edil, T. B. (2001) Predicting leakage through composite landfill liners. *J. Geotech. Geoenviron.* 127(6), 510–520.

Fortin, J. P., Turcotte, R., Massicotte, S., Moussa, R., Fitzback, J., Villeneuve, J. P. (2001) Distributed watershed model compatible with remote sensing and GIS data. I. Description of the model. *J. Hydrol. Engng* 6(2), 91–99.

Fournier, V. (2007). Plan de conservation de la tourbière de Covey Hill. Rapport d'étape dansle cadre d'un projet de maîtrise sur la caractérisation hydrologique du milieu. Rapport présenté à Conservation de la Nature. 20 p.

Fournier, V. (2008). Hydrologie de la tourbiere du Mont Covey-Hill et implications pour la conservation. MSc thesis Université du Québec à Montréal : 93 pp.

Franke, O. L., Reilly, T. E. (1987). The effects of boundary conditions on the steady-state response of three hypothetical ground-water systems: Results and implications of numerical experiments. *U.S. Geol. Surv. Water Supply Pap.* 2315, U.S. Geological Survey, Denver, CO, USA.

Gagné, S., (2010). Apport de l'eau souterraine aux cours d'eau et estimation de la recharge sur le Mont Covey Hill. MSc thesis Université du Québec à Montréal. 104 pp.

Gambolati, G., Teatini, P. (1996). A block iterative finite element model for nonlinear leaky aquifer systems. *Water Resour. Res.* 32(1): 199-204.

Gauthier, M. J., Camporese, M., Rivard, C., Paniconi, C., Larocque, M. (2009). A modeling study of heterogeneity and surface water-groundwater interactions in the Thomas Brook catchment, Annapolis Valley (Nova Scotia, Canada). *Hydrol. Earth Syst. Sci.* 13 :1-14.

Globensky, Y. (1986). Géologie de la région de Saint-Chrysostome et de Lachine (sud).Ministère de l'énergie et des ressources. 166 p.

Godin, R., Rouleau, A. (2006). Essais perméamétriques en forage dans le socle rocheux du bassin de la rivière Châteauguay. Report provided to the Ministère du Développement durable, de l'Environnement et des Parcs, Centre d'études sur les ressources minérales, Université du Québec à Chicoutimi. 108 p.

Gunduz, O., Aral, M.M. (2005). River networks and groundwater flow: a simultaneous solution of a coupled system. *J. Hydrol.* 301: 216-234.

Hantush, M. M. (2005). Modeling stream-aquifer interactions with linear response functions. *J. Hydrol.* 311: 59-79.

Hantush, M. S. (1960). Modification of the theory of leaky aquifers. *J. Geophys. Res.* 65(11): 3713-3725.

Hantush, M. S. (1949). Plane potential flow of ground water with leakage. PhD thesis, Department of Civil Engineering, University of Utah: 89 pp.

Hantush, M. S., Jacob, C. E. (1955). "Non-steady radial flow in an infinite leaky aquifer." *Trans. Amer. Geophys. Union* 36(1): 95-100.

Hantush, M. S., Jacob, C. E. (1954). Plane potential flow of groundwater with linear leakage. *Trans. Amer. Geophys. Union* 35(6): 917-937.

Haitjema, H. M. (1995). Analytic element modeling of groundwater flow.394 pp. Academic Press, San Diego, CA, USA.

Harman C., Sivapalan, M. (2009a). A similarity framework to assess controls on shallow subsurface flow dynamics in hillslopes. *Water Resour. Res.*, 45(W01417): doi:10.1029/2008WR007067.

Harman C., Sivapalan, M. (2009b). Effects of hydraulic conductivity variability on hillslope-scale shallow subsurface flow response and storage-discharge relations. *Water Resour. Res.*, 45(W01421): doi:10.1029/2008WR007228.

Hemker, C. J. (1984). Steady groundwater flow in leaky multiple aquifer systems. *J. Hydrol.* 72: 355-374.

Herrera, I. (1970). Theory of multiple leaky aquifers. *Water Resour. Res.* 6(1): 185-193.

Herrera-Pantoja, M., Hiscock, K. M. (2008). The effects of climate change on potential groundwater recharge in Great Britain. *Hydrol. Processes* 22(1): 73-86.

Hilberts, A. G. J., van Loon, E. E., Troch, P. A., Paniconi, C. (2004). The hillslope-storage Boussinesq model for non-constant bedrock slope. *J. Hydrol.* 291: 160-173.

Hilberts, A. G. J., Troch, P. A., Paniconi, C. (2005) Storage-dependent drainable porosity for complex hillslopes. *Water Resour. Res.* 41 (W06001): doi:10.1029/2004WR003725.

Hilberts, A. G. J., Troch, P. A., Paniconi, C., Boll, J. (2007). Low-dimensional modeling of hillslope subsurface flow: Relationship between rainfall, recharge, and unsaturated storage dynamics. *Water Resour. Res.* 43(W03445): doi:101029/2006WR004964.

Hopp, L., McDonnell, J. J. (2009). Connectivity at the hillslope scale: Identifying interactions between storm size, bedrock permeability, slope angle and soil depth. *J. Hydrol.*: doi:10.1016/j.jhydrol.2009.07.047.

Hunt, R. J. (2006). Ground water modeling application using the analytic element method. *Ground Water* 44(1): 5-15.

Jacob, C. E. (1946). Radial flow in a leaky artesian aquifer. *Trans. Amer. Geophys. Union* 27: 198-205.

Jayawickrama, P. W., Brown, K. W., Thomas, J. C., Lytton, R. L. (1988). Leakage rates through flaws in membrane liners. *J. Environ. Engrg., ASCE* 114(6): 1401-1420.

Jiao, J. J., Tang, Z. (1999). An analytical solution of groundwater response to tidal fluctuation in a leaky confined aquifer. *Water Resour. Res.* 35(3): 747-751.

Jones, J. P., Sudicky, E. A., Brookfield, A. E., Park, Y.-J. (2006). An assessment of the tracer-based approach to quantifying groundwater contributions to streamflow. *Water Resour. Res.* 42, W02407, doi:10.1029/2005WR004130.

Kacimov, A.R., Obnosov, Y.V., Perret, J. (2004). Phreatic surface flow from a near-reservoir saturated tongue. *J. Hydrol.* 296: 271-281.

Karpf, C., Krebs, P. (2005). Application of a leakage model to assess exfiltration from sewers. *Water Sci. Technol.* 52(5): 225-231.

Kollet, S. J., Maxwell, R. M. (2006). Integrated surface-groundwater flow modeling: A free-surface overland flow boundary condition in a parallel groundwater flow model. Adv. *Wat. Resour. Res.* 29: 945-958.

Koussis, A. D., Smith, M. E., Akylas, E., Tombrou, M. (1998). Groundwater drainage flow in a soil layer resting on an inclined leaky bed. *Water Resour. Res.* 34(11), 2879–2887.

Kraemer, S. R. (2007). Analytic element ground water modeling as a research program (1980 to 2006). *Ground Water* 45(4): 402-408.

Kuhlman, K. L., Neuman, S. P. (2009). Laplace-transform analytic-element method for transient porous media flow. *J. Eng. Math.* 64 (2): 113-130.

Kuhlman, K. L, Neuman S. P. (2006). Recent advances in Laplace transform analytic element method (LT-AEM) theory and application to transient groundwater flow. Eos Trans. AGU, 87(52), Fall Meet. Suppl., Abstract H41B-0397.

LaBolle, E. M., Ahmed, A. A., Fogg, G. E. (2003). Review of the Integrated Groundwater and Surface-Water Model (ISGM). *Ground Water* 41(2): 238-246.

Larocque, M., Leroux, G., Madramootoo, C., Lapointe, F.J., Pellerin, S., Bonin, J. (2006).Mise en place d'un laboratoires National sur le mont Covey Hill (Québec, Canada). *VertigO* 7(1): 1-11.

Lasalle, P. (1981). Géologie des sédiments meubles de la région de St-Jean-Lachine. Ministère de l'Énergie et des Ressources du Québec, Direction générale de l'exploration géologique et minérale, DPV, 780 pp.

Lavigne, M.-A. (2006). Modélisations numériques de l'écoulement régional de l'eau souterraine dans le bassin versant de la rivière Châteauguay. Institut national de la recherche scientifique. Québec, Université du Québec. M.Sc thesis.: 98.

Le Maitre D. C., Colvin C. A. (2008). Assessment of the contribution of groundwater discharges to rivers using monthly flow statistics and flow seasonality. *Water SA* 34(5): 549-564.

Liang, X., Xie, Z. (2003). Important factors in land-atmosphere interactions: surface runoff generations and interactions between surface and groundwater. *Global Planet. Change* 38: 101-114.

Matonse, A., Kroll, C. (2009). Simulating low streamflows with hillslope-storage models. *Water Resour. Res.,* 45, W01407, doi:10.1029/2007WR006529.

Maurer, E. P., Adam, J. C., Wood, A. W. (2009). Climate model based consensus on the hydrologic impacts of climate change to the Rio Lempa basin of Central America. *Hydrol. Earth Syst. Sci.* 13(2): 183-194.

MDDEP (2007). Données hydrogéologique. Région administrative de Saint-Jean-Chrisostome, http://www.mddep.gouv.qc.ca/eau/souterraines/sih/index.htm.

Mitchell-Bruker, S., Haitjema, H.M. (1996). Modeling steady state conjunctive groundwater and surface water flow with analytic elements. *Water Resourc. Res.*, 32(9): 2725-2732.

Morita, M., Yen, B.C. (2002). Modeling of conjunctive two-dimensional surface - three-dimensional subsurface flows. *J. Hydraul. Eng.* 128(2): 184-200.

Nastev, M., Lamontagne, C., Tremblay, T., Lavoie, D., Hardy, F., Lamothe, M., Croteau, A.,Blanchette, D., Lavigne, M.A., Roy, N., Paradis, D., Benoit, N., Lefebvre, R., Marcotte,D., Gaudin R. et Rouleau, A. (2004). Hydrogeological overview of the transboundary aquifers in the Châteaugua River Basin, Canada-United States. 5ième conférence conjointe AIH-CNC/CGS, Québec. 7 p.

Nastev, M., Rivera, A., Lefebvre, R., Martel, R., Savard, M. (2005). Numerical simulation of groundwater flow in regional rock aquifers, southwestern Quebec, Canada. *Hydrol. J.* (13): 835-848.

Neuman, S. P., Witherspoon, P. A. (1969a). Theory of flow in a confined two aquifer system. *Water Resour. Res.* 5(4): 803-816.

Neuman, S. P., Witherspoon, P. A. (1969b). Applicability of current theories of flow in leaky aquifers. *Water Resour. Res.* 5(4): 817-829.

Noël, P., Rousseau, A., Paniconi, C. (2010). An algortihm for delineating and extracting hillslopes and hillslope width functions from gridded elevation data. *Hydrol. Earth Syst. Sci.*, submitted.

Oliver, L. D., Christakos, G. (1996). Boundary condition sensitivity analysis of the stochastic flow equation. *Adv. Water Resour.* 19(2): 109-120.

Panday, S., Huyakorn, P. S. (2004). A fully coupled physically-based spatially-distributed model for evaluating surface/subsurface flow. *Adv. Water Resour.* 27: 361-382.

Paniconi, C., Troch, P. A., van Loon, E. E., Hilberts, A. G. J. (2003). Hillslope-storage Boussinesq model for subsurface flow and variable source areas along complex hillslopes: 2. Intercomparison with a three-dimensional Richards equation model. *Wat. Resour. Res.* 39(11), 1317, doi:10.1029/2002WR001730.

Paniconi, C., Putti, M. (1994). A comparison of Picard and Newton iteration in the numerical solution of multidimensional variably saturated flow problems. *Wat. Resour. Res.* 30(12): 3357-3374.

Rastogi, A. K. (1988). Flow studies through porous and permeable sub-surface water bearing bodies having sloping base. *Irrigation and Power* 45(1): 84-90.

Reggiani, P., Sivapalan, M., Hassanizadeh, S.M. (1999). A unifying framework for watershed thermodynamics: balance equations for mass, momentum, energy and entropy, and the second law of thermodynamics. *Advances in Water Resources* 22(4): 367-398.

Reggiani, P., S.M. Hassanizadeh, M. Sivapalan, W.G. Gray (1999). A unifying framework for watershed thermodynamics: constitutive relationships. *Adv. Wat. Res.* 23: 15-39.

Rocha, D., Feyen, J., Dassargues, A. (2007). Comparative analysis between analytical approximations and numerical solutions describing recession flow in unconfined hillslope aquifers. *Hydrogeol. J.* 15: 1077–1091.

Rosa, E., Larocque, M., Pellerin, S., Gagné, S., Fournier, B. (2008). Determining the number of manual measurements required to improve peat thickness estimations by ground penetrating radar. *Earth Surf. Process. Landforms :* DOI: 10.1002/esp.1741.

Scibek, J., Allen, D. M. (2006). Comparing modelled responses of two high-permeability, unconfined aquifers to predicted climate change. *Global Planet. Change* 50(1-2): 50-62.

Smakhtin, V. U. (2001). Low flow hydrology: a review. *J.Hydrol.* 240: 147-186.

Sophocleous, M., Perkins, S. P. (2000). Methodology and application of combined watershed and ground-water models in Kansas. *J. Hydrol.* 236(3-4): 185-201.

Sophocleous, M. (2002). Interactions between groundwater and surface water: The state of the science. *Hydrol. J.* 10(1): 52-67.

Strack, O. D. L. (1989). Groundwater mechanics, 732 pp., Prentice Hall, Englewood Cliffs, NJ, USA.

Therrien, R., McLaren, R. G., Sudicky, E. A., Panday, S. M. (2005). HydroGeoSphere A three-dimensional numerical model describing fully-integrated subsurface and surface

flow and solute transport, 322 pp., Groundwater Simulation Group, Univ. of Waterloo, Waterloo, Ont., Canada.

Therrien, R., Sudicky, E. A., (1996). Three-dimensional analysis of variably-saturated flow and transport in porous media. *J. Contam. Hydrol.* (23): 1-44.

Thompson, D. M., (2006). Changes in pool size in response to a reduction in discharge: a flume experiment. *River Res. Applic.* (22): 343-351.

Thoms, R. B., Johnson, R.L. (2005). Modelling groundwater/surface water interactions using MODFLOW-WhaT. Proceedings of the 4th International Groundwater Quality Conference, Waterloo, Ont., Canada. IAHS Publ. 297 : 466-472.

Tremblay, T. (2008). Hydrostratigraphie et géologie du quaternaire dans le bassin-versant de la rivière Châteauguay, Québec. MSc thesis Université du Québec à Montréal : 233 pp.

Troch, P. A., Paniconi, C., van Loon, E. E. (2003). Hillslope-storage Boussinesq model for subsurface flow and variable source areas along complex hillslopes: 1. Formulation and characteristic response. *Wat. Resour. Res.* 39(11), 1316, doi:10.1029/2002WR001728.

Tromp-van Meerveld, H. J., Weiler, M. (2008). Hillslope dynamics modeled with increasing complexity. *J. Hydrol.* 361: 24-40.

Tromp-van Meerveld, H. J., Peters, N. E., McDonnell, J. J. (2007). Effect of bedrock permeability on subsurface stormflow and the water balance of a trenched hillslope at the Panola Mountain Research Watershed, Georgia, USA. *Hydrol. Process.* 21: 750-769.

Uchida, T., Asano, Y., Ohte, N., Mizuyama, T. (2003). Seepage area and rate of bedrock groundwater discharge at a granitic unchanneled hillslope. *Water Resour. Res.* 39(1): 1018, doi:10.1029/2002WR001298.

VanderKwaak, J. E. (1999). Numerical simulation of flow and chemical transport in integrated surface-subsurface hydrologic systems, Ph.D. thesis, Univ. of Waterloo, Waterloo, Ont., Canada: 217 pp.

VanderKwaak, J. E., Loague, K. (2001). Hydrologic-response simulations for the R-5 catchment with a comprehensive physics-based model. *Water Resour. Res.* 37, 999-1013.

Werner, A. D., Gallagher, M. R., Weeks, S. W. (2006). Regional-scale, fully coupled modelling of stream-aquifer interaction in a tropical catchment. *J. Hydrol.* 328: 497-510.

Wilkinson, W. B., Cooper, D. M. (1993). The response of idealized aquifer/river systems to climate change. *Hydrol. Sci. J.* 38(5): 379-390.

Winter, T. C., Harvey, J. W., Franke, O. L., Alley, W. M. (1998). Ground water and surface water: A single resource, *U.S. Geol. Surv. Circular N.* 1139, Denver, CO.

Yang, D., Srikantha, H., Musiake, K. (2002). A hillslope-based hydrological model using catchment area and width functions. *Hydrol. Sci. J.* 47(1): 49-65.

Yusoff, I., Hiscock, K. M., Conway, D. (2002). Simulation of the impacts of climate change on groundwater resources in eastern England. *Geol. Soc. Lond. Spec. Publ.* 193: 325-344.